DEVELOPMENTAL REMODELING OF AMPA AND NMDA SUBUNIT COMPOSITION AT THE ROD BIPOLAR CELL DYAD SYNAPSE IN THE MOUSE RETINA

Tesis entregada a la

UNIVERSIDAD DE VALPARAÍSO

en Cumplimiento Parcial de los requisitos para optar al grado de

Doctor en Ciencias con Mención en Neurociencia

Facultad De Ciencias

Por

Sebastian Felipe Estay Vizcarra

Enero 2024

Dirigida por: Profesor Andrés E. Chávez Navarrete

Universidad de Valparaíso
CHILE

Facultad de Ciencias
COORDINACIÓN DE POSTGRADO

ACTA OFICIAL EXAMEN DE GRADO

Nombre: SEBASTIÁN FELIPE ESTAY VIZCARRA

Rut: 17.392.587 - 5

Programa: DOCTORADO EN CIENCIAS MENCIÓN NEUROCIENCIA

Título Tesis: "Developmental remodeling of AMPA and NMDA subunit composition at the Rod Bipolar Cell dyad synapse in the mouse retina".

Fecha: 25 de enero 2024

Nombre Académico	Comisión	Firma	Nota Tesis Escrita	Nota Tesis Oral
Dr. Marco Fuenzalida (UV)	Revisor Interno Presidente de la Comisión		7.0	7.0
Dr. Jeff Diamond (NIH, USA)	Revisor Externo		7.0	7.0
Dra. Chiayu Chu (UV)	Revisora Interna		7.0	7.0
Dr. Álvaro Ardiles (UV)	Revisor Interno		7.0	7.0
Dr. Andrés Chávez (UV9	Tutor		7.0	7.0

Promedio Tesis Escrita	7.0
Promedio Tesis Oral	7.0
PROMEDIO TESIS FINAL	7.0

Dra. Ana María Cárdenas D.
Directora
Doctorado en Ciencias mención Neurociencia
Facultad de Ciencias

ACKNOWLEDGEMENTS

Mis más sinceros agradecimientos a las personas que han estado durante este largo proceso, muchas veces gratificante y otras tantas no.

Gracias a mi familia (Miriam, Héctor, Javier, Felipe y gatito) por su apoyo y cariño incondicional, sin su apoyo no hubiera llegado tan lejos.

Gracias Odra por estar más de 15 años en las buenas y en las malas, creer en mi cuando yo no lo hacía. Sin duda tu presencia me ha me ha enseñado a ser incondicional hacia las personas que queremos y siempre me ha incentivado a mejorar como persona.

Gracias Claudia por ampliar mi visión del mundo y compartir tu mundo conmigo. Gracias por enseñarme la tolerancia y los límites, sacarme de mi zona de confort y por tu apoyo y amistad.

Gracias Glyxia morena (y perdón por tan poco) por enseñarme que hay cosas más allá de la ciencia, por volver a despertar mi curiosidad, por hacerme volver a apreciar la música, el arte y los pequeños detalles. En otra línea temporal no me habría perdido la fiesta de gatitos por nada del mundo:).

Gracias Ale por tu amistad, apoyo y por cada conversación que siempre fue un gusto porque aprendí o me enteré de algo nuevo. Y por los berlines y galletas también!

Gracias Cami por siempre creer en mi trabajo, por los memes de perritos, por el cafecito conversado en los pasillos y por ser mi amiga.

Gracias Andrés por darme la oportunidad de ingresar al laboratorio hace más de 8 años, por el apoyo incondicional en todo ámbito. Por la paciencia con los tiempos.

Gracias Fran y Cami por las conversaciones de pandemia y por los memes compartidos jeje.

Gracias gente que he conocido escalando en tornamesa (gabo, carla, esteban, cote, kevin, mati, cami, dani, daniprrr) por el apañe, buena onda. Sin duda han sido un gran aporte este último año.

FUNDING

This work was supported by:

- **Programa de doctorado en Ciencias Biológicas mención Neurociencia**, Facultad de Ciencias, Universidad de Valparaíso.

- **Proyecto FONDECYT 1151091 y 1201848.**

- **Centro Interdisciplinario de Neurociencia (CINV): Proyecto código P09-022F**

LIST OF CONTENTS

LIST OF FIGURES AND TABLES

ABBREVIATIONS

ACs: Amacrine cells

ACSF: artificial cerebrospinal fluid

AMPA: α-Amino-3-hydroxy-5-methyl-4-isoxazolepropionic acid

AMPAR: AMPA receptor

BC: Bipolar cell

BK: Calcium-activated potassium channels

CGE: Caudal ganglionic eminence

CaMKII: Ca^{2+}/calmodulin-dependent protein kinase II

CBC: Cone bipolar cell

cGMP: Cyclic guanosine monophosphate

CI-AMPARs: Calcium-impermeable AMPARs

CICR: Calcium-induced calcium release

CKAMPS: Cysteine-knot AMPA receptor modulating protein

CNGCs: Cyclic nucleotide-gated channels

CNIHs: Cornichons

CNS: Central Nervous System

CP-AMPARs: Calcium-permeable AMPARs

CPPG: (RS)-α-Cyclopropyl-4-phosphonophenylglycine

D-APV: D-2-amino-5-phosphonovalerate

DHT: 5,7-dihydroxytryptamine

DR: Dark-rearing

EM: Electron microscopy

EPSC: Excitatory postsynaptic current

ERG: Electroretinogram

GABA: γ -aminobutiric acid

$GABA_AR$: $GABA_A$ receptor

$GABA_CR$: $GABA_C$ receptor

GABAR: GABA receptor

GAD-67: Glutamic acid decarboxylase 67

GCL: Ganglion cell layer

GlyR: Glycine receptor

GPCR: G protein-coupled receptor

GSG1L: Germ cell-specific gene 1-like protein

IAN: Indolamine-accumulating neurons

iGluR: Ionotropic glutamate receptor

IPL: Inner plexiform layer

IPSC: Inhibitory postsynaptic current

KARs: Kainate receptors

LE: Light-exposure

LRRTM4: Leucine Rich Repeat Transmembrane Neuronal 4

MGE: Medial ganglionic eminence

mEPSC: Miniature EPSC

mGluR: Metabotropic glutamate receptor

MNTB: Medial nucleus of the trapezoid body

NBQX: 2,3-Dioxo-6-nitro-1,2,3,4-tetrahydrobenzo[f]quinoxaline-7-sulfonamide

NMDA: N-methyl-D-aspartate

NMDAR: NMDA receptor

NR: Normal-rearing

ONL: Outer nuclear layer

OPL: Outer plexiform layer

OPs: Oscillatory potentials

PhTx: Philanthotoxin

PKC: Protein Kinase C

RBC: Rod bipolar cell

RGC: Retinal ganglion cell

RI: Rectification index

RIBEYE: Ribbon synapse scaffolding protein

RyRs: Ryanodine receptors

SAPs: Synapse-associated proteins

sEPSC: Spontaneous EPSC

sIPSC: Spontaneous IPSC

SynDIG4: Synapse differentiation-induced gene 4

TARP: Transmembrane AMPA receptor regulatory protein

TPMPA: 1,2,5,6-Tetrahydropyridin-4-yl)methylphosphinic acid

TRPM1: Transient Receptor Potential cation channel subfamily M member 1

TTX: Tetrodotoxin

VGCCs: Voltage-gated calcium channels

VGLUT1: Vesicular glutamate transporter 1

vIPSCs: Voltage-evoked IPSC

ABSTRACT

During postnatal development, synaptic connections undergo dynamic refinement involving structural and functional changes in response to neuronal activity. In the visual system, the onset of visual experience, marked by eye opening (~P14), triggers synaptic remodeling processes, including modifications in synaptic receptor composition. In the retina, the rod pathway, a conserved circuitry across mammalian species, mediates dim light vision. Here, rod bipolar cells (RBCs) provide glutamatergic inputs to GABAergic A17 and glycinergic AII amacrine cells (ACs). While AII ACs transfer signals to ON and OFF pathway, A17 ACs make reciprocal inhibitory feedback synapses onto the same RBC axon terminal, modulating the time course of visual signaling *in vivo*. While at the time of eye opening, these synapses undergo extensive modifications leading to the maturation of fundamental components that enable inhibitory signaling, including GABA receptors (GABARs), it remains unclear whether the maturation and stabilization of RBC dyad synapses during development involve changes in the subunit composition of ionotropic glutamate receptors (iGluRs) and whether these changes require visual experience.

In this thesis, using acute retinal slices from normally- and dark-reared mice and a combination of electrophysiological, pharmacological, and optical approaches, we investigate whether light-dependent synaptic activity (i.e. visual experience), drives a switch in the subunit composition of AMPARs and/or NMDARs at the RBC dyad synapse, allowing for the stabilization of feedforward and feedback synaptic connections of this circuit.

We found that: (1) the mEPSC frequency increases with age in both AII and A17 ACs, but the amplitude and kinetics change only in AII ACs. These changes were unaffected by visual deprivation, except for the mEPSC frequency onto AII ACs, which was enhanced. (2) In the mouse retina, the expression of CP-AMPARs in AII ACs remained unchanged throughout development, while NMDARs were not functionally expressed. No changes were induced by visual deprivation. (3) In A17 amacrine cells, AMPARs transition from calcium-impermeable (with an atypical pharmacological profile) to

calcium-permeable, while NMDARs transition from GluN2B- to GluN2A-containing receptors. This change in iGluRs subunit composition was not modified by visual deprivation. (4) The GABAergic reciprocal feedback, which requires CP-AMPARs activation, onto RBC axon terminals is absent before eye opening, likely by the lack of expression of CP-AMPARs before eye opening. (5) Interestingly, the synaptic strength of the GABAergic reciprocal feedback is reduced by visual deprivation, an effect that can be reversed by exposing visually deprived animals to light.

Together, our results indicate that extensive refinement of the mechanisms facilitating feedforward excitatory and feedback inhibitory signaling at the RBC dyad synapse occurs during retinal development. Most of these changes are independent of visual experience. Additionally, our findings underscore the distinct iGluRs profiles exhibited by AII and A17 amacrine cells, suggesting that both cell types follow unique programs of synaptic refinement and development.

1 INTRODUCTION

An essential step in understanding how neuronal circuits of the central nervous system (CNS) receive, compute, encode and transmit information is to investigate how they are established and refined during development. Throughout postnatal development, synaptic connections undergo dynamic refinement involving structural and functional changes in response to neuronal activity. In the visual system, it is well-established that the onset of visual experience, marked by eye opening, triggers synaptic remodeling processes, including modifications in synaptic receptor composition (Quinlan et al., 1999; Philpot et al., 2001; Lu and Constantine-Paton, 2004b). The activity-dependent remodeling in receptor composition is crucial for shaping the final synaptic connections and play a significant role in synaptic maturation and stabilization throughout development (Gambrill and Barria, 2011).

The retina, a true part of the CNS, provides an excellent model system for studying the developmental and functional aspects of neuronal communication. There, the rod bipolar cell (RBC) dyad synapse in the rod pathway is a crucial and conserved circuitry across mammalian species, playing a pivotal role in mediating vision under low-light conditions (scotopic vision). Although the glutamatergic feedforward signaling from RBC to AII amacrine cell and the reciprocal GABAergic feedback from A17 amacrine cell to RBC have been extensively studied in the adult retina (Singer and Diamond, 2003; Chavez et al., 2006; Chavez and Diamond, 2008; Grimes et al., 2009; Chavez et al., 2010; Oesch and Diamond, 2011; Grimes et al., 2015; Graydon et al., 2018; Hartveit et al., 2018; Veruki et al., 2019; Egger and Diamond, 2020), recent efforts have been directed toward investigating these processes during retinal development. While evidence suggest that the excitatory and inhibitory signaling at the RBC dyad synapse is functional before eye opening (Schubert et al., 2008), recent studies have clearly established that at the time surrounding eye opening, these synapses undergo extensive modifications leading to the maturation of fundamental components that enable inhibitory and excitatory signaling (Schubert et al., 2013; Okawa et al., 2019; Sinha et al., 2020; Sinha et al., 2021; Kim et al., 2023; Wisner et al., 2023). However, it remains unclear whether the maturation and stabilization of RBC dyad synapses during development involve changes in the subunit composition of

iGluRs, as observed in other synapses of the CNS (Quinlan et al., 1999; Philpot et al., 2001; Kumar et al., 2002; Matta et al., 2011; Matta et al., 2013) and whether these possible changes required visual-experience.

In this thesis, our aim was to demonstrate whether light-dependent synaptic activity (i.e. visual experience), drives a switch in the subunit composition of AMPARs and/or NMDARs at the RBC dyad synapse, allowing for the stabilization of feedforward and feedback synaptic connections of this circuit. Therefore, in this chapter, I provide a brief overview of the organization and physiology of the mammalian retina, with emphasis on the rod pathway and the molecular mechanisms underlying the feedforward and feedback signaling at this synapse. Subsequently, I delve into the current knowledge surrounding the development of RBC dyad synapses and explore the possible role of visual experience in synaptic refinement of these connections.

1.1 Structural organization and physiology of the mammalian retina

The mammalian retina, the first station of visual processing, is a highly structured neural tissue localized at the back surface of the eye. It is organized in a laminar way, where cell bodies reside in *nuclear layers* and synaptic contact occur within *plexiform layers*. The retina is composed by five main classes of neurons which include photoreceptors, horizontal, bipolar, amacrine and ganglion cells plus one class of glial cell, the Müller cell. The photoreceptor cell bodies are localized in the outer nuclear layer (ONL), whereas the cell bodies of bipolar, horizontal and amacrine cells are distributed along the inner nuclear layer (INL). Retinal ganglion cells (RGCs) and some “displaced” amacrine cells (ACs) are localized in the ganglion cell layer (GCL). Synaptic contact between photoreceptors, bipolar and horizontal cells occur in the outer plexiform layer (OPL), whereas bipolar, amacrine and retinal ganglion cells make synaptic contact in the inner plexiform layer (IPL) (Reviewed by Rodieck, 1998; Masland, 2001; Wassle, 2004; **Figure 1**).

Visual processing in the retina initiates when light reach the photoreceptors, which are the light-sensitive cells responsible for converting photons into electrochemical signals. Two types of photoreceptors exist: rods and cones. Rods are well-suited for low-light conditions, enabling scotopic

vision, while cones are specialized for daylight vision, facilitating photopic vision. In darkness, a steady inward cationic current known as "dark current" flows through cyclic nucleotide-gated channels (CNGCs), localized on the outer segment membrane of rods and cones, leading to their depolarization and the continuous release of glutamate. When light reaches the outer segments of the photoreceptors, specialized photopigments (rhodopsin in rods and opsin in cones) are activated. This activation initiates a series of signaling cascades that lead to the closure of CNGCs, hyperpolarizing the photoreceptor cell membrane and ultimately decreasing glutamate release (Fu and Yau, 2007).

Photoreceptors transfer this light-evoked signal to bipolar cells (BCs) via glutamatergic synaptic connections. In the last two decades, based on morphology, physiology, and molecular markers, 13 subtypes of BCs have been described in the mouse retina (Ghosh et al., 2004; Helmstaedter et al., 2013; Euler et al., 2014). More recently this classification has been extended to 15 different subtypes, of which 14 receive direct glutamatergic inputs from cones, but only one, the RBC, receives inputs exclusively from rod photoreceptors (Shekhar et al., 2016). Visual information coming from the photoreceptors is segregated in ON and OFF pathways mediated by BCs that are depolarized (ON-BCs) or hyperpolarized (OFF-BCs) in response to light (Euler et al., 2014). These functional differences are determined by the expression of glutamate receptors. ON-BCs express the metabotropic glutamate receptor 6 (mGluR6; Nomura et al., 1994) which prevent Transient Receptor Potential cation channel subfamily M member 1 (TRPM1)-mediated depolarization (Morgans et al., 2009; Shen et al., 2009; Koike et al., 2010a; Koike et al., 2010b), while OFF-BCs hyperpolarize in response to light due to expression of, α-amino-3-hydroxy-5-methyl-4-isoxazolepropionic acid receptor (AMPARs) and Kainate receptors (KARs; DeVries, 2000), two different iGluRs. Furthermore, ON and OFF-BCs make synaptic contact with RGCs in the inner and the outer half of the IPL, respectively, making these pathways anatomically segregated (Euler et al., 2014). RGCs are the principal output of information to the rest of the CNS, and in the mouse retina, at least 30 different types have been identified according to their morphology, light responses and genetic markers (Sanes and Masland, 2015; Baden et al., 2016).

The vertical flow of information through this excitatory pathway is highly regulated by horizontal cells in the outer retina and by amacrine cells (ACs) in the inner retina (**Figure 1**). In the mammalian retina, two to three types of horizontal cells (Peichl and Gonzalez-Soriano, 1994; Guo et al., 2010; Puller et al., 2014), provide feedback and feedforward inhibition to photoreceptors and bipolar cells, respectively. Although the specific mechanisms underlying this regulation are currently under debate (Thoreson and Mangel, 2012), their contribution to generate the initial center-surround receptive field organization, a fundamental feature that shape RGCs responses, has been demonstrated (Stroh et al., 2018). Contrary to horizontal cells, ACs comprise a highly heterogeneous group of at least 63 different subtypes (Yan et al., 2020) which are broadly classified, according to the diameter of their dendritic trees, as narrow or wide-field amacrine cells. Narrow-field cells are commonly glycinergic, whereas wide-field cells are commonly GABAergic (Strettoi and Masland, 1996; MacNeil and Masland, 1998; Zhang and McCall, 2012; Helmstaedter et al., 2013). ACs lack axons, instead, they use their dendrites for synaptic input-output, suggesting an extensive and complex dendritic processing. They receive inputs from BCs and other ACs and provide feedback and feedforward inhibition to BCs and RGCs, regulating by this mean the spatial and temporal properties of light responses (Masland, 2012; Diamond, 2017). One of the best characterized circuits where glutamate release from axons is regulated by a robust feedback inhibition is the RBC dyad synapse, which is part of the rod pathway.

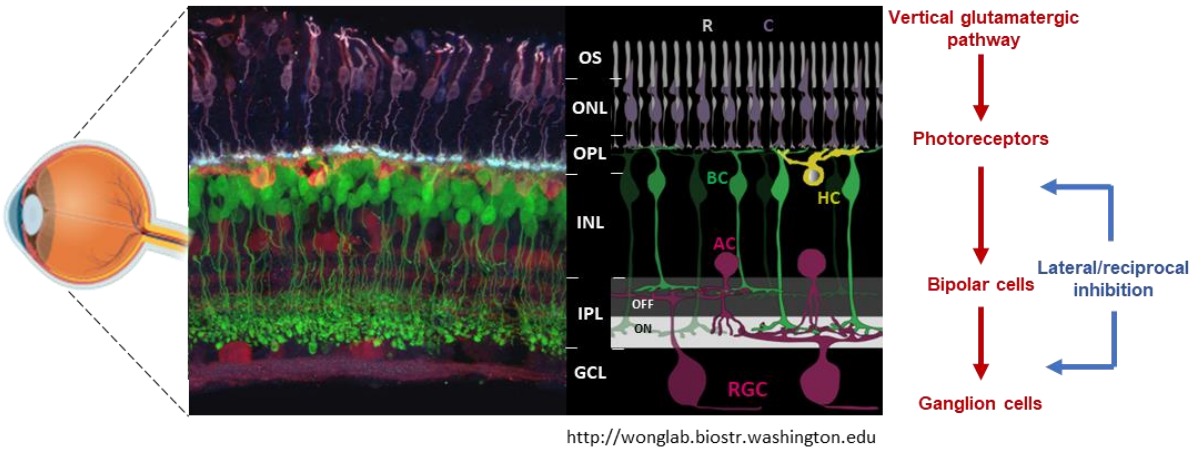

Figure 1. General organization of the mammalian retina.

The retina, a neural tissue located at the back surface of the eye (left), serves as the first station of visual processing. As shown in the vertical section and in the representative scheme, it is organized in layers (center), with cell bodies in nuclear layers and synaptic contacts occurring within plexiform layers. The main neuron types composing the retina include cone (C) and rod (R) photoreceptors, bipolar cells (BCs), ganglion cells (GCs), amacrine cells (ACs), and horizontal cells (HCs). Additionally, glial cells such as Müller cells (M), microglia (Mi), and astrocytes (AS) provide metabolic and immunological support (not shown). The retina is divided into different layers (from the most internal to the outer layers): ganglion cell layer (GCL), inner plexiform layer (IPL), inner nuclear layer (INL), outer plexiform layer (OPL), outer nuclear layer (ONL), and outer segment layer (OS). The conversion of light to an electrochemical signal occurs in the photoreceptors. The neural signal is then transferred via parallel glutamatergic synapses to bipolar cells, which, in turn, contact retinal ganglion cells—the principal output to the CNS. This vertical glutamatergic pathway is regulated by horizontal and amacrine cells, providing lateral inhibition at the OPL and IPL, respectively (right). Adapted from Dr. Rachel Wong lab website (http://depts.washington.edu/wonglab/research.html).

1.2 Rod pathway in the mammalian retina

Our visual system is capable of operating across an extensive range of light intensities, that covers more than nine orders of magnitude (Rodieck, 1998). In this scenario, the rod pathway acts as a highly sensitive circuit which can encode the absorption of a single photon (Baylor, 1996), making it well-suited to mediate vision in low-light conditions (Scotopic vision; Bloomfield and Dacheux, 2001). In the classic rod pathway, rod photoreceptors provide glutamatergic inputs to RBCs, which in turn make glutamatergic synapses with the glycinergic AII and GABAergic A17 ACs (Kolb and Nelson, 1983; Dacheux and Raviola, 1986; Raviola and Dacheux, 1987; Strettoi et al., 1990; **see Figure 2**).

AII amacrine cells are the most abundant ACs in the mammalian retina, comprising approximately 11% of the total AC population (Casini et al., 1995; Strettoi and Masland, 1996; MacNeil and Masland, 1998; Helmstaedter et al., 2013). They have a narrow bistratified dendritic field that extend through the IPL. Their lobular processes form sign-inverting glycinergic synapses onto OFF-CBCs (Tsukamoto et al., 2001; Graydon et al., 2018) and some OFF-RGCs (van Wyk et al., 2009) in the outer half of the IPL. Additionally, their arboreal processes form sign-conserving electrical synapses onto ON-CBCs (Famiglietti and Kolb, 1975) in the inner half of the IPL, a unique wiring, that enables AII ACs to relay rod-mediated signals to the cone pathway under scotopic conditions. The high sensitivity of this circuitry is achieved through three principal characteristics that enable high-gain amplification for the detection of a single photon: 1) Divergence at the rod photoreceptor output, where one rod connects with two RBCs, 2) Convergence at the RBC-AII synapse, with each RBC contacting ~4-5 AII ACs via ~53 ribbon synapses, resulting in signal replication and cancellation of synaptic noise and 3) Spatial unification of neighboring AII ACs through electrical coupling. These characteristics contribute to the rod pathway's ability to reduce the signal-to-noise ratio and achieve a robust amplification of the signal from a single photon (Tsukamoto and Omi, 2013). Despite of their pivotal role in scotopic vision, several reports indicate that electrical synapses onto ON-BCs can operate in the opposite direction under mesopic and photopic conditions, providing crossover inhibition to a subset of OFF-RGCs (Manookin et al., 2008), and playing an essential role in the detection of

approaching objects during daylight conditions (Munch et al., 2009; Oesch and Diamond, 2009; Strettoi et al., 2018).

On the other hand, the second postsynaptic element identified at the RBC dyad synapse is the A17 AC, which is classified as wide-field GABAergic amacrine cell and it is morphologically identified by their wide (~100-300 µm) dendritic arbors with several unbranched neurites extended through the IPL (Menger and Wassle, 2000). A17 ACs dendritic arbors contain several varicosities, each of which receives glutamatergic excitatory synaptic input exclusively from a single RBC (Nelson and Kolb, 1985) and makes local reciprocal inhibitory feedback synapses onto the same RBC terminal (Nelson and Kolb, 1985; Dacheux and Raviola, 1986; Hartveit, 1999; Zhang et al., 2002), regulating neurotransmitter release (Chavez et al., 2006). *Ex vivo* studies have provided evidence that this reciprocal feedback is crucial in modulating the gain and dynamic range of the feedforward signaling between RBCs and AII ACs (Volgyi et al., 2002; Grimes et al., 2010). Furthermore, ablation of indolamine-accumulating neurons (IAN), including A17 ACs, by intravitreal injection of the neurotoxic agent 5,7-dihydroxytryptamine (DHT), strongly suggest that A17 ACs-mediated feedback inhibition regulates the temporal properties of light-evoked signaling *in vivo* (Nakatsuka and Hamasaki, 1985; Dong and Hare, 2003). In addition to reciprocal feedback inhibition, RBC axon terminals also receive inhibitory inputs from other non-reciprocal GABAergic and glycinergic ACs that also contribute to shape the temporal course and properties of light-evoked responses within the rod pathway (Eggers and Lukasiewicz, 2006b; Chavez and Diamond, 2008; Chavez et al., 2010).

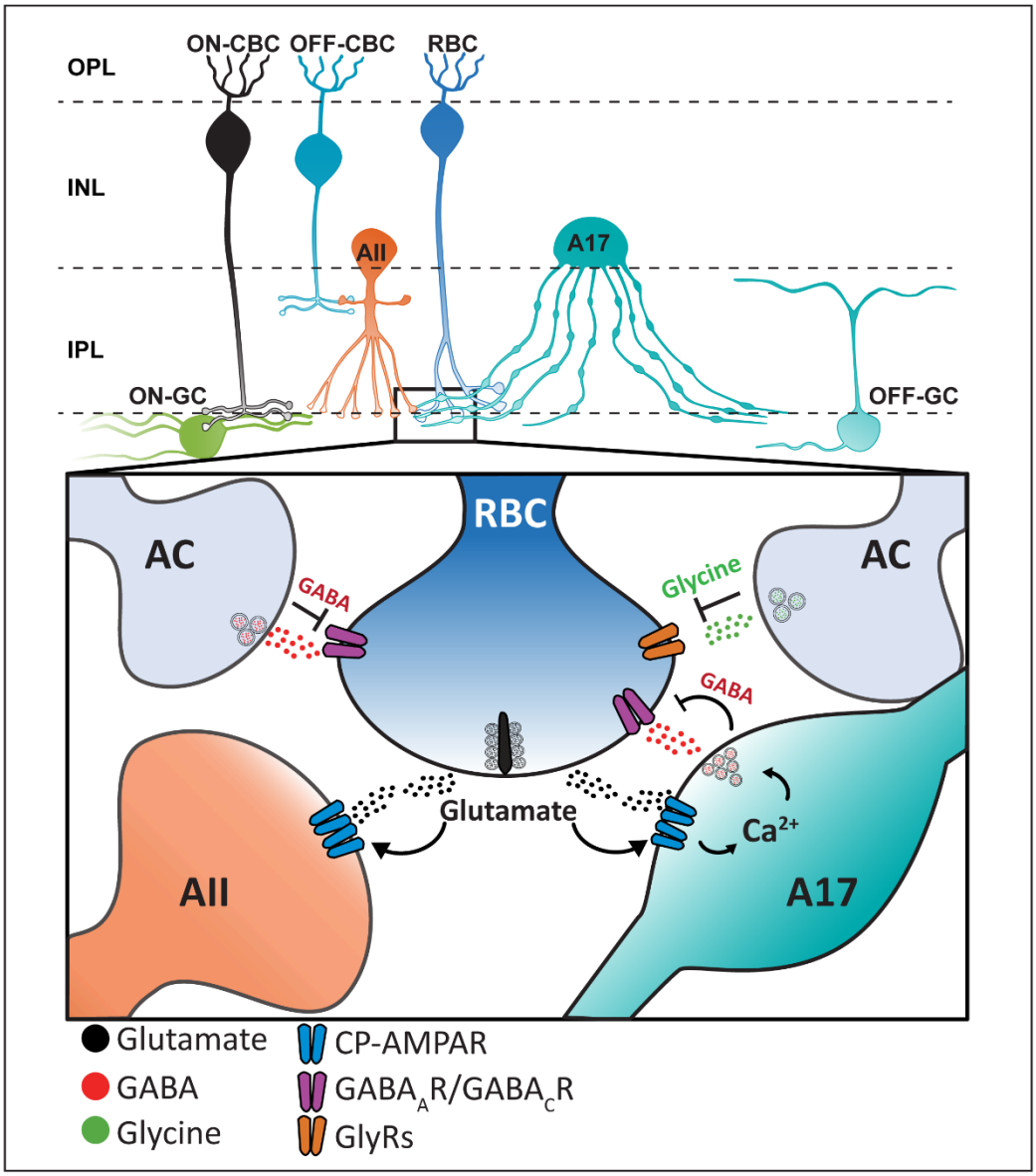

Figure 2. The rod bipolar cell dyad synapse.

Schematic representation of the basic organization of the RBC dyad synapse. In the classic rod pathway, rod photoreceptors (not shown) provide glutamatergic inputs to RBCs, which, in turn, form glutamatergic ribbon synapses with the glycinergic AII and GABAergic A17 amacrine cells. AII ACs transfer rod signals to the cone pathway, dividing them into ON and OFF components by making sign-conserving gap junctions with ON-CBCs and forming inhibitory, glycinergic synapses onto OFF-CBCs. A17 ACs make a reciprocal, inhibitory synapses onto the RBC, thereby modulating the feedforward signaling at the RBC-AII synapse. Additionally, feedforward signaling at the RBC dyad synapse is also regulated by glycinergic and non-reciprocal GABAergic synapses from other types of ACs.

1.3 Feedforward excitatory synaptic transmission at the RBC dyad synapse

In the last two decades, the molecular and physiological mechanisms underlying excitatory feedforward signaling at the RBC dyad synapse have been described in detail in several species including rabbits, rodents and primates (Dacheux and Raviola, 1986; Chun et al., 1993; Menger and Wassle, 2000; Dong and Hare, 2003; Volgyi et al., 2004; McLaughlin et al., 2020).

1.3.1 Glutamate release at the RBC dyad synapse

It is well established that glutamate release from RBC axon terminals is triggered mainly by the activation of L-type (CaV1; Protti and Llano, 1998; Singer and Diamond, 2003) and to a minor extent T-type (CaV3; Pan, 2000; Pan et al., 2001) voltage-gated calcium channels (VGCCs), even though recent reports indicate that P/Q-type (CaV2.1) and N-type (CaV2.2) VGCCs might also contribute to transmitter release in the mouse retina (Zhang et al., 2022b).

VGCCs are organized in nanodomains tightly coupled to specialized electron-dense structures called synaptic ribbons, which allows high rates of neurotransmitter release compared to conventional synapses. Synaptic ribbons act as conveyor belts, with synaptic vesicles tethered to them. The vesicles located at the base of the ribbon are primed for rapid transmitter release, making them well-suited for signaling the onset of stimuli, meanwhile, the vesicles positioned further up the ribbon contribute to sustained release, likely representing the intensity and duration of the light stimulus (For reviews see: Lagnado and Schmitz, 2015; Moser et al., 2020). This unique dual-component responses allow ribbon synapses to encode luminance and contrast in RBCs (Oesch and Diamond, 2011). Furthermore, the one-to-one coupling between VGCCs opening and vesicle release, enable the transition from univesicular to multivesicular transmitter release, facilitating the codification of the RBC presynaptic graded potential over a wide dynamic range (Singer et al., 2004; Jarsky et al., 2010). It is important to note that while synaptic ribbons are believed to play a crucial role in organizing presynaptic active zones and facilitating transmitter release, evidence suggests that transmitter release can occur independently of ribbons (Mehta et al., 2014). Furthermore, the removal of synaptic ribbons in BCs has been found to impair evoked, but not spontaneous transmitter release (Maxeiner et

al., 2016), suggesting that ribbons are essential for synchronized release, but not for the release *per se*.

1.3.2 Glutamatergic receptors mediating synaptic transmission at the RBC dyad synapse: NMDA and AMPA receptors

In the retina, like in the rest of the CNS, fast excitatory synaptic transmission is mediated by iGluRs, which can be classified into three functional classes: NMDA (N-methyl-D-aspartate) receptors and non-NMDARs which include AMPARs and kainate receptors. Additionally, delta (δ) glutamate receptors are also considered as a fourth class of iGluRs based on sequence homology, however, whether they are assembled in functional channels remains uncertain, although they are thought to act as trans-synaptic organizers (Hansen et al., 2021).

NMDARs are heterotetrameric ligand-gated ion channels composed by two GluN1 subunits in combination with either two GluN2 subunits (diheteromeric) or a combination of GluN2 and GluN3 subunits (triheteromeric). Activation of NMDARs require simultaneous binding of glutamate and glycine (or D-Serine) as a co-agonist. These receptors are characterized by their: 1) Slow activation kinetics, 2) Mg^{2+}-dependent block at hyperpolarized potentials and 3) permeability to monovalent (Na^{+}, K^{+}) and divalent cations (Ca^{2+}). NMDARs serve as coincidence detectors that require simultaneous presynaptic release of glutamate and postsynaptic depolarization to produce the slow Ca^{2+}-permeable component of the excitatory postsynaptic current (EPSC) (Paoletti et al., 2013; Hansen et al., 2017).

In the RBC dyad synapse it was originally assumed that AII and A17 ACs did not express NMDARs (Boos et al., 1993; Menger and Wassle, 2000), but emerging evidence from the rat retina suggest that both AII and A17 ACs express functional NMDARs (Hartveit and Veruki, 1997; Zhou et al., 2016), that are likely localized at extra-synaptic sites (Veruki et al., 2019). AII ACs express GluN2B-containing NMDARs, while A17 ACs express GluN2A-containging NMDARs. Although the specific role of these receptors remains to be determined, evidence suggest that NMDARs activation increase the reciprocal GABA release from A17 ACs (Veruki et al., 2019). Moreover, experiments performed in AII ACs from rabbit retina, indicate that NMDAR activation could regulate the gap

junction coupling through CaMKII (Ca^{2+}/calmodulin-dependent protein kinase II)-dependent phosphorylation of Connexin-36 (Kothmann et al., 2012; Veruki et al., 2018).

On the other hand, AMPARs play a crucial role in excitatory synaptic transmission, serving as the primary mediators of fast excitatory signals in the mature brain. AMPARs are ligand-gated ion channels and consist of four core subunits (GluA1-4). These subunits can combine to form homo- or hetero-tetramers, giving rise to a wide variety of AMPAR subtypes. Each subunit uniquely contributes to channel kinetics, ion selectivity, and receptor trafficking properties, thereby adding to the functional diversity of AMPARs (Traynelis et al., 2010; Hansen et al., 2021). Unlike other iGluRs, AMPARs are associated with a diverse range of auxiliary and interacting proteins forming a large multimolecular signaling machine that is believed to encompass over 30 distinct proteins (Catsburg and MacGillavry, 2020; Kamalova and Nakagawa, 2021). Some AMPARs auxiliary proteins include TARPs (Transmembrane AMPA receptor regulatory protein; Chen et al., 2000; Tomita et al., 2003; Kato et al., 2008), cornichons (CNIHs; Schwenk et al., 2009), CKAMPS (Cysteine-knot AMPA receptor modulating proteins; von Engelhardt et al., 2010; Farrow et al., 2015), GSG1L (Germ cell-specific gene 1-like protein; Schwenk et al., 2012; Shanks et al., 2012), and SynDIG4 (Synapse differentiation-induced gene 4; Matt et al., 2018). These auxiliary proteins are known to influence several aspects of AMPAR function, including localization, trafficking, pharmacology, ion permeation, and block by intracellular polyamines (Hansen et al., 2021; Kamalova and Nakagawa, 2021).

RNA sequencing and immunocytochemical staining studies conducted in rabbits, primates, and rodents have revealed that AII ACs predominantly express AMPARs composed of GluA2, GluA3, and GluA4 subunits (Grunder et al., 2000a; Ghosh et al., 2001; Li et al., 2002; Yan et al., 2020; Percival et al., 2022). In contrast, the specific identity of AMPARs expressed in A17 ACs is less clear. In the rabbit retina, it was found that GluA1-GluA4 subunits do not co-localize with A17 AC varicosities. Instead, these varicosities were found to express δ 1/2 glutamate receptors (Ghosh et al., 2001; Li et al., 2002). Immunogold electron microscopy (EM) studies in the rat retina have shown that A17 AC varicosities primarily contain the GluA3 subunit. Inconsistent immunostaining was observed

for GluA4, whereas GluA1/2 subunits were not detected (Grimes et al., 2015). Interestingly, single-cell RNA sequencing analyses in the adult mouse retina indicate a high expression of GluA2/3 and GluA4 subunits in A17 ACs (Yan et al., 2020).

It is important to note that the functional diversity of AMPARs is enhanced through alternative splicing and RNA editing. AMPAR subunits exist in two forms, the "flip" and "flop" variants, which arise from alternative splicing of two exons encoding a part of the ligand-binding domain (Sommer et al., 1990). These isoforms exhibit distinct kinetic properties and pharmacology, with "flop" versions desensitizing more rapidly than the "flip" versions and being less sensitive to the desensitization blocker cyclothiazide (Sommer et al., 1990; Pei et al., 2009). Furthermore, RNA editing of GluA subunits expands receptor diversity by generating distinct isoforms. Notably, the GluA2 subunit plays a critical role in defining AMPAR functional properties. Through post-transcriptional editing of GluA2 RNA in the pore-lining region, a glutamine (Q) residue at position 607 is replaced with an arginine (R) residue. This modification renders GluA2-containing AMPARs impermeable to calcium (Ca^{2+}) ions and make them resistant to blockade by endogenous polyamines, resulting in linear current-voltage (I-V) relationships (Sommer et al., 1991; Verdoorn et al., 1991). Conversely, GluA2-lacking AMPARs, known as Ca^{2+}-permeable (CP-AMPARs), exhibit higher single-channel conductance and display voltage-dependent blockade by endogenous polyamines, leading to inwardly rectifying I-V relationships (Bowie and Mayer, 1995; Kamboj et al., 1995; Koh et al., 1995; Dingledine et al., 1999). In the rodent retina, it is well-established that glutamate released from RBCs primarily activates AMPARs, which exhibit GluA2-lacking Ca^{2+}-permeable characteristics, and are expressed in both AII and A17 ACs (Menger and Wassle, 2000; Mørkve et al., 2002; Singer and Diamond, 2003; Veruki et al., 2003; Osswald et al., 2007). In A17 ACs, the expression of Ca^{2+}-permeable AMPA receptor is fundamental to trigger GABAergic reciprocal feedback onto RBCs (Chavez et al., 2006).

1.4 Mechanism underlying reciprocal GABAergic feedback at the A17-RBC synapse

At most CNS synapses, transmitter release requires VGCCs-dependent Ca^{2+}-influx (Catterall, 1998; Catterall, 2011), however, functional evidence indicate that GABA release from A17 ACs can be triggered independently of VGCCs activation, instead it require Ca^{2+}-influx through CP-AMPARs (Chavez et al., 2006). Moreover, this Ca^{2+} signal mediated by CP-AMPARs can be boosted by Ca^{2+}-induced calcium release (CICR) from intracellular stores via activation of Ryanodine receptors (RyRs; Chavez et al., 2006). Although, GABA release from A17 ACs require CP-AMPAR activation, additional studies suggest that L-type VGCCs are also expressed in A17 varicosities, but their activation is limited by Ca^{2+}-activated K^+ (BK) channels. Under certain conditions such as strong activation of A17 AC dendrites, VGCCs can be recruited to enhance GABA release (Grimes et al., 2009; Diamond, 2017).

GABA released from A17 ACs exerts its function through the activation of ionotropic GABA receptors (GABARs), which form pentameric complexes and can be divided in the $GABA_A$ (α1-6, β1-4, γ1-4, δ, ε subunits) and $GABA_C$ (ρ1 and ρ2 subunits) receptors. For $GABA_A$Rs, it has been suggested that α, β and γ are required for their functional assembly, typically in a 2:2:1 ratio. For $GABA_C$Rs homo or heteropentameric assemblies of ρ1 or ρ2 subunits can be formed (Chebib and Johnston, 1999; Moss and Smart, 2001). Molecular and functional studies have shown that both GABARs subtypes are expressed in the RBC terminals; however, they do not co-localize at the same synapses (Fletcher et al., 1998; Koulen et al., 1998b; Schubert et al., 2013). In fact, spontaneous GABA release (Frech and Backus, 2004; Eggers and Lukasiewicz, 2006a) and reciprocal feedback elicited by depolarizing RBCs primarily activate $GABA_A$Rs (Chavez et al., 2006), composed of α1 or α3 subunits (Schubert et al., 2013; Sinha et al., 2021). However, when the release from A17 ACs is enhanced, a $GABA_C$R-mediated component can be observed in the reciprocal feedback inhibitory postsynaptic currents (IPSC; Hartveit, 1999; Singer and Diamond, 2003; Chavez et al., 2006). Interestingly, further studies have shown that in the same RBC terminal each A17 varicosity return a proximal and a distal reciprocal synapse located at ~200 nm and ~500 nm, respectively, from the synaptic ribbon. GABA release from the proximal synapse depends on the activation of CP-AMPARs and activates principally

$GABA_AR$s, whereas the second synapse activate $GABA_CR$s and its activation is modulated by VGCCs-BK channel complexes (Grimes et al., 2010; Grimes et al., 2015). Compared to $GABA_AR$s, $GABA_C$ receptors have a higher affinity for GABA, but lower activation/inactivation kinetics, desensitization and channel conductance (Bormann, 2000), thus it has been suggested that the two receptors regulate different aspects of glutamate release from RBCs under different conditions (Eggers and Lukasiewicz, 2006b; Moore-Dotson et al., 2015).

1.5 Synaptic development of the RBC dyad synapse

At the time of eye opening in rodents, postnatal day 14-15 (P14-P15; Henneberger et al., 2005), morphological features and molecular components resemble those of adult animals suggesting that retinal circuits are mature (Hoon et al., 2014). Nonetheless, during this critical period, eye opening drives a series of changes in circuitry development, synaptogenesis and synaptic receptor composition at different levels of the retinothalamo-cortical pathway (Yoshii et al., 2003; Lu and Constantine-Paton, 2004a; Zhao et al., 2006), including the retina (Feller, 2003; Tian and Copenhagen, 2003; Tian, 2004).

In the rod pathway, the onset of GABAergic spontaneous activity onto RBCs can be detected as soon as P8 (Schubert et al., 2008). Moreover, before eye opening (<P15), both $GABA_AR$s and $GABA_CR$s are already expressed at the RBC axon terminals, and apposition between dendritic processes of GAD-67 positive ACs – presumably A17 ACs – and Protein Kinase C (PKC)-immunolabeled RBC axon terminals can be observed at P10 (Schubert et al., 2013). Similarly, essential components of the glutamatergic system, including endogenous ligands (Fletcher and Kalloniatis, 1997), receptors (Grunder et al., 2000a; Grunder et al., 2000b; Hack et al., 2002), vesicular transporters (Johnson et al., 2003), and the fundamental machinery responsible for vesicular release (Dhingra et al., 1997; Greenlee et al., 2002; von Kriegstein and Schmitz, 2003), are also expressed before eye opening. Likewise, ribbon synapses appear around P11 (Fisher, 1979), and RIBEYE, a ribbon synapse scaffolding protein, can be immunodetected by P10 (Johnson et al., 2003). Co-localization of the vesicular glutamate transporter 1 (VGLUT1) with PKC-labeled RBCs can already

be detected as early as P7 (Johnson et al., 2003; Sherry et al., 2003), coinciding with the start of spontaneous glutamatergic activity onto AII and A17 ACs, which initiates around the same time (Schubert et al., 2008).

Although, at a first glance, the expression of the principal components of the glutamatergic and GABAergic systems suggest that feedforward and feedback synaptic transmission may be functional at the RBC dyad synapse before eye opening, *in vivo* ERG recordings have shown an increase in ERG amplitudes and oscillatory potentials (OPs) in the rodent retina (el Azazi and Wachtmeister, 1991; He et al., 2013), implying that major changes are taking place at RBC synapses (Liao et al., 2023) at the time surrounding eye opening. In line with this, before eye opening, $GABA_AR$s expressed at RBC axon terminals undergo a switch in subunit composition from α3-containing to α1-containing $GABA_AR$s (Sinha et al., 2021). Previous reports indicate that GABAergic synaptogenesis is independent of GABAergic or glutamatergic neurotransmission. However, GABA release onto RBC axon terminals is necessary for the maintenance of α1-containing, but not α3-containing $GABA_AR$s nor $GABA_CR$s (Schubert et al., 2013). Therefore, during postnatal development, there is a major refinement of inhibitory synapses onto RBC axon terminals.

On the other hand, it is well-established that in the rodent retina mature excitatory synapses onto AII and A17 ACs express GluA2-lacking CP-AMPARs (Singer and Diamond, 2003; Chavez et al., 2006; Grimes et al., 2015; Hartveit et al., 2018; Percival et al., 2022) and extra-synaptic GluN2B-containing and GluN2A-containing NMDARs (Zhou et al., 2016; Veruki et al., 2019), respectively. However, even though there have been reports of functional CP-AMPAR expression in AII ACs before eye opening (Osswald et al., 2007), there is no evidence regarding the expression of other iGluRs and their functional properties at early stages of postnatal development.

Interestingly, in neurons of the neocortex (Kumar et al., 2002; Shin et al., 2005; Brill and Huguenard, 2008), the medial nucleus of the trapezoid body (MNTB; Lujan et al., 2019) and the CA3 region of the hippocampus (Ho et al., 2007), the subunit composition of AMPARs undergoes a switch from GluA2-lacking AMPARs (Ca^{2+}-permeable; CP-AMPARs) to GluA2-containing AMPARs (Ca^{2+}-

impermeable; CI-AMPARs) during postnatal development. Similarly, in the cortex (Sheng et al., 1994; Quinlan et al., 1999; Liu et al., 2004) and the hippocampus (Bellone and Nicoll, 2007; Matta et al., 2011; Rodenas-Ruano et al., 2012), NMDARs change from GluN2B-containing to GluN2A-containing receptors, a switch that is fundamental for synaptic incorporation of AMPARs (Hall et al., 2007; Gray et al., 2011; Ferreira et al., 2015) and synapse stabilization (Gambrill and Barria, 2011). Whether similar processes occur at excitatory synapses onto AII and A17 amacrine cells remains unclear. *Therefore, our first aim was to investigate the functional properties of iGluRs in AII and A17 amacrine cells before and after eye opening to provide further insight on these potential developmental changes.*

1.6 Activity-dependent changes in receptor subunit composition: Role of visual experience

Classical studies using visual deprivation or monocular deprivation have demonstrated that visual experience shapes the connectivity and functional maturation of the visual system (Hooks and Chen, 2020). At the synaptic level, visual experience during the critical period is required for the functional maturation of GABARs (Chen et al., 2001), NMDARs (Carmignoto and Vicini, 1992; Quinlan et al., 1999; Philpot et al., 2001; Matta et al., 2011) and AMPARs (Han et al., 2017; Tan et al., 2020) in the visual cortex. In the rodent retina, visual experience is required for the expression and correct localization of mGluR6s in ON-CBCs, but not in RBCs (Dunn et al., 2013). Moreover, recent findings indicate that visual deprivation prevents the developmental switch in the subunit composition of $GABA_A$Rs at the RBC axon terminal (Wisner et al., 2023), suggesting that the functional maturation of inhibitory synapses onto RBCs is an activity-dependent process.

At excitatory synapses, acute light stimulation of the mature retina, can induce changes in AMPAR subunit composition in RGCs (Jones et al., 2012; Casimiro et al., 2013), whereas visual deprivation alter AMPARs properties in AII ACs (Osswald et al., 2007) and prevent the maturation of NMDARs in synaptic fractions of the retina (Xue and Cooper, 2001) and in RGCs (Guenther et al., 2004). However, whether light-driven synaptic activity influences the developmental expression profile

of AMPAR and NMDARs in AII and A17 ACs in the mouse retina is unknown. Thus, the second aim of this thesis was to determine *whether visual experience is required for the functional maturation of AMPARs and NMDARs in both AII and A17 amacrine cells, and if so, the functional consequences in the maturation and stabilization of feedforward and feedback RBC dyad synapses*.

2 HYPOTHESIS AND OBJECTIVES

Hypothesis

Light-dependent synaptic activity during a critical period (eye opening) drives a differential switch in AII and A17 amacrine cell's AMPAR and NMDAR subunit composition throughout the postnatal development of the mouse retina modifying the stabilization and maturation of the RBC dyad synapse.

General aim

To evaluate the functional role of AMPA and NMDA receptors subunit composition at RBC dyad synapse and to determine whether their expression profile depends on light-driven synaptic activity over the time course of the eye opening.

Specific aims

1. To examine the functional role of AMPA and NMDA receptors in the synaptic transmission at RBC-AII synapses over the time course of the eye opening in normal and dark-reared mice.

1.1. To evaluate the contribution of AMPARs and NMDARs to synaptic transmission at RBC-AII synapses by electrophysiological recordings of spontaneous currents (sEPSC) in normal and dark-reared mice.

1.2. To evaluate the functional properties of AMPARs and NMDARs expressed in AII amacrine cells by electrophysiological recordings of evoked EPSC (eEPSC) in normal and dark-reared mice.

2. To examine the functional role of AMPA and NMDA receptors in the synaptic transmission at RBC-A17 synapses over the time course of the eye opening in normal and dark-reared mice.

2.1. To evaluate the contribution of AMPARs and NMDARs to synaptic transmission at RBC-A17 synapses by electrophysiological recordings of sEPSC in normal and dark-reared mice.

2.2. To evaluate the functional properties of AMPARs and NMDARs in A17 amacrine cells by electrophysiological recordings of eEPSC in normal and dark-reared mice.

3 EXPERIMENTAL METHODS

3.1 Animals

In this study, we used normally reared (NR: 12:12 light-dark cycle, **Figure 3A**) wildtype (WT) C57BL/6J mice of both sexes and GluA2$^{-/-}$ knockout mice (Jackson Laboratories, JAX:002913) provided by Dr. Susumu Tomita from Yale University, USA. Animals were housed at 20-22°C with *ad libitum* access to food and water. The day of birth was designated as postnatal day 0 (P0). As eye opening in mice occurs around ~P14 (Henneberger et al., 2005), we divided the animals into two experimental groups: the first group consisted of mice aged P10-P13 (before eye opening), while the second group consisted of animals aged P20-P40 (after eye opening). Only mice with closed eyes at P13 were used for the study, and those with open eyes were excluded. All experimental procedures were conducted in accordance with the bioethics regulations of the Chilean Research Council (ANID) and approved by the bioethics committee of the Universidad de Valparaíso (Chile, BEA159-20, CBC40/2022).

3.2 Dark-rearing and Light-Exposure

To investigate the impact of visual experience on the development and establishment of the RBC dyad synapse, we conducted experiments using P20-P40 mice that were reared in complete darkness from birth (DR; 24-hour dark cycle). The DR mice were kept in a separate facility, under the same conditions as NR mice, and received animal care twice a week under infrared illumination (850 nm) using homemade night vision goggles. To examine the effect of light exposure on the DR mice, we randomly selected mice for recovery experiments (**Figure 17**) and exposed them to room light (60-80 lux) for 1 hour one or two consecutive days, as indicated in **Figure 3B**. After the light exposure, mice were returned to the dark room until the day of the electrophysiological recordings. On the same day of the experiments, we used non-exposed DR littermates as controls.

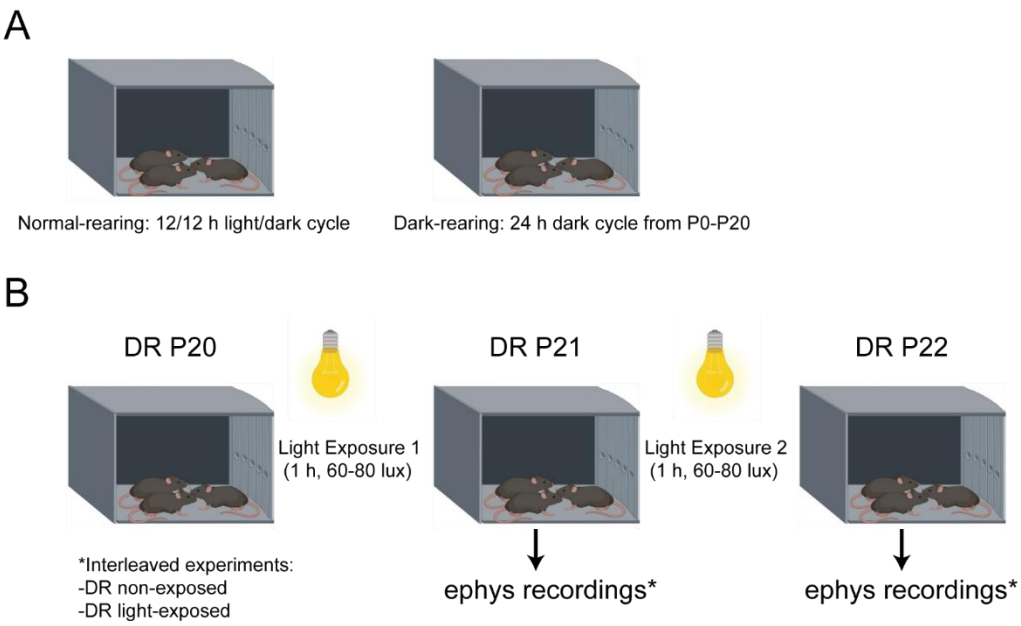

Figure 3. Experimental design for Dark-Rearing and Light-Exposure.

(A) To determine the effects of age and visual experience on the development of the RBC dyad synapse, mouse retinas isolated from normally-reared (12/12h light-dark cycle) and dark-reared (24 h dark cycle) mice were used in this study. (B) Recovery experiments were performed by exposing DR mice to light (60-80 lux) for 1 h on one or two consecutive days. After exposure, DR mice were returned to a separate home cage, and electrophysiological recordings were performed the next day. Interleaved control experiments were performed in non-exposed DR mice on the same day of the recordings.

3.3 Ex vivo electrophysiological recordings

3.3.1 Retinal slice preparation

Retinal slices were obtained under room light conditions. In brief, animals were decapitated following isoflurane (Forane®, Abbot laboratories, USA) anesthesia, eyes were enucleated, the cornea, lens and vitreous humor were removed and the retina was isolated at room temperature (RT) in artificial cerebrospinal fluid (ACSF) composed by (in mM): 119 NaCl, 26 $NaHCO_3$, 1,25 Na_2HPO_4,

2,5 KCl, 2,5 $CaCl_2$, 1,5 $MgSO_4$, 10 Glucose, 2 Na-pyruvate and 4 Na-lactate (290-295 mOsm). The ACSF was bubbled with carbogen (95% O_2/5% CO_2) and the pH was adjusted to 7.4 with NaOH. The retina was cut in halves and a section of ~1mm^2 was embedded in 3% (w/v) low-melting point agarose (in ACSF with $NaHCO_3$ substituted for HEPES (10 mM)). The agar block was mounted and cut in 210 µm sections (**Figure 4A**) using a Leica Vibratome VT1200S (Leica Microsystems AG, Wetzlar, Germany). Slices were used after a 30 min stabilization period and were maintained up to 6 hours in ACSF continuously bubbled with carbogen.

3.3.2 Whole-cell voltage clamp recordings

Individual retinal slices were transferred to a recording chamber mounted on an upright fixed-stage Nikon FN1 microscope. The recording chamber was superfused at a rate of 2-3 mL/min with ACSF and was kept at 28°C by an automatic temperature controller (TC-324C, Warner Instrument). Whole-cell voltage clamp recordings were made using electrodes with a resistance between 8 to 10 MΩ for RBCs and 6 to 8 MΩ for AII-A17 ACs. All experiments were done under room light conditions. For RBCs, we used a cesium-based intracellular solution composed by (in mM): 100 Cs-methanesulfonate, 20 Tetraethylammonium chloride (TEA-Cl), 10 HEPES, 1.5 BAPTA, 10 Na_2-phosphocreatine, 4 Mg-ATP, 0.4 Na-GTP y 10 glutamic acid (~285 mOsm). Intracellular solution for A17 and AII recordings contained (in mM): 100 Cs-methanesulfonate, 20 TEA-Cl, 10 HEPES, 10 EGTA, 10 Na-phosphocreatine, 4 Mg-ATP, 0.4 Na-GTP (~285 mOsm). The pH was adjusted to 7.2-7.3 with CsOH.

To visualize cells, we used infrared differential interference contrast (IR-DIC) microscopy with a water immersion objective lens (40x, Nikon) and identified them by cellular morphology using fluorescent dyes Alexa-488 or Alexa-594 hydrazide added to the intracellular solution (10 µM; Invitrogen-ThermoFischer Scientific). RBCs were characterized by their goblet-shaped somas localized in the external limit of the OPL and the extension of a single axon to the sublamina 5 of the IPL, adjacent to the GCL, where the axon ended in a series of varicosities (**Figure 4B**). Furthermore, RBCs were identified by their high input resistances (>1 GΩ), and small, sustained Ca^{2+}-currents

(Singer and Diamond, 2003), contrary to the larger and transient Ca^{2+}-currents observed in CBCs (Hartveit, 1999; Pan, 2000). AII ACs were recognized by their diamond-shaped soma located in the INL and slightly displaced toward IPL (**Figure 4B**)**.** Moreover, AII ACs can be easily distinguished by their bistratified dendritic trees formed by lobular appendages and arboreal dendrites at the distal and proximal parts of the IPL, respectively (Demb and Singer, 2012). A17 ACs were distinguished by their large dome-shaped somas localized in the INL/IPL border and by their highly branched dendritic tree, that extend at least 100 µm, with dozen of neurites that present varicosities at a regular intervals (Menger and Wassle, 2000; Singer and Diamond, 2003; Grimes et al., 2010).

All experiments, unless otherwise stated, were conducted in the presence of strychnine 3 µM and TTX 0.5 µM to block glycinergic feedback and TTX-sensitive non-reciprocal feedback onto RBC terminals, respectively (Chavez et al., 2006; Chavez et al., 2010). Series (Rs) and input resistance (Rin) were continuously monitored throughout all the recording and Rs was left uncompensated. Cells with changes in Rs >20% during the experiment were excluded from the analysis. Signals were recorded using a Multiclamp 700B amplifier (Molecular Devices), acquired at 10 kHz, and low-pass filtered at 2 kHz before acquisition. Data were acquired and analyzed using a custom-made routine written in Igor Pro 6.37 (Wavemetrics, Portland, OR, USA) and visualized with Origin software (Microcal, Northampton, MA, USA).

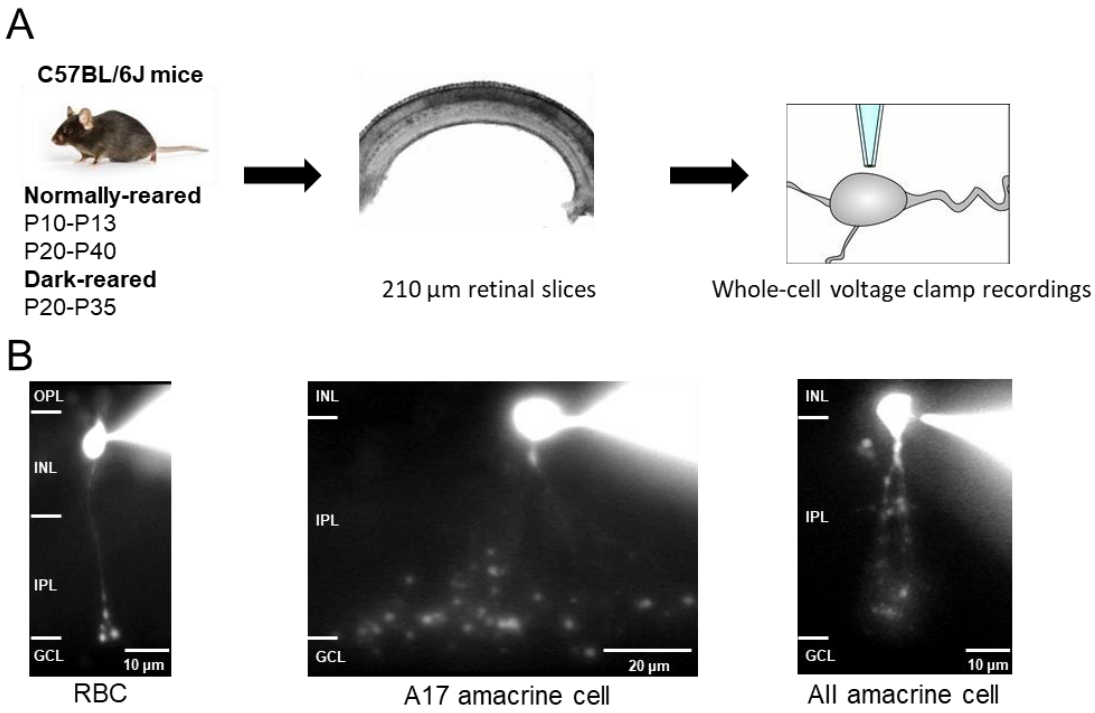

Figure 4. Experimental methods and retinal neurons recorded.

(A) Animals used in this work were divided in two experimental groups that comprises ages between P10-P13 (before eye opening) and P20-P40 (after eye opening; *left*). Eyes were enucleated and acute retinal slices (210 µm) were obtained using a vibratome (*middle*). Electrophysiological recordings were done using whole-cell voltage clamp technique (*right*). **(B)** RBC, AII and A17 amacrine cells were identified under epifluorescence using Alexa-488 hydrazide (10 µM) in the intracellular solution. Ganglion cell layer (GCL), inner plexiform layer (IPL), inner nuclear layer (INL), outer plexiform layer (OPL) are indicated in the microphotographs.

3.3.3 Recording methods and analysis

Spontaneous miniature excitatory postsynaptic currents (mEPSCs)

Spontaneous miniature excitatory postsynaptic currents (mEPSC) were recorded from AII and A17 amacrine cells voltage clamped at -60 mV in the continuous presence of SR95531 (10 µM), TPMPA (50 µM), strychnine (3 µM), APV (25 µM) and TTX (0.5 µM) to block $GABA_ARs$, $GABA_CRs$, GlyRs, NMDAR and NaV currents, respectively. All mEPSC recordings started 2-3 min after break-in to allow cell dialysis and stabilization. For experiments presented in **Figures 5 and 6** mEPSC activity

was recorded for 5 min. The last 2 min of the baseline were concatenated and analyzed offline using the MINI analysis software (Synaptosoft). For figures 7-8 and 12-13, the CP-AMPARs channel blocker IEM1460 (25 µM) was bath applied for 10 min. Pairwise comparisons were performed between the last 2 min of the baseline and the last 2 min of drug application. Signals were low-pass filtered at 1.5 kHz to improve the signal-to-noise ratio and the threshold amplitude for event detection was set (-5 pA) above the root mean square noise level (2 pA). Events were subsequently checked manually for accuracy. Cumulative plots for inter-event intervals and amplitude were generated by grouping the events of all datasets.

For the analysis of kinetics properties of AMPAR-mediated mEPSCs, events with an exponential decay, and a monotonic rising phase, which could be clearly discriminated from the background noise, were manually collected (150-200 events per cell). The kinetics parameters were calculated from the scaled average aligned to 50% of the rise time. Rise time was calculated as 10-90% time to the peak. Half-width as the time to 50% peak amplitude and to calculate the decay time the mEPSC waveform was fitted to a single exponential to obtain tau (time to 37% of the peak amplitude).

AMPAR and NMDAR-mediated currents

To evaluate the functional features of AMPARs, we took advantage of the voltage-dependent blockade of GluA2-lacking receptors by polyamines, which produces a characteristic inwardly rectifying current-voltage (I-V) relationship (Kamboj et al., 1995; Koh et al., 1995; Rozov and Burnashev, 1999). Toward this end, we added the polyamine spermine (250 µM) to the intracellular solution and constructed I-V plots of AMPAR-mediated currents (I_{AMPA}) recorded at different holding potentials (from -60 mV to +40 mV with 20 mV step increments).

To elicit I_{AMPA}, glutamate (500 µM, 100 ms for A17 or 25 ms for AII ACs) was applied by pressure-induced release (“puff”), directly onto AII/A17 processes located in sublamina 5 of the IPL. I_{AMPA} were pharmacologically isolated by adding antagonists against $GABA_AR$s (SR-95531 10 µM), $GABA_CR$s (TPMPA 50 µM), GlyRs (strychnine 3 µM) and NMDARs (APV 25 µM). As control

experiments, we made AII and A17 recordings in the absence of this polyamine in the intracellular solution. The rectification index (RI) was calculated as the ratio of I_{AMPA} at 40 mV/-60 mV and normalized to 1. In figures 8 and 13 I_{AMPA} was elicited by a puff of AMPA (100 µM, 25 ms) onto AII or A17 (V_{HOLD}=-60 mV) amacrine cell processes and IEM1460 (25 µM) was bath applied for 10 min to determine the contribution of CP-AMPARs to the total I_{AMPA}.

To examine the functional features of NMDARs across retinal development. NMDAR-mediated currents (I_{NMDA}) were elicited by puff application of NMDA (1 mM, 500 ms) onto AII or A17 dendrites. I_{NMDA} were pharmacologically isolated by adding antagonists against $GABA_A$Rs (SR-95531 10 µM), $GABA_C$Rs (TPMPA 50 µM), GlyRs (strychnine 3 µM) and AMPARs (NBQX 10 µM). These experiments were done in Mg^{2+}-free ACSF and in the continuous presence of the NMDAR co-agonist D-Serine (200 µM) and Tricine (10 mM) to chelate Zn^{2+} traces. To determine NMDAR subunit composition, we bath applied for 10 min $ZnCl_2$ (40 µM) which is equivalent to a free Zn^{2+} of 200 nM (Fayyazuddin et al., 2000) to block NR2A-containing NMDARs. Subsequently, we bath applied Ro-256981 (1 µM) for 10 min to block NR2A-containing NMDARs. Recordings were performed in the presence of Tricine (10 mM) to chelate any traces of endogenous Zn^{2+}.

All puff agents were applied using a Picospritzer II (General Valve) at 6 PSI using pulled glass pipettes (4-5 MΩ). Puffed agents were dissolved in ACSF buffered with HEPES (10 mM) pH= 7.4. ACSF-HEPES alone did not evoke any response when puffed in the OPL or IPL (data not shown). Puff was applied at intervals of 20-30 s and puff evoked response was measured as the difference between the peak of the response and the baseline before stimulation. Comparisons were performed between the average responses (4-6) of the last 2 min of each condition.

Voltage-evoked inhibitory postsynaptic currents (vIPSCs)

To evaluate the reciprocal GABAergic feedback inhibition at RBC terminals, we voltage-evoked inhibitory postsynaptic currents (vIPSC) by depolarizing RBCs from -60 mV to -10 mV for 100 ms at 20 s intervals (Chavez et al., 2006). Depolarization of voltage-clamped RBCs elicited sustained inward calcium currents, upon which were superimposed transient, feedback inhibitory postsynaptic

currents (IPSCs). vIPSC amplitude was measured as the difference between the onset and the peak of the IPSC as described previously (Chavez et al., 2006). VGCC currents were measured as the difference between baseline and the last 20 ms of the voltage step (100 ms).

Paired recordings

Paired RBC-AII or RBC-A17 recordings were performed in retinal slices from normally-reared P10-P13 mice to evaluate the function of synaptic connections at RBC-AII and RBC-A17 synapse. Depolarizing voltage steps (from -60 to -10 mV; 100 ms) were used to elicit glutamate release from the presynaptic RBC onto postsynaptic AII or A17 amacrine cells.

3.4 Statistics

All values are presented as mean ± SEM. The number of cells and animals, as well as the statistical test used for each experiment, is specified in the figure legends and **Supplementary Table 1**. Statistical analyses were performed using Origin Pro 2018 (v9.5.1.195, OriginLab). Outliers were identified using the ROUT test (with 1% confidence level; Graphpad Prism). The Shapiro-Wilk test was used to assess normality of the datasets. For parametric data, two-group comparisons were performed using a paired or unpaired t-test, and comparisons between more than two groups were performed using one-way ANOVA or repeated-measures ANOVA, followed by a Tukey post-hoc test. For non-parametric data, two-group comparisons were performed using the Mann-Whitney test or paired Wilcoxon rank test, while comparisons between more than two groups were performed using Kruskal-Wallis ANOVA (KWANOVA), followed by the Dunn's post-hoc test, or Friedman test for repeated measures, followed by the Wilcoxon-Nemenyi-McDonald-Thompson (WNMT) post-hoc test. Cumulative distributions were compared using the Kolmogorov-Smirnov test. Statistical significance is indicated by asterisks (*$p < 0.05$; **$p < 0.01$; ***$p < 0.001$), while non-significance ($p > 0.05$) is not indicated.

4 RESULTS

The main objective of this thesis was to gain a better understanding of the contribution of AMPA and NMDA receptors to synaptic transmission at the RBC dyad synapse during the period surrounding eye opening. To achieve these goals, we performed electrophysiological recordings in acute retinal slices obtained from normally reared (NR) mice of two different age groups: P10-P13 (before eye opening) and P20-P40 (after eye opening). Additionally, we aimed to investigate how visual experience, i.e., light-driven synaptic activity at the time of the eye opening, influences the development of the essential features of this synapse, which play a pivotal role mediating scotopic vision in mammals. To evaluate this, we performed experiments in dark-reared mice at P20-P40 to study the impact of visual deprivation on synapse development.

Effects of age and dark-rearing on AMPAR-mediated synaptic transmission onto AII amacrine cells

First, we evaluated mEPSCs at the developing RBC-AII synapse by single cell voltage-clamp recordings on visually identified AII ACs (V_{hold}= -60 mV; See methods). Sample traces obtained in NR P10-P13 (N=8 cells /6 animals), P20-P40 (N=8 cells/6 animals), and DR (N=9 cells/7 animals) mice are shown in **Figure 5A**. Following eye opening the cumulative distribution of mEPSCs inter-event intervals (IEI; **Figure 5B**) exhibited a significant shift towards shorter times (P<0.0001, KS test), indicating an increase in mEPSCs frequency (P=0.013, one-way ANOVA). In contrast, the cumulative distributions of mEPSCs amplitudes (**Figure 5C**) were shifted to smaller values (P=0.0004, KS test), indicating a decrease in the mean mEPSCs amplitude after eye opening (P=0.0004, one-way ANOVA).

Several factors can contribute to the shape of excitatory postsynaptic currents. To further investigate the postsynaptic changes that occur during this period, we analyzed the kinetic properties of AMPAR-mediated mEPSCs. Scaled average waveforms, generated from ~150 events per cell, are shown in **Figure 5D** for the three groups studied. The analysis (**Figure 5E**) revealed a significant

increase in the rise (P=0.0003, one-way ANOVA), decay (P=0.004, one-way ANOVA), and half-width times (P=0.004, KWANOVA) after eye opening.

If these developmental changes required visual experience at the time of the eye opening, then, dark-rearing should prevent them. Contrary to this prediction, following eye opening, the shift in IEI cumulative distribution (P<0.0001, KS test) and the increment in mEPSCs mean frequency (P<0.0001, one-way ANOVA) were still observed in DR mice. However, compared to NR P20-P40 group, this increase in synaptic activity is exacerbated, resulting in cumulative distributions shifted toward shorter IEI (P<0.0001, KS test) and a higher mEPSCs mean frequency (P<0.0001, one-way ANOVA, Figure 5B). Although the presynaptic neurotransmitter release is enhanced in DR mice, the cumulative distribution and mean mEPSCs amplitudes remained unchanged compared to both, P10-P13 (P=0.09, KS test; P=0.059, one-way ANOVA, respectively) and P20-P40 groups (P=0.25, KS test; P=0.077, one-way ANOVA, respectively, **Figure 5C**), suggesting that the decrease in mEPSC amplitude observed in NR mice following eye opening might be delayed in DR mice. Further analysis showed that the slowdown in the kinetic properties of AMPARs following eye opening was unaffected in DR mice and was comparable to NR P20-P40 mice, except for the rise time, which showed a slight but significant increase (P=0.04, one-way ANOVA, **Figure 5E**).

Altogether, these results suggest that pre- and post-synaptic modifications of AMPAR-mediated inputs are taking place at the RBC-AII synapse during the period of eye opening. Additionally, our findings indicate that DR significantly exacerbate presynaptic changes but does not alter the postsynaptic element at RBC-AII synapse.

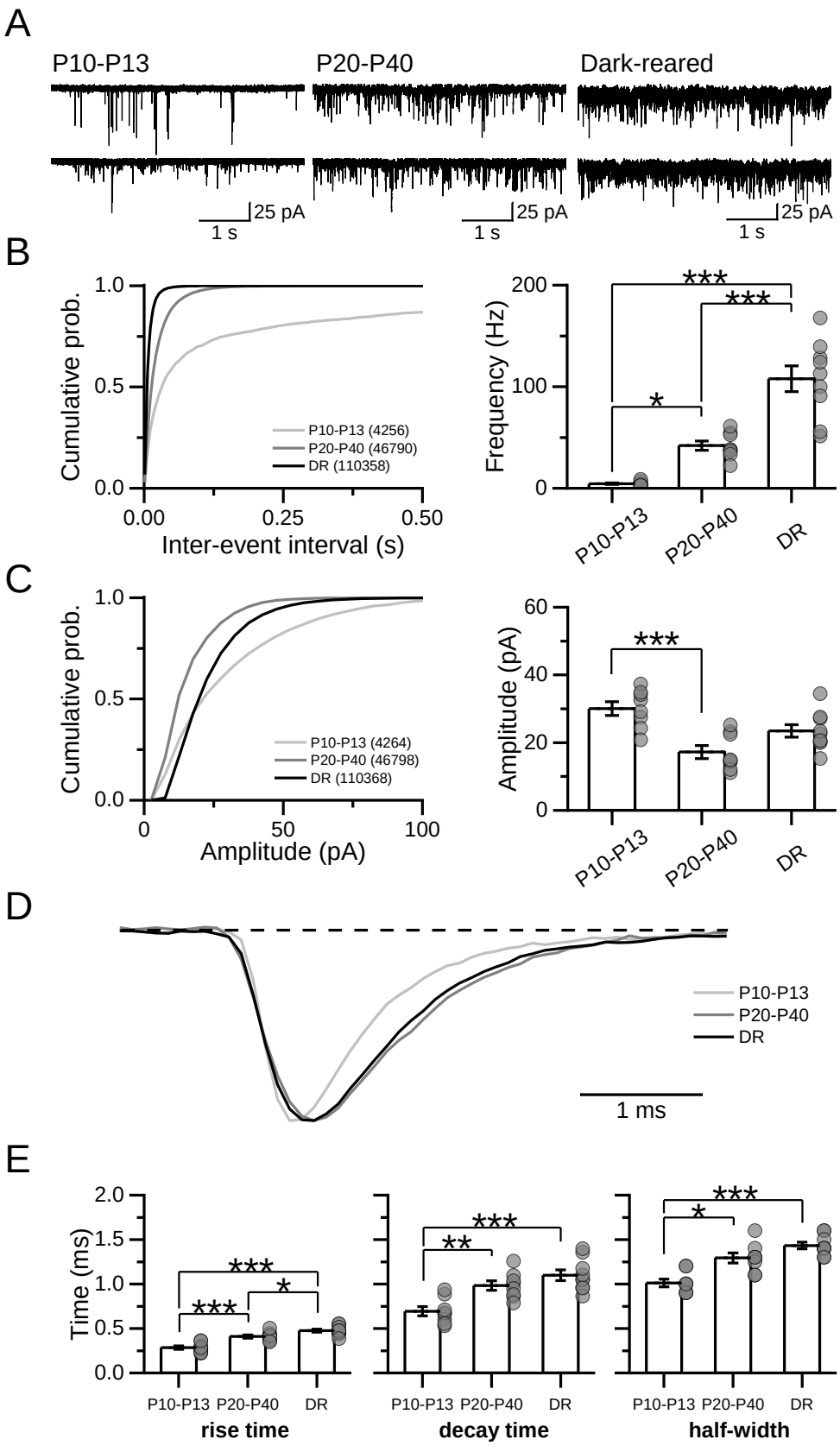
A
P10-P13
P20-P40
Dark-reared
25 pA
1 s
B
Cumulative prob.
Inter-event interval (s)
P10-P13 (4256)
P20-P40 (46790)
DR (110358)
Frequency (Hz)
P10-P13
P20-P40
DR
C
Cumulative prob.
Amplitude (pA)
P10-P13 (4264)
P20-P40 (46798)
DR (110368)
Amplitude (pA)
D
P10-P13
P20-P40
DR
1 ms
E
Time (ms)
rise time
decay time
half-width

Figure 5. Effects of eye opening and dark-rearing on AMPAR-mEPSCs and kinetics in AII ACs.

(A) Representative traces of AMPAR-mEPSCs recorded at -60 mV in AII amacrine cells from P10-P13 (left), P20-P40 (middle) normally-reared, and P20-P40 dark-reared mice (right). **(B)** Cumulative distributions of mEPSCs inter-event interval times (left) and average mEPSC frequency (right) show an increment following eye opening, enhanced by visual deprivation **(C)** Cumulative distributions (left) and average mEPSC amplitude (right) showed a decrease following eye opening, unaltered by visual deprivation. The number of events detected is indicated on the cumulative plots. **(D)** Averaged scaled waveforms from mEPSCs recorded in AII amacrine cells from P10-P13 (light gray), P20-P40 (gray) normally-reared and P20-P40 (black) dark-reared mice. Averages were generated from ~150 events per cell. Only events with monophasic waveforms, which could be clearly discriminated from the background noise, were considered. **(E)** Average rise, decay and half-width times increased after eye opening and were not altered by visual deprivation. N=cells/animals. P10-P13: n=8/6, P20-P40: n=8/6, DR: n=9/7. Experiments were performed in the continuous presence of strychnine (3 µM), SR95531 (10 µM), TPMPA (50 µM), APV (25 µM) and TTX (0.5 µM). Data are presented as mean ± SEM. *p<0.05, **p < 0.01, *** p< 0.001.

Functional properties of AMPARs in AII amacrine cells across retinal development

Presynaptic changes can be explained by the ongoing ribbon synapse stabilization prior to eye opening (Okawa et al., 2019), while postsynaptic changes in the amplitude and the slowdown in the kinetic properties of AMPAR-mEPSCs might result from a switch in the subunit composition of AMPARs as it has been previously reported in other areas of the CNS (Kumar et al., 2002; Blair et al., 2013). To elucidate the mechanisms underlying the refinement in AMPAR-mediated synaptic transmission during postnatal development, we evaluated the functional properties of AMPARs expressed in AII ACs. Currents mediated by CP-AMPARs are blocked at depolarized membrane potentials by endogenous polyamines giving rise to inwardly rectifying current-voltage (I-V) relationships (Bowie and Mayer, 1995; Donevan and Rogawski, 1995; Koh et al., 1995). Thus, we took advantage of this property, and evaluated the inward rectification of AMPAR-mediated currents (I_{AMPAR}) elicited at different holding potentials (-60 mV to +40 mV, 20 mV step increments) by a exogenous puff (pressure-induced focal release) application of glutamate (500 μM, 25 ms, 6 PSI) onto AII ACs from NR P10-P13, P20-P40, and DR mice without (-) or with (+) spermine (250 μM) in the intracellular solution (**Figure 6A).** As shown in **Figure 6B and C**, before and after eye opening, AMPAR I-V relationships displayed a strong inward rectification at depolarized voltages, resulting in a lower rectification index (RI) compared to I_{AMPA} recorded in the absence of spermine (P10-P13: Spermine (-) N=6 cells/4 animals; (+) N=6 cells/5 animals, P<0.0001; P20-P40: (-) N=4 cells/4 animals; (+) N=5 cells/4 animals, P=0.0002, unpaired *t* test), indicating that CP-AMPARs are expressed prior eye opening. Furthermore, AMPAR I-V relationships showed a similar RI in DR mice compared to P20-P40 mice (DR: N=4 cells/4 animals, P=0.96, unpaired *t* test), suggesting that CP-AMPARs developmental expression do not depend on visual experience.

These results suggest that CP-AMPARs are functionally expressed in AII ACs prior to eye opening, which is consistent with earlier findings in the rat retina (Osswald et al., 2007). However, Osswald et al. (2007) reported a reduction in the sensitivity to CP-AMPAR channel blockers such as IEM1460 and philanthotoxin (PhTx) following eye opening. In contrast, we did not observe this

phenomenon in our recordings using intracellular spermine. Therefore, to investigate this difference, we evaluated the sensitivity of AMPARs expressed in AII ACs from P10-P13 and P20-P40 NR mice to IEM1460, a specific open-channel blocker of CP-AMPARs (Magazanik et al., 1997; Twomey et al., 2018; Figure 7). We recorded I_{AMPAR} (V_{hold}=-60 mV) evoked by a puff of AMPA (100 μM, 25 ms) before and after bath application of IEM1460 (25 μM, for 10 min). IEM1460 led to a significant reduction in both the peak amplitude (**Figure 7B**) and charge (Q; **Figure 7C**) of I_{AMPAR} before (Amplitude: P=0.012; Charge: P=0.04, N=4 cells/3 animals, paired *t* test) and after eye opening (Amplitude: P=0.012; Charge: P=0.005, N=5 cells/4 animals, paired *t* test). Moreover, the percentage of block produced by IEM1460 was similar (~70%) between both groups (P=0.72, unpaired *t* test, **Figure 7D**), indicating that the sensitivity to IEM1460 remain unchanged during AII ACs development.

While the previous experiments provide strong evidence that CP-AMPARs are functionally expressed in AII ACs at early stages of retinal development, it remains unclear whether their contribution to synaptic transmission changes over the developmental time windows examined in this study. To further investigate this possibility, we recorded pharmacologically isolated AMPAR-mediated mEPSCs in P10-P13 (N=8 cells/6 animals) and P20-P40 (N=7 cells/5 animals) NR mice (**Figure 8**), before and after bath application of IEM1460 (25 μM, for 10 min). Before eye opening (**Figure 8A-B**), the cumulative distribution of IEI (P=0.30, KS test) and the mEPSCs mean frequency (P=0.15, paired *t* test) were unchanged, whereas both the cumulative distribution (P=0.01, KS test) and the mEPSCs mean amplitude (P=0.002, paired *t* test) were significantly reduced. Interestingly, after eye opening (**Figure 8D**), the cumulative distribution of IEI was pronouncedly shifted toward longer event intervals (P<0.0001, KS test), indicating a decrease in the mEPSCs mean frequency (P=0.02, Wilcoxon rank test), while the cumulative distribution (P<0.0001, KS test) and the mEPSCs mean amplitude (P=0.002, paired *t* test) were also strongly reduced. Although, the percentage of block induced by IEM1460 on mEPSCs amplitudes did not differ between groups (P=0.40, unpaired t-test, **Figure 8E**), it was lower (~50%) than the block observed by direct activation of AMPARs by puff application (**Figure 7D**, ~70%). To investigate this discrepancy, histograms of mEPSCs amplitudes were constructed

(**Supplementary Figure 1**). IEM1460 treatment shifted the distribution in both age groups (P10-P13 and P20-P40), causing it to overlap with the distribution of electrical noise. This observation suggests that a proportion of mEPSCs events with small amplitude are being masked by the electrical noise in the presence of IEM1460, resulting in the under-sampling of mEPSCs events. This could explain the discrepancy observed between the percentage of block on mEPSCs and I_{AMPA} experiments, and the observed decrease in mEPSCs frequency (**Figure 8D**). Altogether, these results demonstrate that CP-AMPARs are functionally expressed in AII ACs before eye opening. Moreover, they indicate that the sensitivity of these receptors to blockers remains unchanged during postnatal development in the mouse retina and its expression is not affected by visual deprivation.

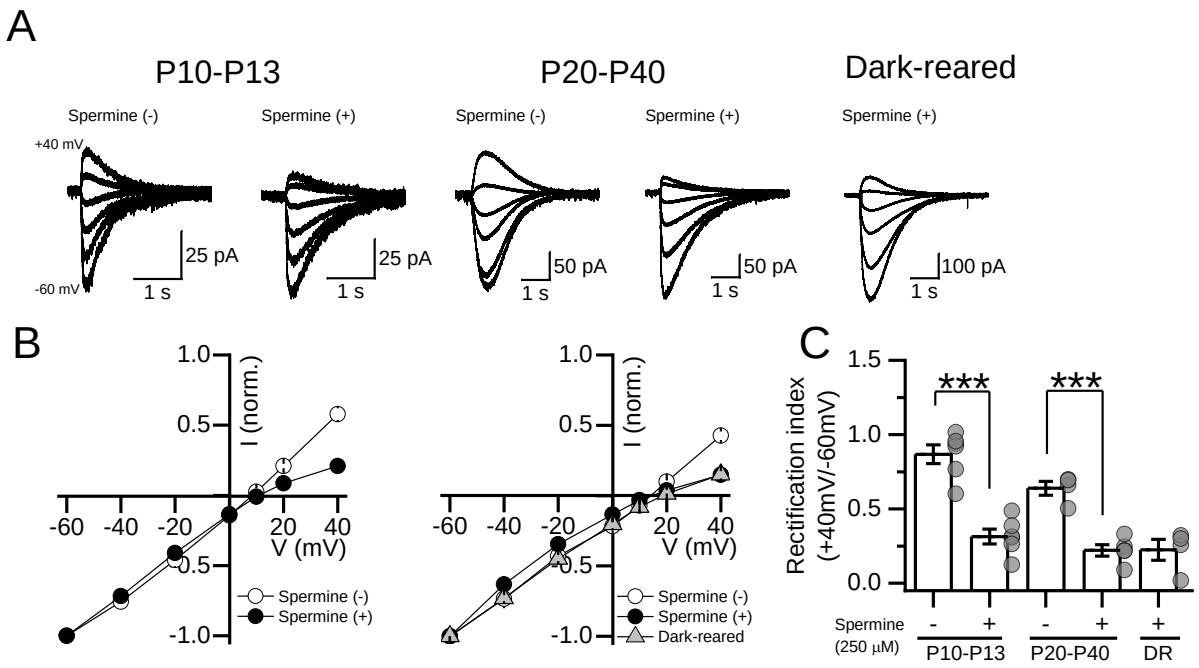

Figure 6. The polyamine block of AMPARs remains unchanged throughout AII AC maturation.

(A) Averaged AMPAR-mediated currents recorded at different holding potentials (from -60 mV to +40 mV, 20 mV steps) in P10-P13 (left), P20-P40 (middle) normal-reared, and P20-P40 dark-reared mice. AMPAR-mediated currents were elicited by puff application of glutamate (500 μM; 25 ms, 5-6 PSI) directly to AII ACs' arboreal dendrites located at the sublamina 5 in control conditions (without spermine) or including spermine (250 μM) in the intracellular solution. **(B)** Normalized current-voltage relationships (I-V) from P10-P13 (left) and P20-P40 mice (right; normal- and dark-reared). **(C)** In both, P10-P13 and P20-P40, the average rectification index (RI) exhibited a similar decrease compared with control conditions. Dark-rearing did not alter RI of AMPAR-mediated currents. The RI was calculated as the ratio of the peak amplitudes at +40 and -60 mV normalized to 1. N=cells/animals. Spermine (-): P10-P13: n=6/4, P20-P40: n=4/4. Spermine (+): P10-P13: n=6/5, P20-P40: n=5/4, DR: n=4/4. Experiments were performed in the continuous presence of strychnine (3 μM), SR95531 (10 μM), TPMPA (50 μM), APV (25 μM) and TTX (0.5 μM). Data are presented as mean ± SEM. ***p<0.001.

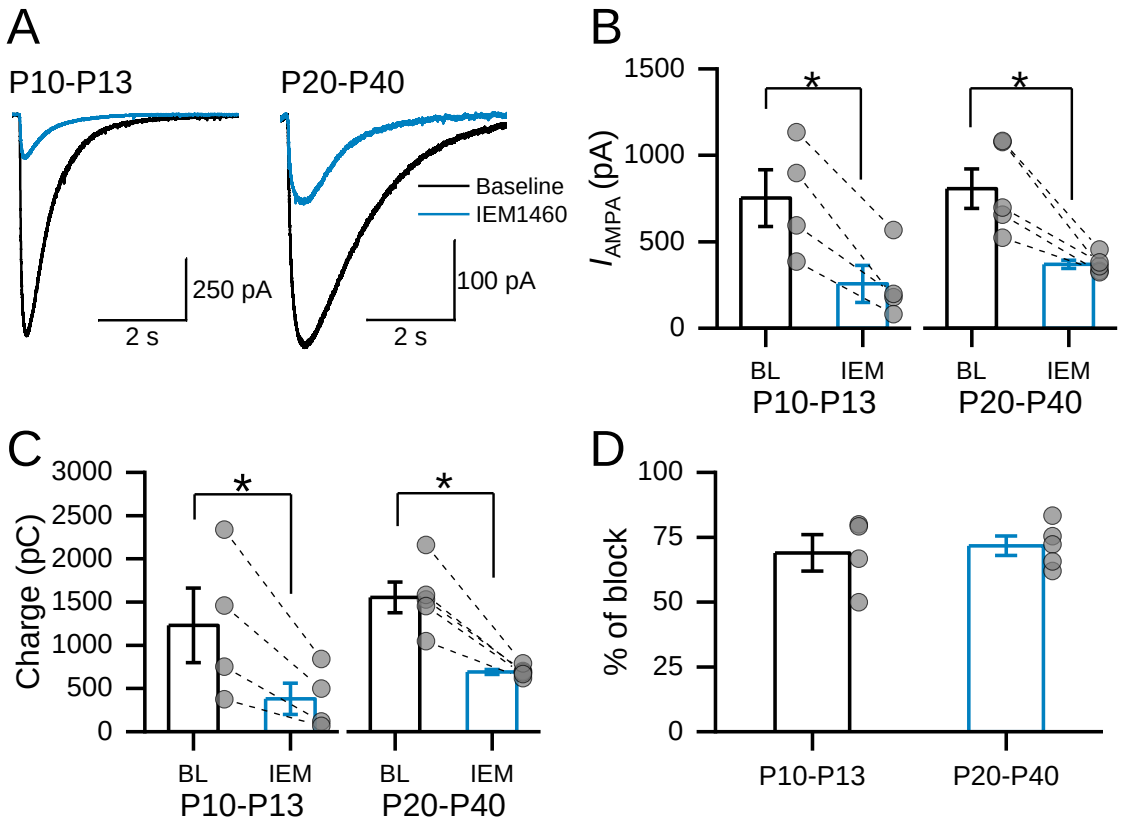

Figure 7. The functional expression of CP-AMPAR does not change during AII AC maturation.

(A) Averaged AMPA-evoked currents (I_{AMPA}) recorded at -60 mV in P10-P13 (left) and P20-P40 (right) groups before (black) and after (blue) bath application of the CP-AMPAR antagonist, IEM1460 (25 µM). I_{AMPA} was elicited by puff application of AMPA (100 µM, 25 ms, 5-6 PSI) directly to AII ACs' arboreal dendrites located at the sublamina 5 of the IPL. (**B)** The mean peak amplitude and **(C)** charge of I_{AMPA} were significantly reduced after the addition of IEM1460, with a similar percentage of block **(D)**, indicating that the functional expression of CP-AMPARs does not change during AII amacrine cell maturation. N=cells/animals. P10-P13: n=4/3, P20-P40: n=5/4. Experiments were performed in the continuous presence of strychnine (3 µM), SR95531 (10 µM), TPMPA (50 µM), APV (25 µM) and TTX (0.5 µM). Data are presented as mean ± SEM. *p<0.05.

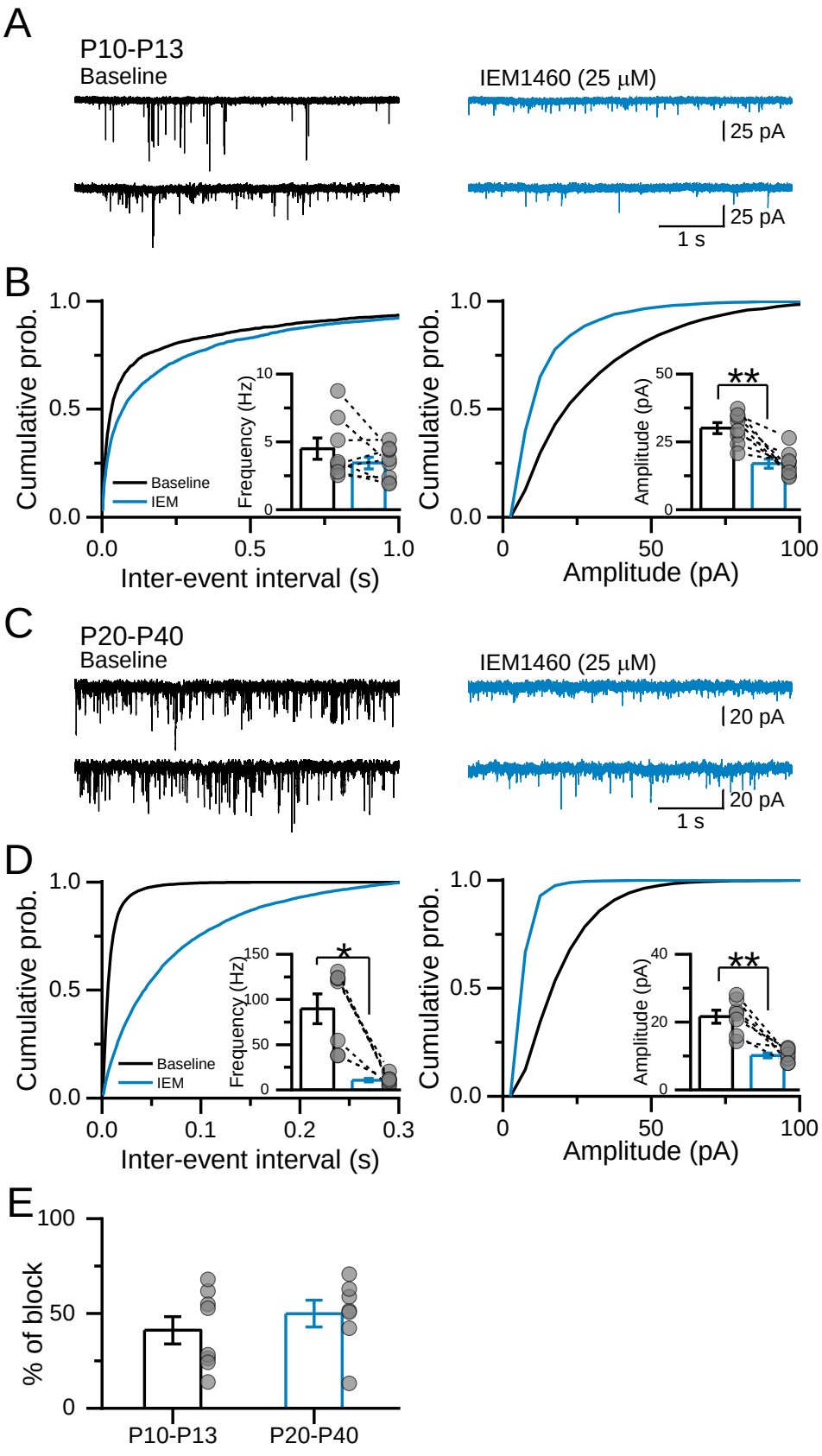
A
P10-P13
Baseline
IEM1460 (25 μM)
25 pA
25 pA
1 s
B
Cumulative prob.
Inter-event interval (s)
Baseline
IEM
Frequency (Hz)
Amplitude (pA)
**
Amplitude (pA)
C
P20-P40
Baseline
IEM1460 (25 μM)
20 pA
20 pA
1 s
D
Cumulative prob.
Inter-event interval (s)
Baseline
IEM
Frequency (Hz)
*
Amplitude (pA)
**
Amplitude (pA)
E
% of block
P10-P13
P20-P40

Figure 8. The contribution of CP-AMPARs to synaptic transmission does not change at the RBC-AII synapse during development.

(A) Representative traces of AMPAR-mEPSCs recorded at -60 mV in AII amacrine cells from P10-P13 before (left) and after (right) bath application of the CP-AMPAR antagonist, IEM1460 (25 µM). **(B) C**umulative distribution plots and the average mEPSCs frequency and amplitude show that IEM1460 decreased mEPSC amplitude before eye opening. **(C)** The same as **(A)** but for P20-P40 mice. **(D) C**umulative distribution plots and the average mEPSCs frequency and amplitude show that IEM1460 decreased both mEPSC frequency and amplitude. **(E)** The percentage of block of mEPSC amplitude was similar in both groups. N=cells/animals. P10-P13: n=8/6, P20-P40: n=7/4. Experiments were performed in the continuous presence of strychnine (3 µM), SR95531 (10 µM), TPMPA (50 µM), APV (25 µM) and TTX (0.5 µM). Data are presented as mean ± SEM. *p<0.05, **p < 0.01.

Functional properties of NMDARs in AII amacrine cells across retinal development

While it was previously believed that AII ACs did not express functional NMDA receptors (Boos et al., 1993; Menger and Wassle, 2000), recent research indicate that rat AII ACs express GluN2B-containing NMDARs localized at extra-synaptic sites (Veruki et al., 2019). This led us to study if the NMDARs subunit composition changes during development and if these changes are regulated by visual experience. First, we elicited NMDAR-mediated currents (I_{NMDA}) by puff application of NMDA (1 µM, 0.5 s) onto AII ACs (V_{Hold}=+40 mV) superfused with Mg^{2+}-free ACSF supplemented with the NMDAR co-agonist D-Serine (200 µM) and Tricine (10 mM) to chelate residual traces of Zn^{2+} (**Figure 9**). Surprisingly, we were unable to elicit I_{NMDA} in P10-P13 (N=7 cells/5 animals) or P20-P40 (N=5 cells/5 animals) mice under our experimental conditions (**Figure 9A**). It should be noted that in DR (N=6 cells/3 animals) mice, we observed a small but significant inward current compared to P10-P13 (P=0.004) or P20-P40 (P=0.03, KANOVA) mice. However, further experiments are necessary to confirm whether this inward current is mediated by the activation of NMDARs. As our results contradict the evidence of extrasynaptic NMDA expression in AII ACs, we performed control experiments under the same conditions in AII ACs from rat retina, where the expression of NMDARs was originally described (Veruki et al., 2019). As previously described, we successfully evoked I_{NMDA} in rat retina (**Figure 9B**), suggesting that NMDAR expression in AII ACs is likely to be species-specific or occur during developmental stages not assessed in this study.

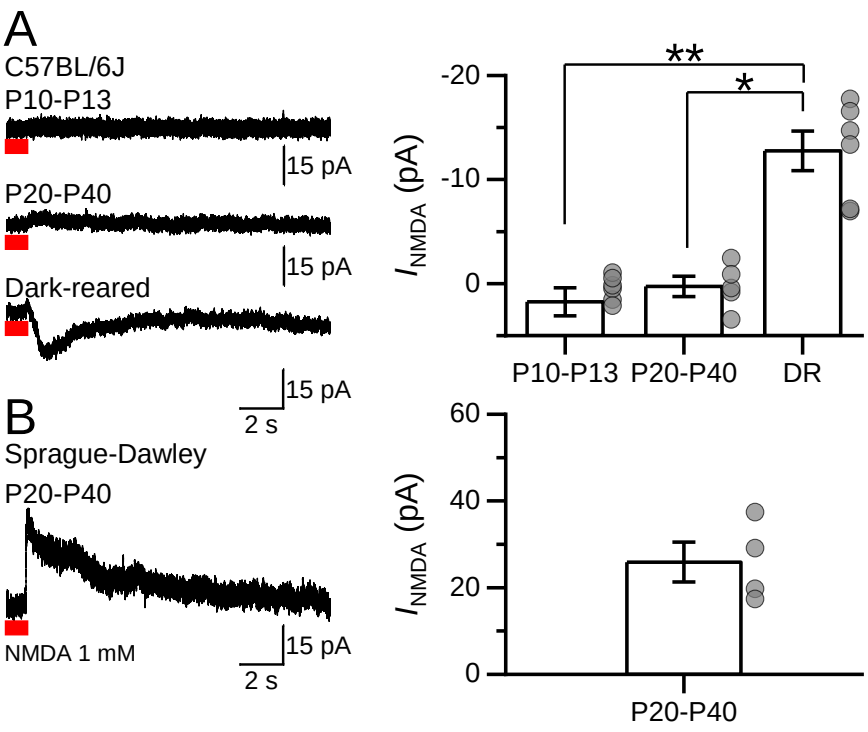

Figure 9. NMDARs are not functionally expressed in AII ACs from the mouse retina.

(A) Averaged NMDAR-mediated currents (I_{NMDA}) recorded from AII amacrine cells at +40 mV from P10-P13 (top), P20-P40 (middle) normal-reared, and P20-P40 (bottom) dark-reared mice. I_{NMDA} was elicited by a puff application of NMDA (1 mM, 1 s, 5-6 PSI) directly to AII ACs' arboreal dendrites located at the sublamina 5 of the IPL in the presence of Mg^{2+}-free ACSF supplemented with the NMDAR co-agonist D-Serine (200 µM). Puff application of NMDA failed to elicit significant I_{NMDA} in normal-reared mice from both groups. AII ACs from the dark-reared group exhibited a small but significant inward current. **(B)** Same as **(A)**, but for AII amacrine cells recorded in P20-P40 rat retinal slices. The summary plot show that, unlike AII amacrine cells from the mouse retina, puff application of NMDA in rat retinal slices evoke a significant I_{NMDA}. N=cells/animals. P10-P13: n=7/5, P20-P40: n=5/5, DR: n=6/3. Experiments were performed in the continuous presence of strychnine (3 µM), SR95531 (10 µM), TPMPA (50 µM), NBQX (10 µM) in order to isolate I_{NMDA}. Data are presented as mean ± SEM. *p<0.05, **p<0.01.

Effects of age and visual deprivation on AMPA receptor-mediated synaptic transmission onto A17 amacrine cells

Next, we performed the same type of experiment at RBC-A17 synapses. Sample traces from recordings obtained in NR P10-P13 (N=8 cells/5 animals), P20-P40 (N=8 cells/6 animals), and DR (N=7 cells/5 animals) mice are shown in **Figure 10A**. After eye opening, the cumulative distribution of IEI showed a leftward shift (P=0.002, KS test) and an increase in the mean mEPSCs frequency (P=0.037, KWANOVA, **Figure 10B**), however, the cumulative distribution (P=0.99, KS test) and mEPSCs mean amplitude remained unchanged (P=0.25, KWANOVA, **Figure 10C**). Further analysis of the kinetic of AMPAR-mEPSCs (**Figure 10D-E**) showed that the rise, decay and half-width times were unaltered (P=0.99, P=0.53, P=0.94 respectively, one-way ANOVA, **Figure 10E**).

Interestingly, when we examined whether visual experience regulates these changes in A17 ACs, we found that the leftward shift in the cumulative distribution (P=0.004, KS test) and the increase in mEPSCs frequency (P=0.013, KWANOVA, **Figure 10B**) was still observed in DR mice, but it was not enhanced compared to P20-P40 mice (P=0.91, KS test; P=1, KWANOVA, respectively). Furthermore, we found that the cumulative distribution and mEPSCs mean amplitude did not change compared to P10-P13 (P=0.20, KS test; P=0.09, one-way ANOVA, respectively) or P20-P40 groups (P=0.25, KS test; P=1, one-way ANOVA, **Figure 10C**). Accordingly, the rise, decay, and half-width times of AMPA-mediated mEPSCs were also unaffected by visual deprivation (P=0.19, P=0.11, P=0.25 respectively, one-way ANOVA, **Figure 10E**). These results suggest that presynaptic rather than postsynaptic modifications are taking place at the RBC-A17 synapse during postnatal development, and these changes are independent of visual experience.

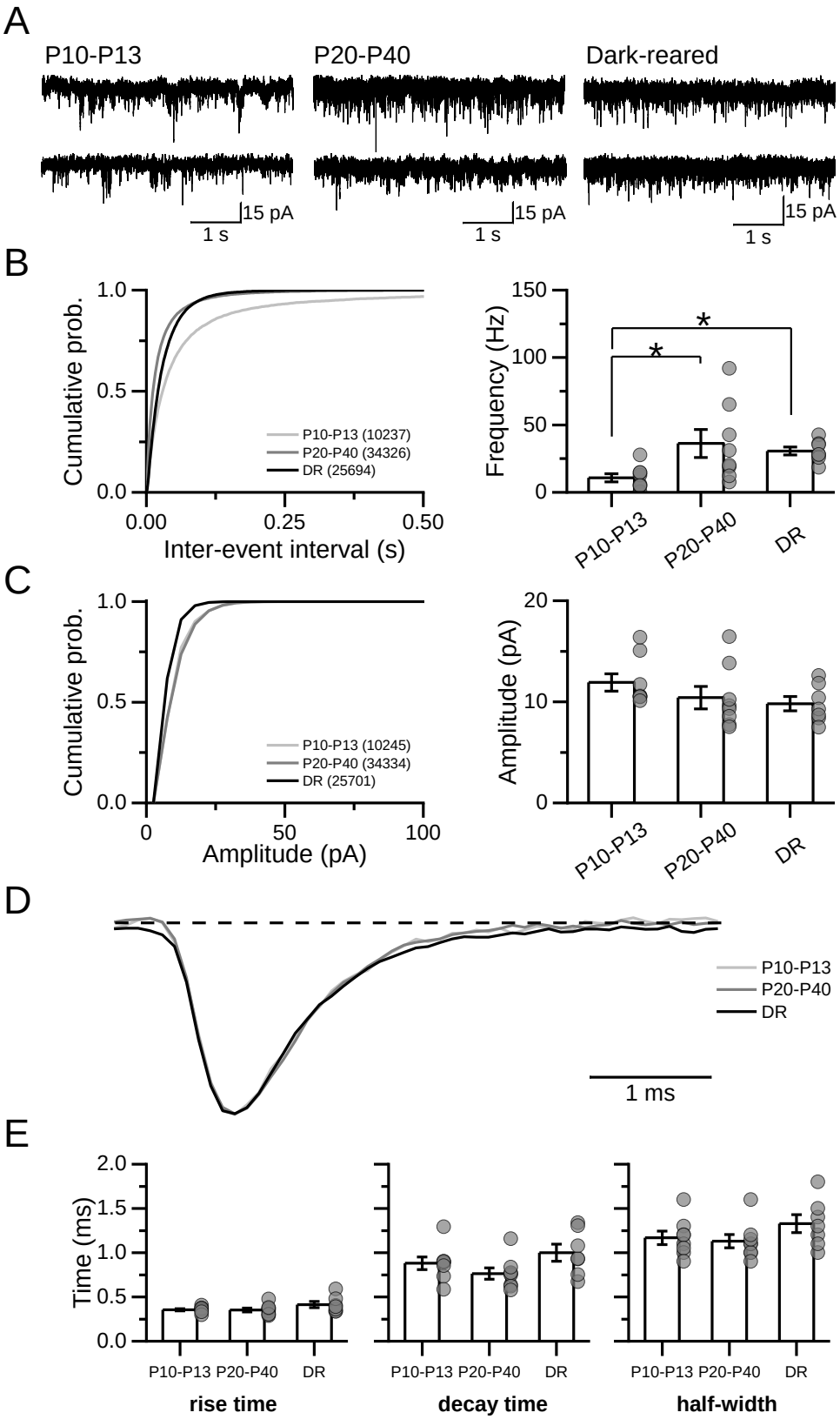
A
P10-P13
P20-P40
Dark-reared
15 pA
1 s
B
Cumulative prob.
Inter-event interval (s)
P10-P13 (10237)
P20-P40 (34326)
DR (25694)
Frequency (Hz)
P10-P13
P20-P40
DR
C
Cumulative prob.
Amplitude (pA)
P10-P13 (10245)
P20-P40 (34334)
DR (25701)
Amplitude (pA)
D
P10-P13
P20-P40
DR
1 ms
E
Time (ms)
rise time
decay time
half-width

Figure 10. Effects of eye opening and dark-rearing AMPAR-mEPSCs and kinetics in A17 ACs.

(A) Representative AMPAR-mEPSCs recorded at -60 mV in A17 amacrine cells from P10-P13 (left), P20-P40 (middle) normally-reared, and P20-P40 dark-reared mice (right). **(B)** Cumulative distributions of mEPSCs inter-event interval times (left) and average mEPSC frequency (right) showed an increase following eye opening, which remained unaffected by visual deprivation. **(C)** Cumulative distributions (left) and average mEPSC amplitude (right) exhibited no significant changes during maturation or after visual deprivation. The number of events detected is indicated on the cumulative graphs. **(D)** Averaged scaled waveforms from mEPSCs recorded at -60 mV in A17 amacrine cells from P10-P13 (light gray), P20-P40 (gray) normal-reared, and P20-P40 (black) dark-reared mice. Averages were generated from ~150 events per cell. Only events with monophasic waveforms, which could be clearly discriminated from the background noise, were considered. **(E)** Average rise, decay and half-width times showed no significant changes during A17 ACs maturation and were unaffected by visual deprivation. N=cells/animals. P10-P13: n=8/5, P20-P40: n=8/6, DR: n=7/5. Experiments were performed in the continuous presence of strychnine (3 µM), SR95531 (10 µM), TPMPA (50 µM), APV (25 µM) and TTX (0.5 µM). Data are presented as mean ± SEM. *p<0.05.

Functional properties of AMPARs in A17 amacrine cells across retinal development

Next, we assessed the properties of the AMPARs expressed in A17 ACs by analyzing the voltage-dependent blockade of CP-AMPARs by intracellular spermine in NR (P10-P13; P20-P40), and DR mice with (+) or without (-) spermine in the intracellular solution (**Figure 11A)**. Notably, AMPAR-mediated currents showed a strong inward rectification and lower RI (**Figure 11B-C**) after (**P20-P40:** Spermine (-) N=7 cells/5 animals; (+) N=8 cells/5 animals, P=0.005, unpaired *t* test), but not before the eye opening (**P10-P13:** Spermine (-) N=6 cells/5 animals; (+) N=8 cells/5 animals, P=0.84, Mann Whitney test), suggesting that these receptors might be calcium-impermeable. Additionally, visual deprivation did not affect the RI compared to P20-P40 mice (DR: N=6 cells/4 animals, P=0.68, unpaired *t* test), which indicate that the development of this feature is independent of visual experience.

Although at a first glance, these results suggest that a switch in AMPARs subunit composition from GluA2-containing calcium-impermeable receptors to GluA2-lacking calcium-permeable receptors is taking place in A17 ACs during retinal development, when we evaluated the sensitivity of AMPARs to IEM1460 (25 μM for 10 min, **Figure 12**) in P10-P13 and P20-P40 normally reared mice, we found that both, the peak amplitude (**Figure 12B**) and charge (Q; **Figure 12C**) of I_{AMPA} were reduced before (Amplitude: P=0.006; Charge: P=0.018, N=5 cells/3 animals, paired *t* test) and after eye opening (Amplitude: P=0.007; Charge: P=0.04, N=5 cells/3 animals, paired *t* test). Moreover, the percentage of block produced by IEM was similar (~75%) between both groups (P=0.75, unpaired *t* test, **Figure 12D**).

Similar results were obtained when we recorded pharmacologically isolated AMPAR-mediated mEPSCs in P10-P13 (N=6 cells/4 animals) and P20-P40 (N=5 cells/3 animals) mice (**Figure 13**), following application of IEM1460 (25 μM, for 10 min). Before eye opening, significant reductions were observed in the cumulative distribution of IEI (P<0.0001, KS test) and the mean frequency of mEPSCs (P=0.047, paired t test), as well as in the cumulative distribution (P=0.02, KS test) and mEPSCs mean amplitude (P=0.036, Wilcoxon rank test, **Figure 13A-B**). After eye opening (**Figure 13C-D**) there was

a significant decrease in the cumulative distribution of IEI (P<0.0001, KS test) and the mean frequency of mEPSCs (P=0.035, paired t test), as well as in the cumulative distribution (P<0.0001, KS test) and mean amplitude of mEPSCs (P=0.038, paired t test) in the presence of IEM1460. The percentage of block induced by IEM1460 on mEPSCs amplitudes did not differ between the groups (P=0.26, unpaired test, **Figure 13E**). However, it was considerably lower (~25%) than the block observed by direct activation of AMPARs by puff application (**Figure 12D**, ~75%). Moreover, mEPSCs amplitudes histograms in A17 ACs (**Supplementary Figure 2**) suggest that a proportion of mEPSCs events with small amplitude are being masked by electrical noise in the presence of IEM1460, leading to the under-sampling of the events. It is worth noting that the mEPSCs mean amplitude in A17 ACs, is considerably smaller (~10 pA) compared with AII ACs (~20-25 pA) at both ages tested, therefore a high proportion of the AMPAR-mediated mEPSCs were near the detection threshold. Additionally, using PhTx (1 μM), we did not observe a decrease in A17 ACs from young P10-P13 mice, as seen in AII ACs (**Supplementary figure 3**)**,** suggesting that the AMPARs expressed in both cell types have different pharmacological properties. However, it remains unclear whether AMPARs in A17 ACs are impermeable to calcium before eye opening.

If AMPARs are impermeable to calcium we expect that they contain GluA2 subunits. To fully determine this, we collaborated with Dr. William Grimes and Dr. Jeffrey Diamond (NIH, USA) and performed whole-cell voltage clamp recordings in retinas from P10-P13 and P20-P40 normally reared GluA2$^{-/-}$ mice (see methods). We analyzed the voltage-dependent blockade of AMPARs by intracellular spermine as described before (**Figure 11**). Consistent with our assumption, we found that in P10-P13 GluA2$^{-/-}$ mice, the AMPAR-mediated currents showed a strong inward rectification (**Figure 14A-B**) with a RI similar to P20-P40 WT mice and significantly lower compared to P10-P13 WT mice (WT P10-P13: N=8 cells/5 animals; GluA2$^{-/-}$ P10-P13 N=6 cells/1 animals, P=0.014, one-way ANOVA, **Figure 14C**). These results strongly suggest that AMPARs expressed in A17 ACs from WT mice contain at least one GluA2 subunit before eye opening. Deletion of GluA2 subunit render AMPARs spermine-sensitive, characteristic that resembles the observations in AMPARs in A17 ACs from mature retinas.

While the role of CP-AMPARs in A17 ACs of adult rodents have been extensively studied, to our knowledge, this is the first report on the properties of AMPARs in A17 ACs prior to eye opening. Moreover, our results suggest that although AMPARs expressed in these cells have a pharmacological profile different from what we expected, showing a mixed set of pharmacological characteristics from both CP-AMPARs (IEM1460-sensitive) and CI-AMPARs (spermine and PhTx insensitive), they indeed are composed by GluA2 subunits, thus, it is very likely that they are calcium impermeable.

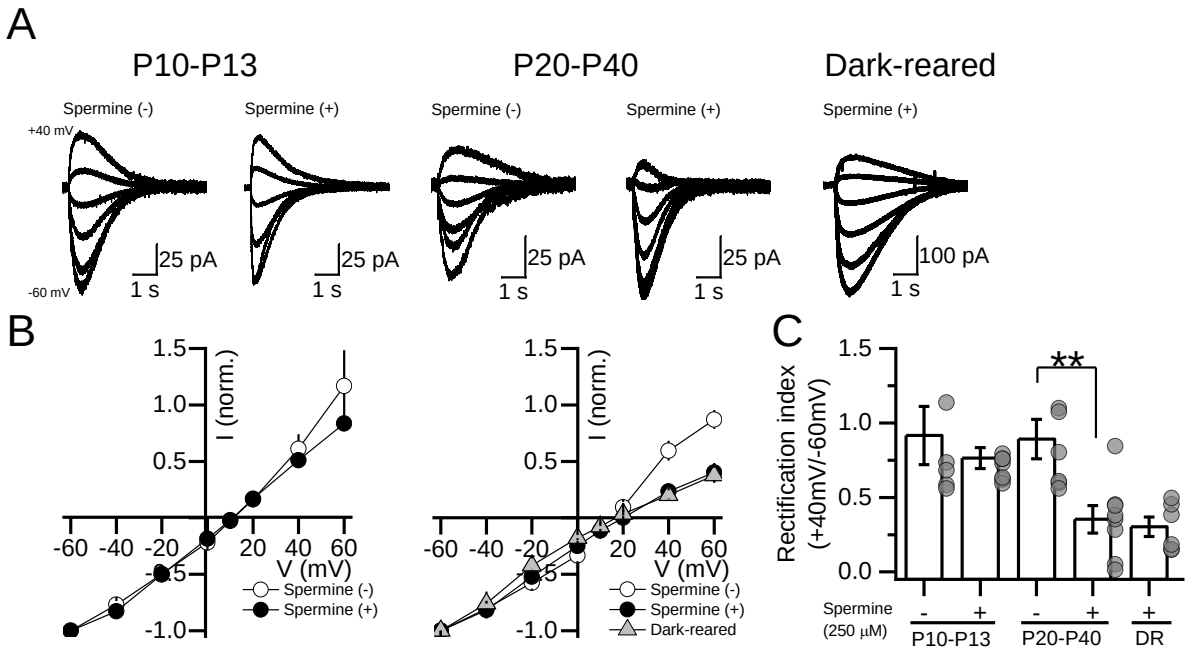

Figure 11. The polyamine block of AMPARs is developmentally regulated in A17 ACs.

(A) Averaged AMPAR-mediated currents recorded at different holding potentials (from -60 mV to +40 mV, 20 mV steps) in P10-P13 (left), P20-P40 (middle) normal-reared and, P20-P40 dark-reared mice. AMPAR-mediated currents were induced by puff application of glutamate (500 μM; 25 ms, 5-6 PSI) directly to A17 ACs' processes extended at the sublamina 5 in control conditions (without spermine) or including spermine (250 μM) in the intracellular solution. **(B)** Normalized current-voltage relationships (I-V) from P10-P13 (left) and P20-P40 (right; normal- and dark-reared). **(C)** AMPAR-mediated currents showed inward-rectification after, but not before eye opening. Visual deprivation did not alter the RI of AMPARs in A17 amacrine cells. The RI was calculated as the ratio of the peak amplitudes at +40 and -60 mV. N=cells/animals. Spermine (-): P10-P13: n=6/5, P20-P40: n=7/5. Spermine (+): P10-P13: n=8/5, P20-P40: n=8/5, DR: n=6/4. Experiments were performed in the continuous presence of strychnine (3 μM), SR95531 (10 μM), TPMPA (50 μM), APV (25 μM) and TTX (0.5 μM). Data are presented as mean ± SEM. ***p<0.001.

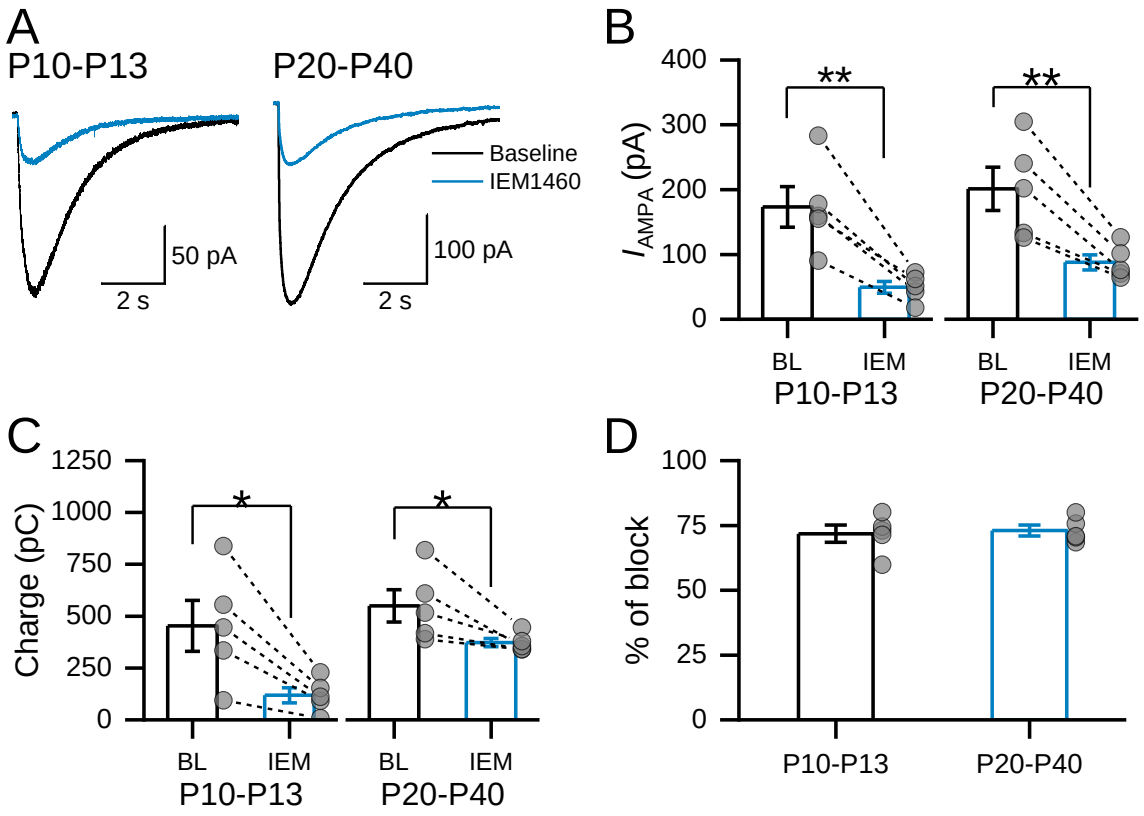

Figure 12. The functional expression of CP-AMPAR does not change during A17 AC maturation.

(A) Averaged AMPA-evoked currents (I_{AMPA}) recorded at -60 mV in P10-P13 (left) and P20-P40 (right) groups before (black) and after (blue) bath application of the CP-AMPAR antagonist, IEM1460 (25 µM). I_{AMPA} was elicited by puff application of AMPA (100 µM, 25 ms, 5-6 PSI) directly to A17 ACs' processes extended at the sublamina 5 of the IPL. **(B)** The mean peak amplitude and **(C)** charge of IAMPA were significantly reduced after the addition of IEM1460, with a similar percentage of block **(D)**, indicating that the functional expression of CP-AMPARs during A17 amacrine cell maturation. N=cells/animals. P10-P13: n=5/3, P20-P40: n=5/3. Experiments were performed in the continuous presence of strychnine (3 µM), SR95531 (10 µM), TPMPA (50 µM), APV (25 µM) and TTX (0.5 µM). Data are presented as mean ± SEM. *p<0.05, **p<0.01.

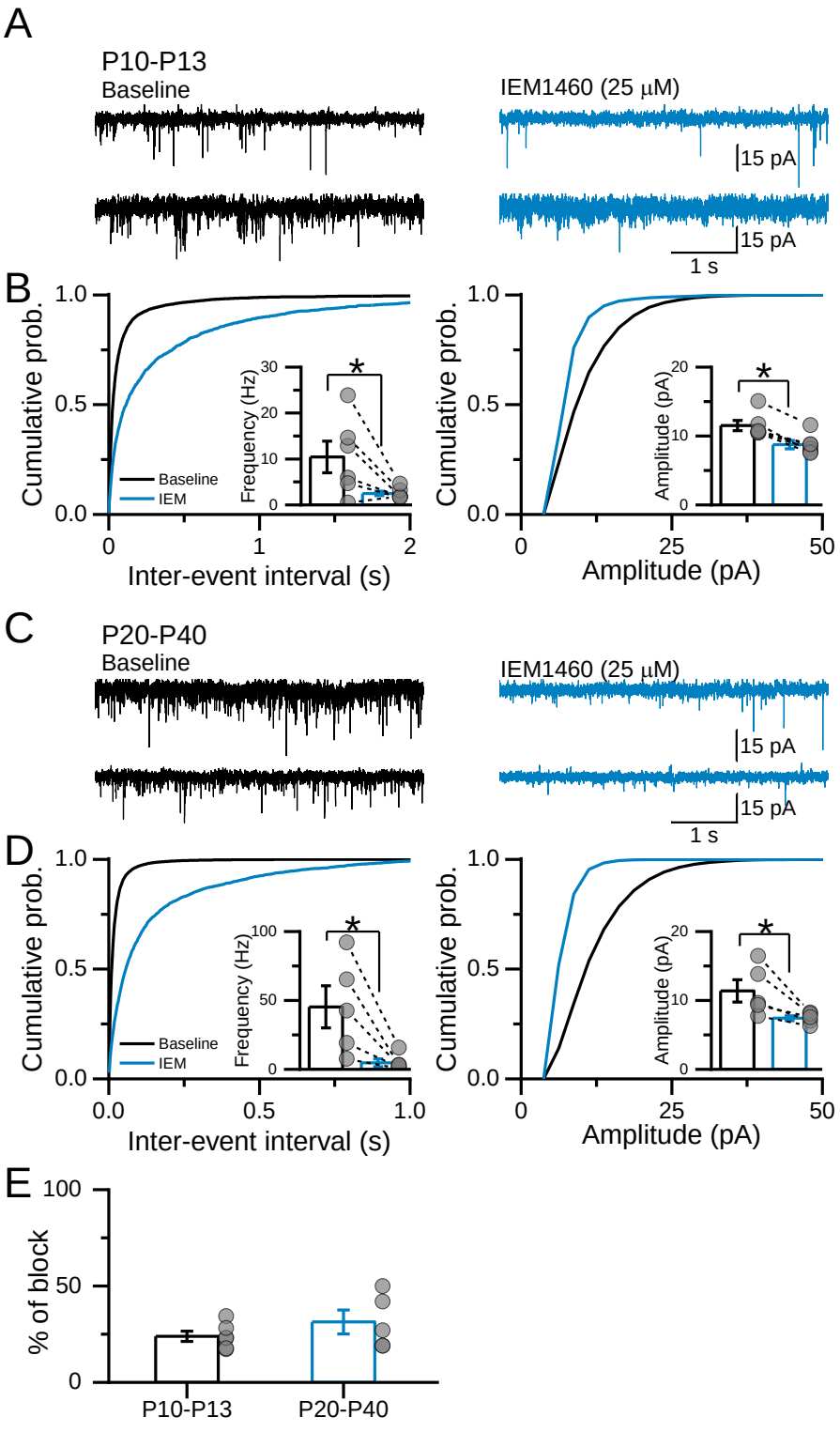
A
P10-P13
Baseline
IEM1460 (25 μM)
15 pA
15 pA
1 s
B
Cumulative prob.
1.0
0.5
0.0
0
1
2
Inter-event interval (s)
Baseline
IEM
Frequency (Hz)
30
20
10
0
*
Cumulative prob.
1.0
0.5
0.0
0
25
50
Amplitude (pA)
Amplitude (pA)
20
10
0
*
C
P20-P40
Baseline
IEM1460 (25 μM)
15 pA
15 pA
1 s
D
Cumulative prob.
1.0
0.5
0.0
0.0
0.5
1.0
Inter-event interval (s)
Baseline
IEM
Frequency (Hz)
100
50
0
*
Cumulative prob.
1.0
0.5
0.0
0
25
50
Amplitude (pA)
Amplitude (pA)
20
10
0
*
E
% of block
100
50
0
P10-P13
P20-P40

Figure 13. The contribution of CP-AMPARs to synaptic transmission does not change at the RBC-A17 synapse during development.

(A) Representative AMPAR-mEPSCs recorded at -60 mV in A17 amacrine cells from P10-P13 before (left) and after (right) bath application of the CP-AMPAR channel blocker, IEM1460 (25 µM). **(B)** Cumulative distribution plots and the average mEPSCs frequency and amplitude show that bath application of IEM1460 decreased both the mEPSC frequency and amplitude before eye opening **(C)** The same as **(A)** but for P20-P40 mice. **(D)** Cumulative distribution plots and the average mEPSCs frequency and amplitude show that IEM1460 decreased both mEPSC frequency and amplitude after eye opening. The percentage of block of mEPSC amplitude was similar in both groups. N=cells/animals. P10-P13: n=6/4, P20-P40: n=5/3. Experiments were performed in the continuous presence of strychnine (3 µM), SR95531 (10 µM), TPMPA (50 µM), APV (25 µM) and TTX (0.5 µM). Data are presented as mean ± SEM. *$p<0.05$, **$p < 0.01$.

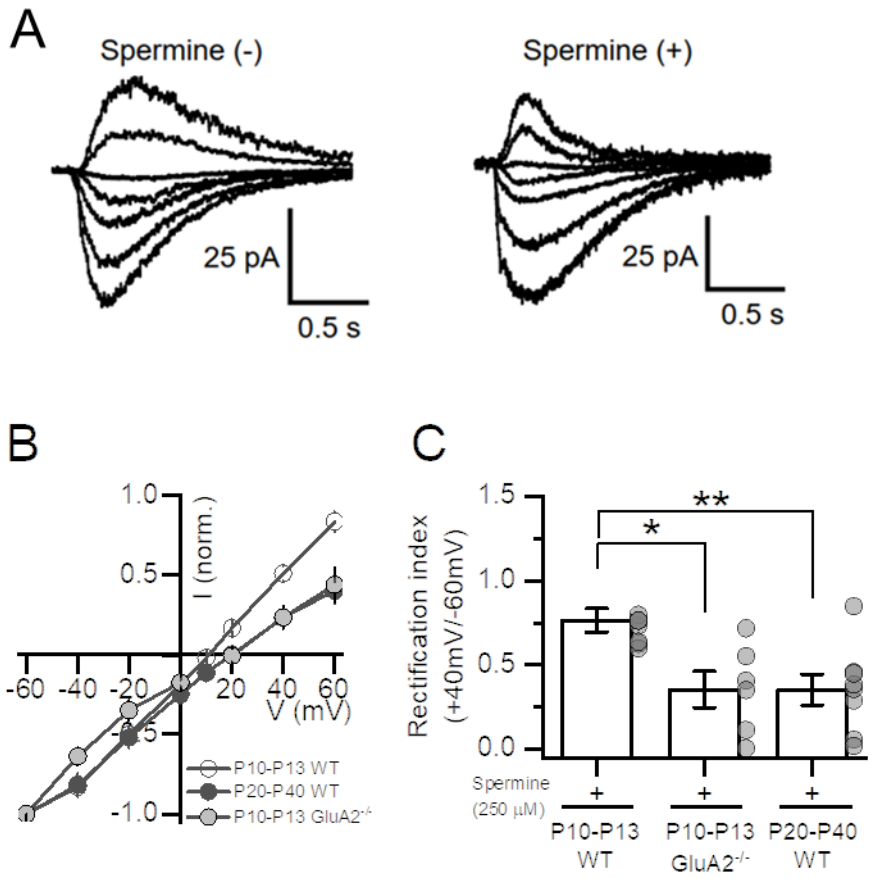

Figure 14. AMPAR-mediated currents are blocked by spermine in A17 amacrine cells from P10-P13 GluA2 $^{-/-}$ mice.

(A) Averaged AMPAR-mediated currents recorded at different holding potentials (from -60 mV to +60 mV, 20 mV steps) in P10-P13 GluA2$^{-/-}$ mice. Currents were elicited by puff application of glutamate (500 µM; 25 ms, 5-6 PSI) directly to A17 ACs' processes extended at the sublamina 5 including spermine (250 µM) in the intracellular solution. **(B)** Comparison of the normalized I-V relationships obtained from P10-P13 WT, P20-P40 WT (**Figure 11**) with P10-P13 GluA2$^{-/-}$ mice. **(C)** The averaged rectification index (RI) of AMPAR-mediated currents recorded in P10-P13 GluA2$^{-/-}$ was significantly lower than in P10-P13 WT mice and similar to P20-P40 WT mice. N=cells/animals. P10-P13 (WT): 8/5, P10-P13 (GluA2$^{-/-}$): n=6/1, P20-P40: n=8/5. Experiments were performed in the continuous presence of strychnine (3 µM), SR95531 (10 µM), TPMPA (50 µM), APV (25 µM) and TTX (0.5 µM). Data are presented as mean ± SEM. **p<0.01.

Reciprocal feedback inhibition at RBC axon terminals is absent before eye opening

To test whether AMPARs expressed in A17 ACs before eye opening were impermeable to calcium, we examined the reciprocal GABAergic feedback inhibition, which requires CP-AMPAR activation (Chavez et al., 2006). Reciprocal feedback inhibition was elicited by depolarization of voltage-clamped RBC (V_{Hold}=-60 mV) by a step pulse of 50 mV (100 ms) that triggered an inward Ca^{2+}-current (I_{Ca}^{2+}) upon which a fast voltage-evoked IPSC is superimposed (vIPSC, black arrow, **Figure 15A**). Recordings were performed in the presence of strychnine (3 µM) and TTX (0.5 µM) to block the glycinergic feedback and the TTX-sensitive non-reciprocal GABAergic feedback. Remarkably, before eye opening, the vIPSC was absent (P10-P13: N=19 cells/15 animals; P20-P40: N=35 cells/21 animals, P<0.0001, Mann-Whitney test, **Figure 15B**), and I_{Ca}^{2+} was slightly but significantly reduced (P<0.0001, Mann-Whitney test, **Figure 15B**) compared to P20-P40 mice. Additionally, increasing the depolarizing step pulse amplitude (from -90 to 50 mV, 20 mV steps, 100 ms) failed to induce a significant vIPSC prior to eye opening (**Figure 15C**). These results strongly support our hypothesis that, despite the atypical pharmacology of AMPARs expressed in A17 ACs, they are indeed calcium impermeable, a characteristic that might underlie the absence of the reciprocal feedback. If this is true, we expect that deletion of the GluA2 subunit should increase calcium permeability and potentially promote the reciprocal GABAergic feedback onto RBCs before eye opening.

Accordingly, analysis of the GABAergic reciprocal feedback in RBCs from P10-P13 GluA2$^{-/-}$ (**Figure 16**) mice revealed that ~41% (13 out of 32 cells) of the recorded RBCs exhibited vIPSC greater than 5 pA. Furthermore, the mean amplitude of the vIPSC was comparable to that of P20-P40 GluA2$^{-/-}$ mice (P10-P13: N=32 cells/5 animals; P20-P40: N=21 cells/3 animals, P=0.12, Mann-Whitney test, **Figure 16B**). In addition, the I_{Ca}^{2+} was reduced compared to P20-P40 GluA2$^{-/-}$ (P=0.0005, Mann-Whitney test, **Figure 16C**), like our findings in WT mice (**Figure 15B**).

It is worth noting that the establishment of the GABAergic reciprocal feedback might not solely rely on the maturation of AMPARs. We previously demonstrated that the absence of reciprocal

feedback cannot be attributed to the reduced I_{Ca}^{2+} observed prior to eye opening (**Supplementary Figure 4**). Additionally, RBC-AII and RBC-A17 pairs are synaptically coupled (**Supplementary Figure 5**). In line with this, we observed that glutamate and GABA release as well as GABARs in RBC-A17 synapse, are functional in early development (**Supplementary Figure 6 and 7**). Therefore, these results strongly suggest that the maturation of AMPARs plays a major role in establishing the reciprocal GABAergic feedback.

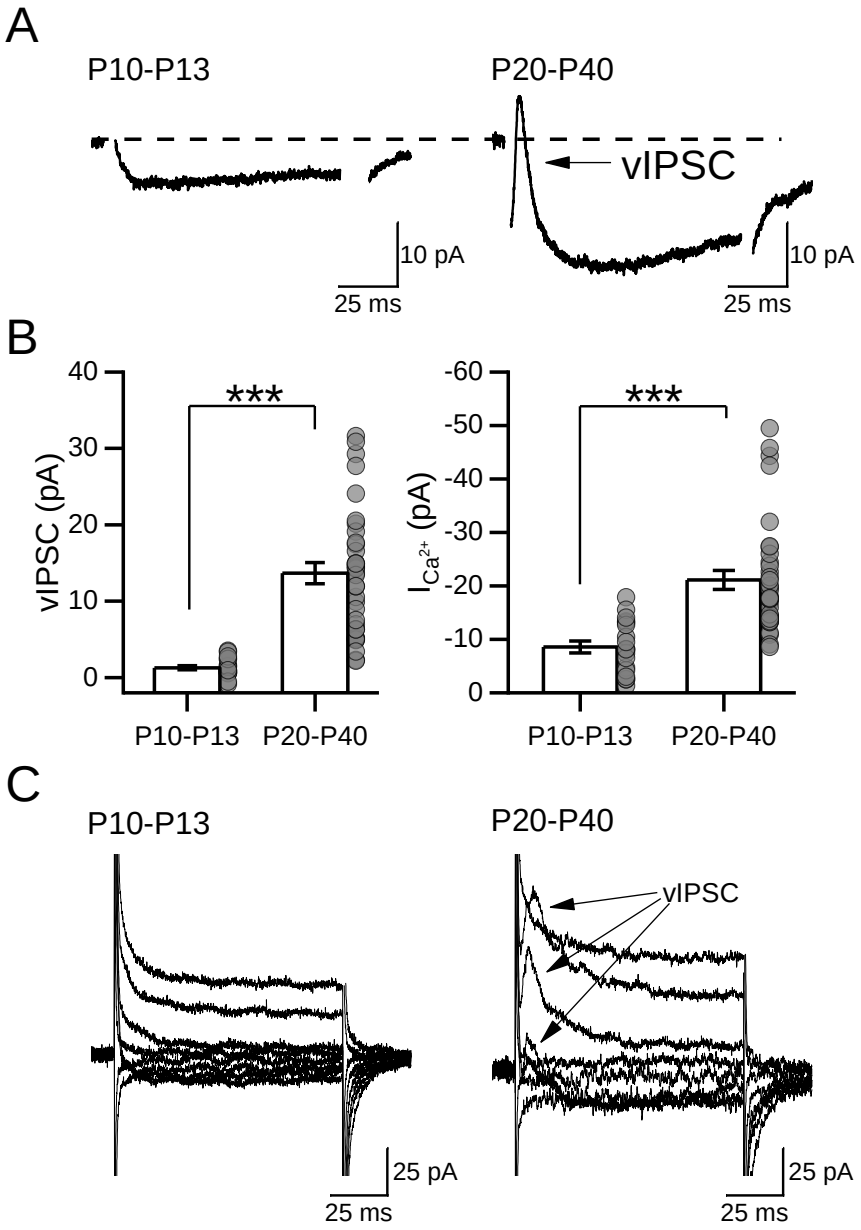

Figure 15. Reciprocal feedback inhibition onto RBCs is absent before eye opening.

(A) Averaged vIPSC currents recorded in P10-P13 and P20-P40 mice. Depolarization of the RBC (100 ms step from -60 to -10 mV) resulted in an inward Ca^{2+} current upon which was superimposed a fast IPSC (black arrow). **(B)** The mean vIPSC amplitude (left) and $I_{Ca^{2+}}$ amplitude (right) increased after the eye opening. N=cells/animals. P10-P13: n=19/15, P20-P40: n=35/21. **(C)** Incrementing the depolarization of RBC (-90 to 50 mV, 20 mV steps) increases reciprocal vIPSC after, but not before, eye opening. Arrows indicate the vIPSC feedback response. Experiments were performed in the presence of strychnine (3 µM) and TTX (0.5 µM) in order to block glycinergic and non-reciprocal GABAergic feedback inputs to RBCs, respectively. Data are presented as mean ± SEM. ***p<0.001.

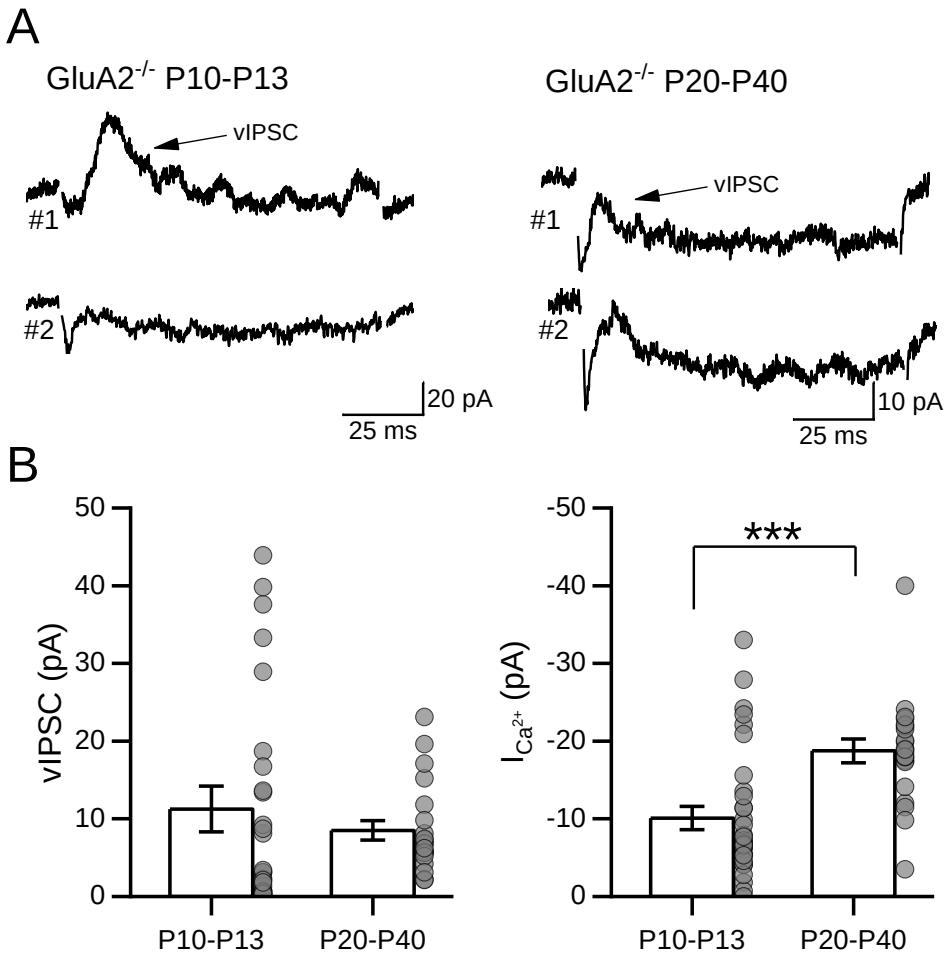

Figure 16. Reciprocal feedback inhibition onto RBCs is functional before eye opening in GluA2$^{-/-}$ mice.

(A) Averaged vIPSC currents recorded in P10-P13 (left) and P20-P40 (right) GluA2$^{-/-}$ mice. The vIPSC is indicated with a black arrow. **(B)** The mean vIPSC amplitude (left) was similar in both groups, while the I_{Ca}^{2+} showed a significant increase after eye opening, similar to WT mice (Fig. 15). N=cells/animals. P10-P13 GluA2$^{-/-}$: 32/5, P20-P40 GluA2$^{-/-3}$: 21/3. Experiments were performed in the presence of strychnine (3 µM) and TTX (0.5 µM) in order to block glycinergic and non-reciprocal GABAergic feedback inputs to RBCs, respectively. Data are presented as mean ± SEM. ***P<0.001.

Reciprocal feedback inhibition at RBC axon terminals is reduced by visual deprivation

As reciprocal feedback is absent prior to eye opening, we wonder if visual experience is required for its development. To determine this, we recorded reciprocal GABAergic feedback from P20-P40 mice dark-reared from P0 (**Figure 17A**). We found that only ~42% of RBCs (25 out of 59) expressed a vIPSC greater than 5 pA, whereas ~85% (23 out of 27) of RBCs expressed significant vIPSC in age-matched normally reared mice. vIPSC mean amplitude was significantly reduced (NR: N=27 cells/5 animals; DR: N=59 cells/20 animals, P<0.0001, Mann-Whitney test, **Figure 17B**), whereas the $I_{Ca^{2+}}$ slightly, but significantly increased in DR mice (NR: 23 cells/5 animals; DR: 59 cells/20 animals, P=0.0009, Mann-Whitney test, **Figure 17B**). To determine whether the reduction in the synaptic strength of the vIPSC can be reversed, a subgroup of DR mice was exposed to light (60-80 lux, 1h) for one (Light-exposure 1) or two (Light-exposure 2) consecutive days (**Figure 18,** see methods). Remarkably, we found that in the LE1 group ~53% (17 out of 32) of the recorded RBCs expressed reciprocal feedback greater than 5 pA. This percentage increased in LE2 group, to ~86% (24 out of 28). When compared with interleaved experiments performed in DR mice on the same day, only ~32% (7 out of 22) of the recorded RBCs expressed vIPSC greater than 5 pA. Consistent with this, the mean amplitude of the vIPSC on LE1 (P=0.04) and LE2 (P<0.0001) was significantly higher compared to interleaved experiments performed in DR mice (DR: N=22 cells/8 animals, LE1: 32 cells/5 animals; LE2: 28 cells/4 animals, KANOVA, **Figure 18B**). No changes were observed in the $I_{Ca^{2+}}$ in any of the groups tested. Together, the results support the idea that visual experience is necessary to trigger the maturation of GABAergic reciprocal feedback. Moreover, exposure to normal lighting conditions can reverse the reduction in the synaptic strength of the reciprocal feedback induced by the visual deprivation.

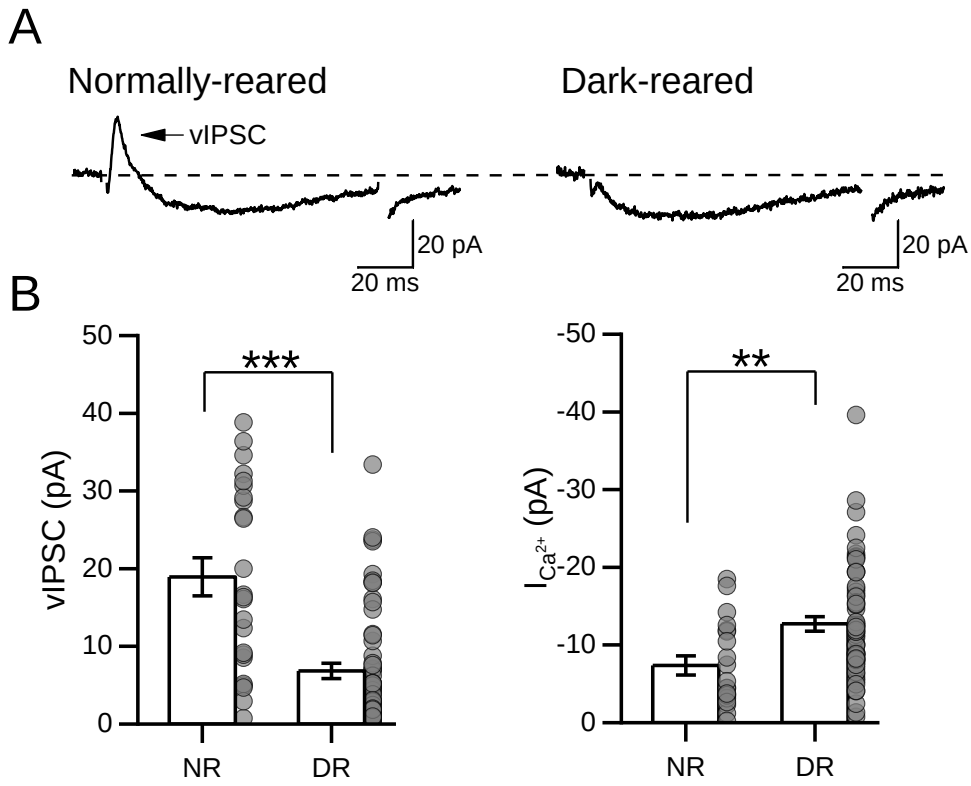

Figure 17. The synaptic strength of the reciprocal feedback inhibition onto RBCs is reduced by visual deprivation.

(A) Averaged vIPSC currents recorded in P20-P40 normally-reared (left) and dark-reared mice (right). The vIPSC is indicated with a black arrow. **(B)** The mean vIPSC amplitude (left) was significantly reduced, while the $I_{Ca^{2+}}$ (right) was slightly, but significantly increased in dark-reared mice. N=cells/animals. P20-P40: 27/5, DR: 59/20. Experiments were performed in the presence of strychnine (3 µM) and TTX (0.5 µM) in order to block glycinergic and non-reciprocal GABAergic feedback inputs to RBCs, respectively. Data are presented as mean ± SEM. **P<0.01, ***P<0.001.

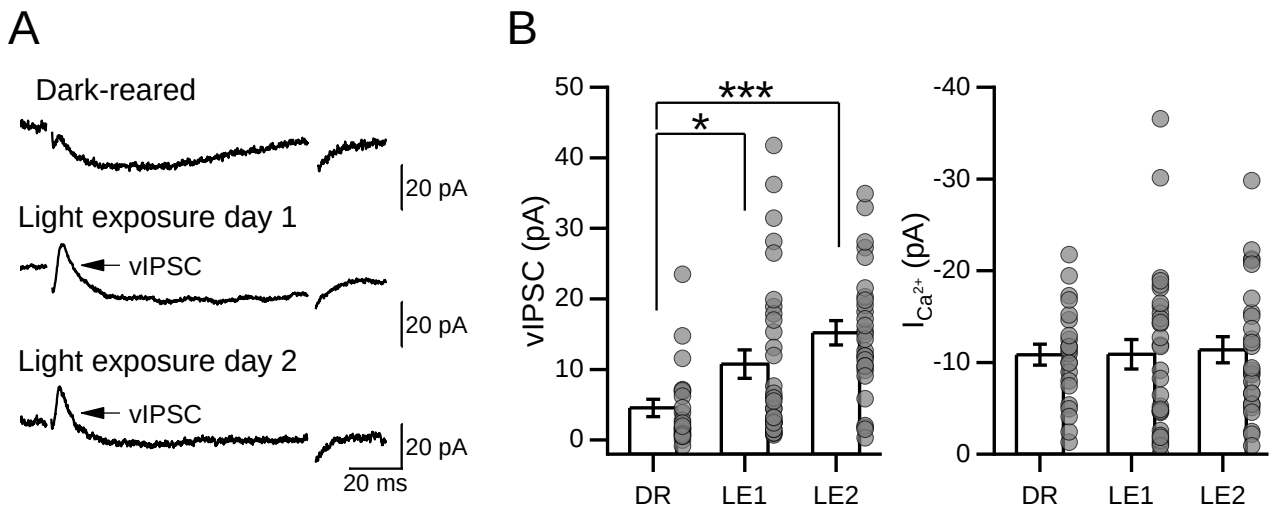

Figure 18. Decreased reciprocal feedback inhibition in dark-reared mice increases following light exposure.

(A) Averaged vIPSC currents recorded from P20-40 dark-reared (top) and from dark-reared mice exposed to light (1h, 60-80 lux) for one (LE1, middle) or two (LE2, bottom) consecutive days. The vIPSC is indicated with a black arrow. **(B)** The vIPSC mean amplitude significantly increased after one and two days of light exposure, whereas no changes in $I_{Ca^{2+}}$ amplitude following light exposure were observed. N=cells/animals. DR: 22/8, LE1: 32/5, LE2: 28/4. Experiments were performed in the presence of strychnine (3 µM) and TTX (0.5 µM) in order to block glycinergic and non-reciprocal GABAergic feedback inputs to RBCs, respectively. Data are presented as mean ± SEM. *P<0.05, **P<0.01.

Functional properties of NMDARS in A17 amacrine cells across retinal development

Finally, we investigated whether NMDARs are functionally expressed in A17 ACs and if their subunit composition could be regulated during retinal development. In contrast to AII ACs, we successfully elicited I_{NMDA} in P10-P13 (N=5 cells/5 animals) and P20-P40 (N=4 cells/3 animals) NR mice, as well as in DR (N=3 cells/2 animals) mice (**Figure 19**). No significant changes were observed in the I_{NMDA} mean amplitude between NR mice, although a trend toward decrease was observed in DR mice compared to both, P10-P13 and P20-P40 NR mice (P10-P13 vs P20-P40, P=0.88; DR vs P10-P13, P=0.17; DR vs P20-P40, P=0.10; one-way ANOVA, **Figure 19B**). Further experiments will be required to confirm this observation. Next, we investigated changes in NMDAR subunit composition (**Figure 20**) and found that, before eye opening, the mean amplitude of I_{NMDA} was significantly decreased by bath application (10 min) of the GluN2A-containing NMDARs blocker, Zn^{2+} (200 nM). Subsequent application (10 min) of the GluN2B-containing NMDARs antagonist, Ro25-6981 (1 µM), further reduced the I_{NMDA} mean amplitude, indicating that, before eye opening, NMDARs are composed by both GluN2A and GluN2B subunits (BL vs Zn^{2+}, P=0.006; Zn^{2+} vs Ro, P=0.038; one-way ANOVA-RM, **Figure 20A**). After eye opening, bath application of Zn^{2+} decreased the I_{NMDA} mean amplitude. However, subsequent application of Ro25-6981, did not further reduced the I_{NMDA} mean amplitude, suggesting that a switch from GluN2B- to GluN2A-containing NMDARs occur in mouse A17 ACs following eye opening (BL vs Zn^{2+}, P=0.024; Zn^{2+} vs Ro, P=0.561; one-way ANOVA-RM, **Figure 20B**).

Lastly, we examined whether this developmental switch in NMDARs subunit composition required visual experience. Bath application of Zn^{2+} decreased the I_{NMDA} mean amplitude. However, subsequent application of Ro25-6981, did not further reduced the I_{NMDA} mean amplitude, suggesting that the transition from GluN2B- to GluN2A-containing NMDARs in A17 ACs occurs independently of visual experience (BL vs Zn^{2+}, P=0.006; Zn^{2+} vs Ro, P=0.557; one-way ANOVA-RM, **Figure 20C**).

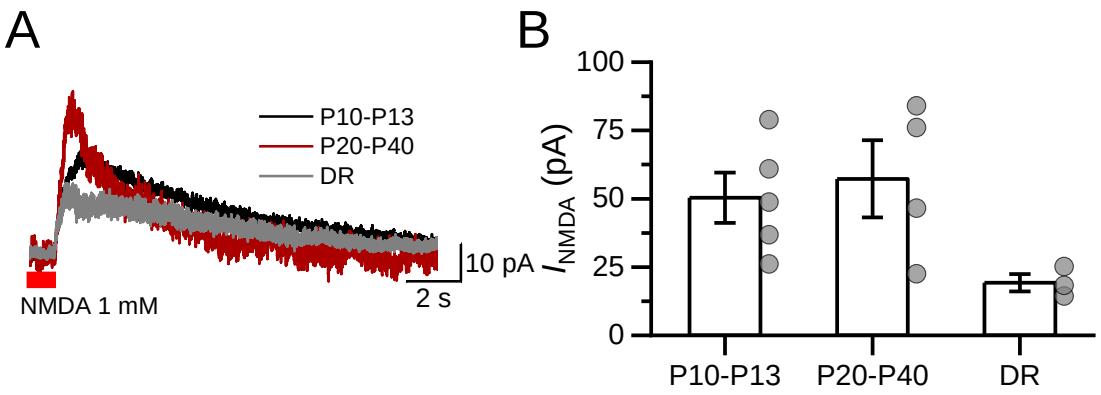

Figure 19. NMDARs are functionally expressed in A17 ACs from the mouse retina.

(A) Averaged NMDAR-mediated currents (I_{NMDA}) recorded from A17 amacrine cells at +40 mV in P10-P13 (black), P20-P40 (red) normally-reared and P20-P40 dark-reared mice (gray). I_{NMDA} was elicited by puff application of NMDA (1 mM, 1 s, 5-6 PSI) directly to A17 ACs processes located at the sublamina 5 of the IPL in the presence of Mg^{2+}-free ACSF supplemented with the NMDAR co-agonist D-Serine (200 µM) and tricine (10 mM) to chelate endogenous Zn^{2+}. **(B)** The mean amplitude of I_{NMDA} was unchanged through retinal development and was unaffected by dark-rearing. N=cells/animals. P10-P13: n=5/5, P20-P40: n=4/3, DR: n=3/2. Experiments were performed in the continuous presence of strychnine (3 µM), SR95531 (10 µM), TPMPA (50 µM), NBQX (10 µM) in order to isolate I_{NMDA}. Data are presented as mean ± SEM. *p<0.05, **p<0.01.

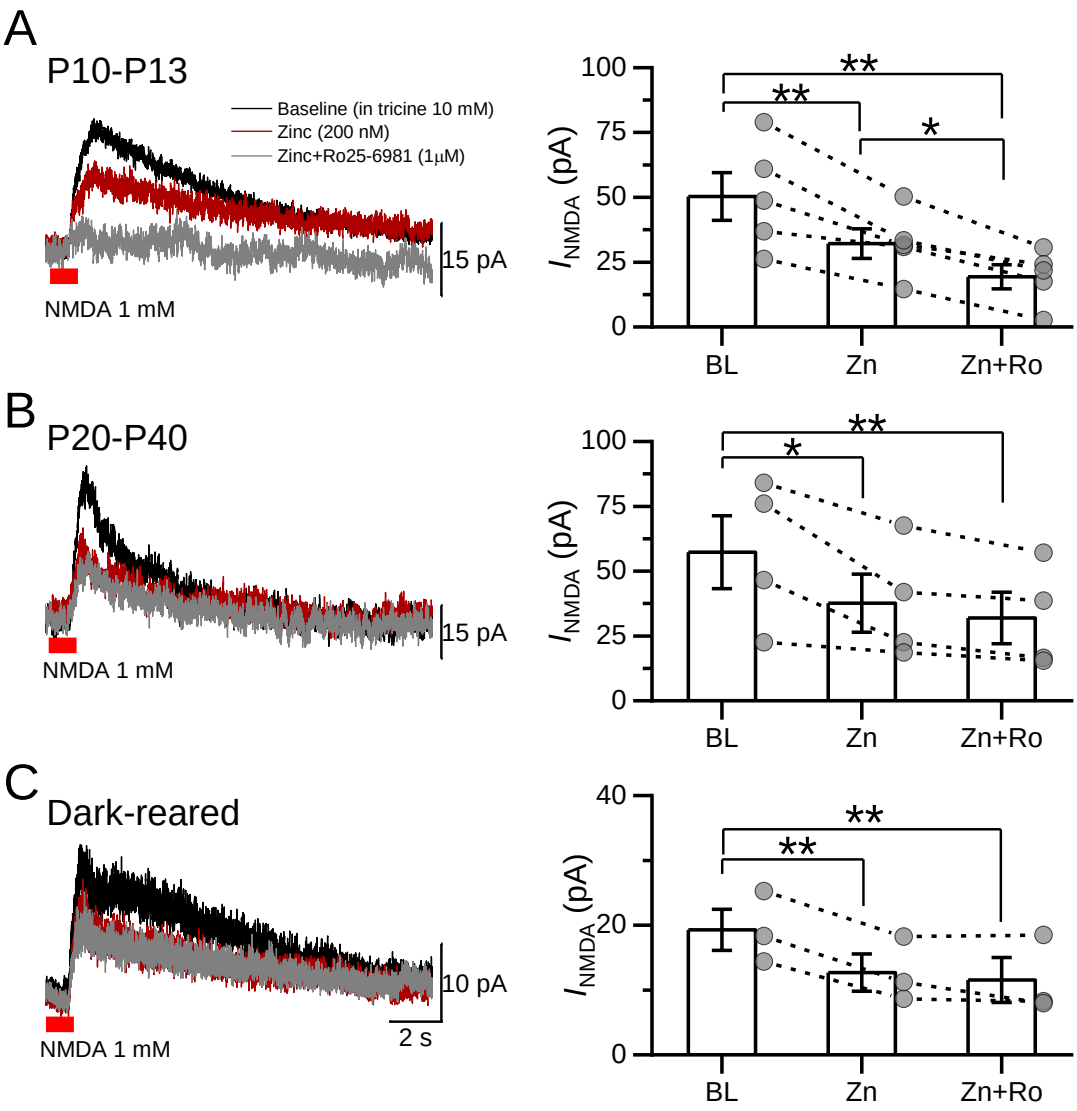
A
P10-P13
Baseline (in tricine 10 mM)
Zinc (200 nM)
Zinc+Ro25-6981 (1μM)
15 pA
NMDA 1 mM
100
75
50
25
0
I_{NMDA} (pA)
**
**
*
BL
Zn
Zn+Ro
B
P20-P40
15 pA
NMDA 1 mM
100
75
50
25
0
I_{NMDA} (pA)
**
*
BL
Zn
Zn+Ro
C
Dark-reared
10 pA
2 s
NMDA 1 mM
40
20
0
I_{NMDA} (pA)
**
**
BL
Zn
Zn+Ro

Figure 20. NMDAR subunit composition undergoes visual experience-independent changes in A17 ACs throughout development.

(A) Averaged NMDAR-mediated currents (I_{NMDA}, left) recorded from A17 amacrine cells at +40 mV in P10-P13 mice before (black) and after the application of Zn^{2+} (red) and Ro25-6981 (gray). I_{NMDA} were induced by puff application of NMDA (1 mM, 1 s, 5-6 PSI) directly to A17s processes located at the sublamina 5 of the IPL in the presence of Mg^{2+}-free ACSF supplemented with the NMDAR co-agonist D-Serine (200 µM) and tricine (10 mM) to chelate endogenous Zn^{2+}. The I_{NMDA} mean amplitude (right) was significantly reduced after the bath application of Zn^{2+} (200 nM) and the subsequent application of Ro25-6981 (1 µM) suggesting that before eye opening NR2A- and NR2B-containing NMDARs contributed to the total I_{NMDA}. **(B)** Same as **(A)** but for P20-P40 mice (left). The I_{NMDA} mean amplitude (right) was reduced by the bath application of Zn^{2+}, but not by Ro25-6981, suggesting that after eye opening NR2A-containing NMDARs contributed to the total I_{NMDA}. **(C)** Same as **(A)**, but for dark-reared mice (left). Similar to NR mice, the I_{NMDA} mean amplitude (right) was reduced only by the bath application of Zn^{2+} suggesting that the change in NMDAR subunit composition is independent of the visual experience at the time of the eye opening. N=cells/animals. P10-P13: n=5/5, P20-P40: n=4/3, DR: n=3/2. Experiments were performed in the continuous presence of strychnine (3 µM), SR95531 (10 µM), TPMPA (50 µM), NBQX (10 µM) to isolate I_{NMDA}. Data are presented as mean ± SEM. *p<0.05, **p<0.01.

5 DISCUSSION

Feedforward and feedback signaling play a crucial role at the RBC dyad synapse in the rod-pathway, reliably transmitting the rod photoreceptor signaling and allowing the adaptation to varying luminance conditions. While the cellular and molecular mechanisms governing these signaling processes are well-understood in the adult rodent retina, their establishment and refinement during postnatal development remain poorly understood. Here, we employed *ex vivo* electrophysiological measurements to unravel the mechanisms determining the establishment and refinement of RBC dyad synapses, critical components of the scotopic circuitry that mediate our vision in dim light conditions.

Our main findings are that: (1) the mEPSC frequency increases with age in both AII and A17 ACs, but the amplitude and kinetics change only in AII ACs. These changes were unaffected by visual deprivation, except for the mEPSC frequency onto AII ACs, which was enhanced. (2) In the mouse retina, the expression of CP-AMPARs remained unchanged throughout development, while NMDARs were not expressed. No changes were induced by visual deprivation. (3) In A17 ACs, AMPARs transition from calcium-impermeable (with an atypical pharmacological profile) to calcium-permeable, while NMDARs transition from GluN2B- to GluN2A-containing receptors. This change in iGluRs subunit composition was not altered by visual deprivation. (4) GABAergic reciprocal feedback, which requires CP-AMPARs activation, onto RBC axon terminals is absent before eye opening likely by the absent of calcium-permeable AMPARs. (5) The synaptic strength of the GABAergic reciprocal feedback is reduced by visual deprivation, an effect that can be reversed by exposing visually-deprived animals to light. Together, our results indicate that extensive refinement of the mechanisms facilitating feedforward excitatory and feedback inhibitory signaling at the RBC dyad synapse occurs during retinal development. Most of these changes are independent of visual experience. Additionally, our data underscores the distinct iGluRs profiles exhibited by AII and A17 amacrine cells, suggesting that both cell types follow unique programs of synaptic refinement and development.

RBC-driven excitatory input onto AII and A17 amacrine cells increase with age

In the mammalian retina, it is well established that the basic machinery involved in vesicular release is expressed prior to eye opening (Dhingra et al., 1997; Greenlee et al., 2002; von Kriegstein and Schmitz, 2003). Previous studies have demonstrated that spontaneous EPSCs can be detected in AII and A17 ACs as early as P7 (Schubert et al., 2008). Using whole-cell voltage clamp recordings, we observed an increase in the frequency of AMPAR-mediated mEPSCs onto AII and A17 ACs after eye opening, suggesting a presynaptic refinement during RBC dyad synapse development **(Figure 5 and 10)**. Similar increments in the excitatory input have been reported in AII ACs (Kim et al., 2023) and RGCs (Tian and Copenhagen, 2001; Johnson et al., 2003).

Transmitter release from RBC axon terminals is triggered and organized by synaptic ribbons (Singer and Diamond, 2003; Singer et al., 2004). Electron microscopy studies have shown that ribbon synapses in the inner retina are detected by P11 (Fisher, 1979), whereas RIBEYE, the principal ribbon synapse marker, can be labeled from P10 in BCs (Johnson et al., 2003). Although ribbons are highly dynamic during this period, they rapidly stabilize and increase in number at the time of eye opening in mouse ON-BCs (Okawa et al., 2019). The stabilization of ribbons after eye opening results in an increase in the sustained, but not the transient, component of light-evoked EPSCs in AII ACs (Kim et al., 2023), suggesting an increment of the readily releasable pool (RRP) of vesicles from RBCs after eye opening.

Previous studies suggest that spontaneous and evoked release are mechanistically distinct (Kaeser and Regehr, 2014; Truckenbrodt and Rizzoli, 2014; Kavalali, 2015) and though RIBEYE deletion do not evidently affect spontaneous release, it alters the nano-domain coupling of Ca^{2+}-channels to the active zone (Maxeiner et al., 2016). Thus, it would be interesting to investigate how the organization of ribbons and their associated proteins during development influence the establishment of spontaneous and evoked release from RBCs.

Feedforward signaling onto AII amacrine cells is enhanced by visual deprivation

Interestingly, in dark-reared mice, we still observed an increase in the frequency of AMPAR-mediated mEPSCs onto AII and A17 ACs after eye opening, indicating that the refinement of the excitatory inputs during retinal development is independent of visual experience. However, this effect was significantly enhanced in AII, but not in A17 ACs (**Figure 5**). Previous studies in the mouse retina have reported that, unlike in ON-CBCs, dark rearing does not affect mGluR6 expression and localization in RBCs dendrites (Dunn et al., 2013). Similar observations have been made in the inner retina, where dark rearing does not alter ribbon synaptogenesis (Fisher, 1979). Nevertheless, Wisner et al. (2023) showed that the resting membrane potential of RBCs is more depolarized in dark-reared conditions due to an immature expression of chloride transporters. Therefore, is plausible that our observations (**Figure 5**) are caused by an increment in transmitter release from presynaptic RBCs. Moreover, Wisner et al. (2023) reported that a small but significant fraction of ribbon synapses were observed in atypical conformations as monads. These findings could explain why feedforward signaling was enhanced in AII, but not A17 ACs. However, further experiments are required to confirm this observation. It is worth noting that our experiments were performed in the presence of antagonists against $GABA_A$, $GABA_C$ and glycine receptors to isolate AMPARs-mediated currents. It would be interesting to examine whether the enhanced release from RBCs is still observed in the presence of the glycinergic and GABAergic inhibition.

AMPAR-mediated inputs are developmentally regulated in AII, but not in A17 amacrine cells

In addition to presynaptic modifications, we observed a decrease in the amplitude and a slowdown in the kinetics properties of AMPAR-mediated mEPSCs in AII, but not in A17 amacrine cells, suggesting that cell-type specific refinement of postsynaptic AMPARs occur at the RBC dyad synapse during retinal development. Moreover, while visual deprivation had a significant effect on presynaptic release onto AII ACs, its impact on mEPSC amplitude and kinetics was modest on AII ACs and did not affect A17 ACs (**Figure 5 and 10**). AMPAR functional properties are primarily determined by their subunit composition which can vary across cell types and change remarkably

during development (Henley and Wilkinson, 2016; Greger et al., 2017). Nevertheless, understanding the regulation of AMPAR subunit expression during retinal development and its impact on specific cell types remains challenging due to the high diversity of retinal cell populations and the lack of specific markers for each subtype.

Using intracellular spermine to examine the functional expression of CP-AMPARs in AII ACs, we observed a strong inward rectification before and after eye opening (**Figure 6**), consistent with previous reports performed in the rat retina (Osswald et al., 2007), indicating that CP-AMPARs are functionally expressed from early development. These observations can be attributed to the specific blockade of GluA2-lacking CP-AMPARs as our recordings in the absence of spermine did not show inward rectification of the I-V relationship. Moreover, experiments performed in dark-reared mice indicate that CP-AMPARs expression is visual experience-independent. Our experiments using IEM1460 on AMPA-evoked I_{AMPA}, further support the notion that CP-AMPARs in AII ACs are expressed early in development and their contribution to the total AMPAR current remained unchanged following eye opening. Our results indicate that prior and after eye opening approximately 75% of the total I_{AMPA} is mediated by CP-AMPARs (**Figure 7**), similarly to studies performed in AII ACs from the primate retina (Percival et al., 2022). The population of CP-AMPARs significantly contribute to excitatory synaptic transmission prior to eye opening, as is demonstrated in our experiments using IEM1460 and PhTX onto spontaneous AMPAR-mediated mEPSCs (**Figure 8 and Supplementary Figure 3**), however, in our experiments we did not observed evidence of the transient polyamine-insensitivity of CP-AMPARs, as it was reported by Osswald et al., (2007) in the rat retina, suggesting that at least in the mouse retina and in the time periods studied here, AMPARs currents do not turn insensitive to these blockers.

These results suggest that the expression of CP-AMPARs remains unchanged throughout AII ACs development, but they do not explain the observed changes in AMPAR-mediated mEPSC amplitude and kinetics (**Figure 5**). It is plausible that a switch in other AMPARs subunits could be contributing to the maturation of AMPARs. For instance, in synapses of the cochlear nucleus, deletion of the GluA3 subunit results in AMPAR-mediated currents with slower rise, decay, and half-width times

(Antunes et al., 2020). Similarly, in hippocampal neurons, a change in the subunit composition of AMPARs from GluA1 to GluA3, accompanied by an increase in the expression of the auxiliary protein TARP, leads to an increase in the decay time of AMPAR currents during postnatal development (Blair et al., 2013). However, while it is known that AMPARs in AII ACs are composed mainly of GluA2, GluA3, and GluA4 subunits (Grunder et al., 2000a; Ghosh et al., 2001; Li et al., 2002; Yan et al., 2020; Percival et al., 2022), how the proportion of these subunits change during retinal development remains to be elucidated.

Furthermore, it is important to consider that other factors, such as RNA editing events, alternative splicing of AMPAR subunits, and the expression of AMPAR auxiliary subunits, may also contribute to the regulation of AMPAR properties throughout retinal development (Henley and Wilkinson, 2016). The “flip/flop” alternative splicing of AMPARs, for instance, is known to be developmentally regulated. The “flip” variant is expressed consistently throughout development, while the “flop” variants are expressed at lower levels during development and gradually reach adult levels around postnatal day 14 in rodents (Monyer et al., 1991). This alternative splicing event significantly impacts channel kinetics, with the “flop” variants exhibiting more rapid desensitization compared to the “flip” variants (Sommer et al., 1990). Consistent with this, Kim et al. (2023) recently reported that the desensitization of evoked EPSCs onto AII ACs was weaker in young mice (P15-P18) compared to adult animals (>P30). It would be interesting to determine how the "flip/flop" alternative splicing refines AMPAR-mediated responses throughout retinal development.

On the other hand, AMPAR auxiliary subunits (Schwenk et al., 2014) and synapse-associated proteins (SAPs) (Sans et al., 2000; Zheng et al., 2010) are also developmentally regulated. The interaction between AMPAR auxiliary proteins and SAPs, such as PSD95 and SAP102, at the postsynaptic density (PSD), plays a fundamental role in AMPAR trafficking and stabilization at the synaptic sites (Chen et al., 2000; Schnell et al., 2002; Elias et al., 2006; Bats et al., 2007; Abdollahi Nejat et al., 2021).

In the mature rodent retina, AII ACs have been shown to express PSD95 (Koulen et al., 1998c; Ghosh et al., 2001; Hartveit et al., 2018), whereas A17 ACs express SAP102 (Koulen et al., 1998a). Interestingly, SAP102 and PSD965 interact with different AMPAR auxiliary subunits. For instance, in CA1 pyramidal neurons SAP102 regulates synaptic AMPAR function through a CNIH-2-dependent mechanism (Liu et al., 2018), and moreover, CNIH-2 and TARP gamma-8 determine the subunit composition of synaptic AMPA receptors by selectively delivering GluA1-containing AMPARs to synaptic sites (Herring et al., 2013). Therefore, it is feasible that AII and A17 ACs express different AMPAR interactomes, contributing to the cell-specific postsynaptic refinement of AMPAR responses observed between both cell types. Currently, no data available exists regarding the expression of AMPAR auxiliary subunits in the developing or mature mammalian retina. Thus, it would be of great interest to investigate the localization, expression, and the potential contribution of these proteins to the developmental maturation of excitatory synapses.

AMPARs subunit composition switch from GluA2-containing to GluA2-lacking in A17 amacrine cells following eye opening

An interesting observation is that in A17 ACs, AMPAR-mediated currents exhibited inward rectification after, but not before eye opening (**Figure 11**). Such transition from spermine-insensitive to spermine-sensitive currents was not affected by visual deprivation and suggest that CP-AMPARs are not functionally expressed before eye opening. However, we found that AMPARs before eye opening were spermine-insensitive, IEM1460-sensitive (**Figure 12-13**), and PhTx-insensitive (**Supplementary Figure 3**), suggesting atypical pharmacological properties with a mixt of GluA2-lacking and GluA2-containing characteristics. Despite this unexpected pharmacology observation, the deletion of the GluA2 subunit rendered AMPARs expressed in P10-P13 mice sensitive to spermine (**Figure 14**), strongly suggesting that, although the pharmacological properties are different, these receptors are likely to be calcium impermeable prior to eye opening.

It is worth noting that AMPARs with atypical pharmacological properties have been observed in other synapses. For instance, slow AMPARs in hippocampal synapses are insensitive to NBQX, a widely used AMPAR antagonist (Pampaloni et al., 2021; Pampaloni and Plested, 2022). This unique characteristic is thought to be influenced by the presence of different AMPAR auxiliary subunits. In cerebellar synapses, the presence of TARP can alter AMPAR pharmacology, causing CNQX, a commonly used antagonist, to act as a partial agonist (Devi et al., 2016). Whether A17 ACs express some auxiliary protein remain unknown.

It is also important to consider that AMPAR auxiliary subunits such as stargazin, cornichon, and GSG1L, have been shown to regulate calcium permeability, and polyamine sensitivity (Henley and Wilkinson, 2016; Bowie, 2018). For instance, stargazin and cornichon can enhance calcium permeability and decrease the polyamine block, while GSG1L enhances the block of CP-AMPARs by endogenous polyamines but reduces the block by exogenous polyamines like PhTX (McGee et al., 2015). Future experiment will be required to determine the expression of auxiliary subunits in A17 ACs and whether these auxiliary proteins can be modified during different developmental stages.

The GABAergic reciprocal feedback is absent before eye opening

To confirm the lack of calcium-permeable AMPARs prior eye opening, we took advantage of reciprocal GABAergic feedback inhibition, which is known to require CP-AMPAR activation in adult retina (Chavez et al., 2006). Notably, reciprocal feedback inhibition was absent and the inward Ca^{2+}-current was smaller prior eye opening compared to P20-P40 mice (**Figure 15**). Accordingly, analysis of the GABAergic reciprocal feedback in RBCs from GluA2$^{-/-}$ mice revealed that ~41% of the recorded RBCs exhibited reciprocal feedback before eye opening (**Figure 16**), supporting our hypothesis that, despite the atypical pharmacology of AMPARs expressed in A17 ACs, they are GluA2-containing calcium-impermeable receptors, a characteristic that might underlie the absence of the reciprocal feedback prior eye opening.

While our data strongly suggests a transition from GluA2-containing to GluA2-lacking AMPAR subunit composition as a potential explanation for the absence of reciprocal feedback, we explored

other possibilities that might contribute to its development. Although our findings suggests that the low presynaptic Ca^{2+} influx onto RBCs observed in young mice (**Figure 15B**) does not account for the absence of reciprocal feedback — increasing the extracellular Ca^{2+} concentration from 2.5 mM to 4 mM only incremented the $I_{Ca}{}^{2+}$ but not the vIPSC amplitude (**Supplementary Figure 4**) — it suggests that VGCCs are not completely mature before eye opening. In the adult retina glutamate release from RBCs is triggered principally by L-type VGCCs (Protti and Llano, 1998; Singer and Diamond, 2003), with a minor but not least important contribution of T-, P/Q- and N-type VGCCs (Pan, 2000, 2001; Pan et al., 2001; Zhang et al., 2022b). It remains to be determined how the expression and function of these different types of VGCCs is regulated at the time surrounding eye opening.

During development, axon-dendrite contacts are temporary and short-lived, with only a small fraction maturing into functional synapses (Catsburg and MacGillavry, 2020). Thus, before eye opening immature contacts between A17 ACs and RBCs might contribute to the absence of reciprocal feedback. However, paired recordings between RBC-AII or RBC-A17 pairs showed that they were functionally coupled prior to eye opening (**Supplementary Figure 5**). Moreover, ultrastructural studies using EM had shown that A17 ACs connect with at least 80% of RBCs at P9, reaching adult-like levels by P11 (Zhang et al., 2022a). Therefore, the lack of reciprocal feedback is unlikely to result from a decreased functional and structural connectivity between A17 ACs and RBCs and support our idea that prior eye opening the lack of calcium-permeable AMPARs might be responsible for the lack of GABAergic feedback inhibition. Moreover, inducing glutamate release onto A17 ACs by depolarizing all ON-BCs, including RBCs, showed no age-related differences in the amplitude of CPPG-evoked currents (**Supplementary Figure 6**), indicating that glutamate release from RBCs is functional, consistent with previous studies showing that AII and A17 ACs receive glutamatergic input before eye opening (Schubert et al., 2008).

Alternatively, it is possible that GABA receptors at the RBC axon terminals or GABA release from A17 ACs may not be functional prior to eye opening. However, consistent with previous reports (Schubert et al., 2013), we did not observe differences in total GABAR-mediated currents elicited by directly activating GABARs onto RBC axon terminals or GABA release from postsynaptic amacrine

cells, including A17 ACs (**Supplementary Figure 7**). Interestingly, a recent study reported a switch, in the subunit composition of $GABA_A$Rs from α3-containing to α1-containing $GABA_A$Rs before eye opening (Sinha et al., 2021). This switch required the recruitment of LRRTM4 (Leucine Rich Repeat Transmembrane Neuronal 4), a transsynaptic adhesion protein critical for the structural development and clustering of $GABA_A$Rs at RBC axon terminals (Sinha et al., 2021). In other areas of the CNS, LRRTM4 has been implicated as a critical factor in the development and clustering of AMPARs at excitatory synapses (Siddiqui et al., 2010; Siddiqui et al., 2013). However, whether LRRTM4 also participates in the organization and clustering of AMPARs at excitatory synapses onto A17 ACs remains to be determined. Together, this evidence suggest that the development and refinement of GABAergic reciprocal feedback likely require both the maturation of GABARs at RBC axon terminals and AMPARs in A17 amacrine cells.

Dark-rearing decreases the synaptic strength of the GABAergic reciprocal feedback

As reciprocal feedback is absent prior to eye opening, we wondered whether visual experience is required for its establishment (**Figure 17**). We found that in dark-reared mice, the synaptic strength of the reciprocal GABAergic feedback was decreased compared to age-matched normally-reared mice, while a slight increase in inward I_{Ca}^{2+} was observed. These findings raise the question of which light-driven mechanisms underlie the refinement of the reciprocal feedback.

In cone and rod photoreceptors, the first-order neurons of the retina, visual deprivation induce structural alterations in the orientation of photoreceptor inner segments (Chai et al., 2020), as well as a functional reduction in photoreceptor-driven a-waves measured using ERG recordings under light-adapted conditions (Tian and Copenhagen, 2001; Vistamehr and Tian, 2004). In the inner retina, visual deprivation decreases cone-driven b-wave responses — which reflect the depolarization of post-photoreceptoral neurons — and alters the expression of mGluR6 in ON-CBCs, but it has no effect on rod-driven b-wave responses or the mGluR6 expression on RBCs (Dunn et al., 2013). While dark-rearing does not seem to alter the rod pathway, it has been reported to strongly reduce oscillatory potentials (Tian and Copenhagen, 2001; Vistamehr and Tian, 2004), a mechanism that is

believed to represent feedback responses of the ACs population. More recently, it has been proposed that these potentials are mediated by RBC-A17 reciprocal synapses (Liao et al., 2023), suggesting that visual deprivation could alter the development of the RBC dyad synapse.

It has been shown that dark-rearing does not induce changes in the morphology, stratification within the IPL (Zhang et al., 2005) or ribbon synaptogenesis in RBCs (Fisher, 1979). Our findings align with these observations, showing that dark-rearing does not influence the glutamatergic input onto A17 ACs (**Figure 10**) or the inward rectification properties of AMPARs (**Figure 11**) in the same cells. However, in dark-reared mice, it has been reported that $GABA_AR$s at RBC axon terminals remain in an immature state (i.e., high levels of α3-containing and low levels of α1-containing $GABA_AR$s), and the contribution of $GABA_AR$s to the total GABAR current was slightly but significantly lower compared to normally-reared mice (Wisner et al., 2023). Given that the reciprocal GABAergic feedback onto RBC axon terminals relies on $GABA_AR$s activation (Chavez et al., 2006), it is plausible that the observed reduction in synaptic strength in our study is attributed to the immature state of $GABA_AR$s. It is important to consider that, although $GABA_AR$s remain in an immature state in dark-reared mice (Wisner et al., 2023), it likely does not imply that the reciprocal inhibitory synapses are completely immature, given the fact that our findings indicate that the reciprocal feedback is completely absent before eye opening (**Figure 15**). Therefore, other factors beyond $GABA_AR$ maturation are likely playing a role in the establishment of reciprocal inhibitory synapses. Of note, Wisner et al. (2003) also reported a reduction in levels and function of $GABA_CR$s and the organizing protein LRRTM4, which could impact non-reciprocal GABAergic inhibition, known to require $GABA_CR$s activation (Chavez et al., 2010).

Exposure to light reverses the reduction in synaptic strength of the GABAergic reciprocal feedback induced by visual deprivation

The reduction in the synaptic strength of the reciprocal GABAergic feedback induced by visual deprivation (**Figure 17**) suggests that the maturation of the A17-RBC synapse requires visual

experience. In the visual cortex, during development, there is a transition in NMDAR subunit composition from GluN2B- to GluN2A-containing receptors (Carmignoto and Vicini, 1992). This shift in NMDAR subunit composition is dependent on visual experience, as dark-rearing blocks this transition, but it can be rapidly reversed by light exposure (Quinlan et al., 1999; Philpot et al., 2001; Matta et al., 2011). Here, we report that introducing dark-reared mice to light (**Figure 18**) for 1 h (60-80 lux) one or two consecutive days (**see methods and Figure 3**) resulted in an increase in the proportion of RBCs showing significant reciprocal feedback compared to RBCs recorded in non-exposed DR mice (interleaved experiments performed on the same day). As mentioned earlier, Wisner et al. (2023) reported that in dark-reared mice, $GABA_AR$s at RBC axon terminals remain in an immature state (i.e., high levels of α3-containing and low levels of α1-containing $GABA_AR$s). In line with our findings, the introduction of dark-reared mice to a 12 h light/dark promote the maturation of $GABA_AR$s within a week (Wisner et al., 2023). Therefore, our results, combined with those reported by Wisner et al., (2023), strongly suggest that visual-experience driven maturation of $GABA_AR$s leads to the functional refinement of the reciprocal GABAergic feedback at RBC axon terminals.

Interestingly, although α1-containing $GABA_AR$s reached normal-rearing levels within a week of cyclic light exposure, $GABA_CR$s expression levels were higher but had not yet reached normal rearing levels (Wisner et al., 2023). This raises an interesting question about the amount of time required to reverse the effects of visual deprivation and whether all the affected components follow similar developmental trajectories. In our study, we exposed dark-reared mice to 1 hour of light (60-80 lux), after which light-exposed mice were reintroduced to a dark cycle, and the experiments were performed the next day. This was sufficient to promote the maturation of the GABAergic reciprocal feedback. In the outer mouse retina, visual deprivation induces a misalignment of inner segments of photoreceptors, which can be reversed by at least two days of cyclic light exposure (Chai et al., 2020). Similarly, in the inner retina, visual deprivation reduce OPs in ERG recordings and sEPSC onto RGCs, alterations that can be reversed after at least 15 and 6 days of introduction to cyclic light, respectively (Tian and Copenhagen, 2001). In the visual cortex, it has been reported that changes in NMDAR subunit composition and function can be reversed after introduction to light within approximately 2

hours (Quinlan et al., 1999; Philpot et al., 2001; Matta et al., 2011), whereas the increase in GABAergic input onto pyramidal neurons, prevented by visual deprivation, can be restored after two days of normal-light rearing (Morales et al., 2002). Consistently, it appears that some components of excitatory circuits have faster recoveries than inhibitory circuits; however, it is evident that there is not a clear consensus on the protocols used to assess the role of sensory experience. To determine the maturational trajectories of different areas and circuitries of sensory systems, it is necessary to establish clear and comparable parameters.

AII amacrine cells in the mouse retina do not express functional NMDA receptors

As a final part of this study, we examined the contribution and properties of NMDARs in AII amacrine cells. We were unable to elicit I_{NMDA} in AII ACs from P10-P13 or P20-P40 NR mice (**Figure 9A**), although in DR mice, we observed a small but significant inward current compared to P10-P13 or P20-P40 NR mice. However, further experiments are necessary to confirm whether this inward current is indeed mediated by the activation of NMDARs. While this differs from previous evidence suggesting functional extrasynaptic NMDARs in AII ACs from the rat and rabbit retina (Hartveit and Veruki, 1997; Zhou and Dacheux, 2004; Kothmann et al., 2012; Zhou et al., 2016; Veruki et al., 2019), single-cell RNA-seq studies in the mouse retina (Yan et al., 2020) indicate minimal expression of NR2A-D (*Grin2a-d*) and NR3D (*Grin3d*) subunits, despite moderate expression levels of the NR1 (*Grin1*) subunit. Further research will be needed to determine if this is reflected in the protein levels of each subunit. In addition, it is worth noting that our observations cannot be attributed to methodological differences, as we were able to successfully elicit I_{NMDA} in AII ACs from the rat retina (**Figure 9B**).

Furthermore, it is essential to consider that our findings add to previous studies reporting differences in the functional properties and molecular markers of AII ACs. For instance, AII ACs in the rat and rabbit retina express the calcium-binding protein parvalbumin (PV; Wassle et al., 1993; Casini et al., 1995; Gabriel et al., 2004), but in the mouse retina, PV-immunolabeling does not target AII ACs (Feigenspan et al., 2001). Moreover, differences in the synaptic strength of connections between OFF-BCs and AII ACs have been reported between rat and mouse retinas. In the rat retina, OFF-CBCs

provide strong excitatory synaptic input to AII ACs (Veruki et al., 2003), while in the mouse retina, the OFF-CBC-AII AC connectivity is functionally weak (Graydon et al., 2018). Future studies are needed to determine the physiological implications of these differences in AII ACs.

NMDA receptor subunit composition switch from GluN2B-containing to GluN2A-containing in A17 amacrine cells after eye opening

Next, we investigated whether NMDARs are functionally expressed in A17 ACs. Unlike AII ACs, we were able to elicit I_{NMDA} in A17 ACs from P10-P13 or P20-P40 NR mice, with no significant age-related changes in the total I_{NMDA} amplitude (**Figure 19**). Our findings align with single-cell RNA-seq studies in the mouse retina (Yan et al., 2020) and functional studies in the rat retina (Veruki et al., 2019), suggesting that A17 ACs in the mature mouse retina express predominantly GluN2A-containing NMDARs. Additionally, we observed a switch from GluN2B- to GluN2A-containing NMDARs in A17 ACs after eye opening. This switch in NMDAR subunit composition is known to play a critical role in the synaptic incorporation of AMPARs and synapse stabilization (Hall et al., 2007; Gray et al., 2011; Ferreira et al., 2015). It would be interesting to investigate whether this subunit switch correlates with the maturation of AMPARs at reciprocal synapses and, consequently, the refinement of the reciprocal GABAergic feedback.

Additionally, we examined whether this developmental switch in NMDAR subunits required visual experience. Recordings in DR mice showed no significant changes in I_{NMDA}, although a trend toward a decrease was observed (**Figure 19**). More experiments are needed to confirm this observation. Moreover, we found that the transition from GluN2B- to GluN2A-containing NMDARs in A17 ACs occurs independently of visual experience (**Figure 20**) consistent with studies performed in the rabbit retina (Chang et al., 2010).

It's important to highlight that in hippocampal interneurons, the developmental origin significantly influences the relative proportion of synaptic transmission carried by AMPARs and NMDARs, as well as their calcium permeability. Cells derived from the caudal ganglionic eminence (CGE) exhibit large NMDAR-mediated EPSCs and CI-AMPARs, while those from the medial

ganglionic eminence (MGE) express relatively small NMDAR-mediated EPSCs and CP-AMPARs. While in the retina all cell types share the same developmental origin (Cepko, 2014), GABAergic ACs emerge before glycinergic ACs during development (Cherry et al., 2009; Voinescu et al., 2009). Our results indicate that before eye opening, AII ACs do not express NMDARs but express CP-AMPARs, while A17 ACs express GluN2B-containing NMDARs and CI-AMPARs. After eye opening, however, the iGluRs profile of AII ACs remains unaltered, while in A17 ACs, NMDARs switch to GluN2A-containing receptors and CP-AMPARs. This suggests that both cell types follow distinct programs of synaptic refinement and development.

6 REFERENCES

Abdollahi Nejat M, Klaassen RV, Spijker S, Guus Smit AB (2021) Auxiliary subunits of the AMPA: The Shisa family of proteins. Curr Opin Pharmacol 58:52-61.

Antunes FM, Rubio ME, Kandler K (2020) Role of GluA3 AMPA Receptor Subunits in the Presynaptic and Postsynaptic Maturation of Synaptic Transmission and Plasticity of Endbulb-Bushy Cell Synapses in the Cochlear Nucleus. The Journal of neuroscience : the official journal of the Society for Neuroscience 40:2471-2484.

Baden T, Berens P, Franke K, Roman Roson M, Bethge M, Euler T (2016) The functional diversity of retinal ganglion cells in the mouse. Nature 529:345-350.

Bats C, Groc L, Choquet D (2007) The interaction between Stargazin and PSD-95 regulates AMPA receptor surface trafficking. Neuron 53:719-734.

Baylor D (1996) How photons start vision. Proceedings of the National Academy of Sciences of the United States of America 93:560-565.

Bellone C, Nicoll RA (2007) Rapid bidirectional switching of synaptic NMDA receptors. Neuron 55:779-785.

Blair MG, Nguyen NN, Albani SH, L'Etoile MM, Andrawis MM, Owen LM, Oliveira RF, Johnson MW, Purvis DL, Sanders EM, Stoneham ET, Xu H, Dumas TC (2013) Developmental changes in structural and functional properties of hippocampal AMPARs parallels the emergence of deliberative spatial navigation in juvenile rats. The Journal of neuroscience : the official journal of the Society for Neuroscience 33:12218-12228.

Bloomfield SA, Dacheux RF (2001) Rod vision: pathways and processing in the mammalian retina. Progress in retinal and eye research 20:351-384.

Boos R, Schneider H, Wassle H (1993) Voltage- and transmitter-gated currents of all-amacrine cells in a slice preparation of the rat retina. The Journal of neuroscience : the official journal of the Society for Neuroscience 13:2874-2888.

Bormann J (2000) The ‘ABC’ of GABA receptors. Trends in Pharmacological Sciences 21:16-19.

Bowie D (2018) Polyamine-mediated channel block of ionotropic glutamate receptors and its regulation by auxiliary proteins. The Journal of biological chemistry 293:18789-18802.

Bowie D, Mayer ML (1995) Inward rectification of both AMPA and kainate subtype glutamate receptors generated by polyamine-mediated ion channel block. Neuron 15:453-462.

Brill J, Huguenard JR (2008) Sequential changes in AMPA receptor targeting in the developing neocortical excitatory circuit. The Journal of neuroscience : the official journal of the Society for Neuroscience 28:13918-13928.

Carmignoto G, Vicini S (1992) Activity-dependent decrease in NMDA receptor responses during development of the visual cortex. Science 258:1007-1011.

Casimiro TM, Nawy S, Carroll RC (2013) Molecular mechanisms underlying activity-dependent AMPA receptor cycling in retinal ganglion cells. Molecular and cellular neurosciences 56:384-392.

Casini G, Rickman DW, Brecha NC (1995) AII amacrine cell population in the rabbit retina: identification by parvalbumin immunoreactivity. The Journal of comparative neurology 356:132-142.

Catsburg LAE, MacGillavry HD (2020) AMPA receptor trafficking in the developing and mature glutamatergic synapse. In: Synapse Development and Maturation, pp 507-525.

Catterall WA (1998) Structure and function of neuronal Ca2+ channels and their role in neurotransmitter release. Cell Calcium 24:307-323.

Catterall WA (2011) Voltage-gated calcium channels. Cold Spring Harbor perspectives in biology 3:a003947.

Cepko C (2014) Intrinsically different retinal progenitor cells produce specific types of progeny. Nature reviews Neuroscience 15:615-627.

Chai Z, Silverman D, Li G, Williams D, Raviola E, Yau KW (2020) Light-dependent photoreceptor orientation in mouse retina. Sci Adv 6.

Chavez AE, Diamond JS (2008) Diverse mechanisms underlie glycinergic feedback transmission onto rod bipolar cells in rat retina. The Journal of neuroscience : the official journal of the Society for Neuroscience 28:7919-7928.

Chavez AE, Singer JH, Diamond JS (2006) Fast neurotransmitter release triggered by Ca influx through AMPA-type glutamate receptors. Nature 443:705-708.

Chavez AE, Grimes WN, Diamond JS (2010) Mechanisms underlying lateral GABAergic feedback onto rod bipolar cells in rat retina. The Journal of neuroscience : the official journal of the Society for Neuroscience 30:2330-2339.

Chebib M, Johnston GAR (1999) The 'Abc' of Gaba Receptors: A Brief Review. Clinical and Experimental Pharmacology and Physiology 26:937-940.

Chen L, Yang C, Mower GD (2001) Developmental changes in the expression of GABA(A) receptor subunits (alpha(1), alpha(2), alpha(3)) in the cat visual cortex and the effects of dark rearing. Brain Res Mol Brain Res 88:135-143.

Chen L, Chetkovich DM, Petralia RS, Sweeney NT, Kawasaki Y, Wenthold RJ, Bredt DS, Nicoll RA (2000) Stargazin regulates synaptic targeting of AMPA receptors by two distinct mechanisms. Nature 408:936-943.

Cherry TJ, Trimarchi JM, Stadler MB, Cepko CL (2009) Development and diversification of retinal amacrine interneurons at single cell resolution. Proceedings of the National Academy of Sciences of the United States of America 106:9495-9500.

Chun MH, Han SH, Chung JW, Wassle H (1993) Electron microscopic analysis of the rod pathway of the rat retina. The Journal of comparative neurology 332:421-432.

Dacheux RF, Raviola E (1986) The rod pathway in the rabbit retina: a depolarizing bipolar and amacrine cell. The Journal of neuroscience : the official journal of the Society for Neuroscience 6:331-345.

Demb JB, Singer JH (2012) Intrinsic properties and functional circuitry of the AII amacrine cell. Visual neuroscience 29:51-60.

Devi SP, Howe JR, Auger C (2016) Train stimulation of parallel fibre to Purkinje cell inputs reveals two populations of synaptic responses with different receptor signatures. The Journal of physiology 594:3705-3727.

DeVries SH (2000) Bipolar Cells Use Kainate and AMPA Receptors to Filter Visual Information into Separate Channels. Neuron 28:847-856.

Dhingra NK, Ramamohan Y, Raju TR (1997) Developmental expression of synaptophysin, synapsin I and syntaxin in the rat retina. Brain Res Dev Brain Res 102:267-273.

Diamond JS (2017) Inhibitory Interneurons in the Retina: Types, Circuitry, and Function. Annual review of vision science.

Dingledine R, Borges K, Bowie D, Traynelis SF (1999) The glutamate receptor ion channels. Pharmacol Rev 51:7-61.

Donevan SD, Rogawski MA (1995) Intracellular polyamines mediate inward rectification of Ca(2+)-permeable alpha-amino-3-hydroxy-5-methyl-4-isoxazolepropionic acid receptors. Proceedings of the National Academy of Sciences of the United States of America 92:9298-9302.

Dong CJ, Hare WA (2003) Temporal modulation of scotopic visual signals by A17 amacrine cells in mammalian retina in vivo. Journal of neurophysiology 89:2159-2166.

Dunn FA, Della Santina L, Parker ED, Wong RO (2013) Sensory experience shapes the development of the visual system's first synapse. Neuron 80:1159-1166.

Egger V, Diamond JS (2020) A17 Amacrine Cells and Olfactory Granule Cells: Parallel Processors of Early Sensory Information. Frontiers in cellular neuroscience 14.

Eggers ED, Lukasiewicz PD (2006a) Receptor and transmitter release properties set the time course of retinal inhibition. The Journal of neuroscience : the official journal of the Society for Neuroscience 26:9413-9425.

Eggers ED, Lukasiewicz PD (2006b) GABA(A), GABA(C) and glycine receptor-mediated inhibition differentially affects light-evoked signalling from mouse retinal rod bipolar cells. The Journal of physiology 572:215-225.

el Azazi M, Wachtmeister L (1991) The postnatal development of the oscillatory potentials of the electroretinogram. III. Scotopic characteristics. Acta Ophthalmol (Copenh) 69:505-510.

Elias GM, Funke L, Stein V, Grant SG, Bredt DS, Nicoll RA (2006) Synapse-specific and developmentally regulated targeting of AMPA receptors by a family of MAGUK scaffolding proteins. Neuron 52:307-320.

Euler T, Haverkamp S, Schubert T, Baden T (2014) Retinal bipolar cells: elementary building blocks of vision. Nature Reviews Neuroscience 15:507-519.

Famiglietti EV, Kolb H (1975) A bistratified amacrine cell and synaptic circuitry in the inner plexiform layer of the retina. Brain research 84:293-300.

Farrow P, Khodosevich K, Sapir Y, Schulmann A, Aslam M, Stern-Bach Y, Monyer H, von Engelhardt J (2015) Auxiliary subunits of the CKAMP family differentially modulate AMPA receptor properties. eLife 4:e09693.

Fayyazuddin A, Villarroel A, Le Goff A, Lerma J, Neyton J (2000) Four residues of the extracellular N-terminal domain of the NR2A subunit control high-affinity Zn2+ binding to NMDA receptors. Neuron 25:683-694.

Feigenspan A, Teubner B, Willecke K, Weiler R (2001) Expression of neuronal connexin36 in AII amacrine cells of the mammalian retina. The Journal of neuroscience : the official journal of the Society for Neuroscience 21:230-239.

Feller MB (2003) Visual System Plasticity Begins in the Retina. Neuron 39:3-4.

Ferreira JS, Schmidt J, Rio P, Aguas R, Rooyakkers A, Li KW, Smit AB, Craig AM, Carvalho AL (2015) GluN2B-Containing NMDA Receptors Regulate AMPA Receptor Traffic through Anchoring of the Synaptic Proteasome. The Journal of neuroscience : the official journal of the Society for Neuroscience 35:8462-8479.

Fisher LJ (1979) Development of retinal synaptic arrays in the inner plexiform layer of dark-reared mice. J Embryol Exp Morphol 54:219-227.

Fletcher EL, Kalloniatis M (1997) Localisation of amino acid neurotransmitters during postnatal development of the rat retina. The Journal of comparative neurology 380:449-471.

Fletcher EL, Koulen P, Wassle H (1998) GABAA and GABAC receptors on mammalian rod bipolar cells. The Journal of comparative neurology 396:351-365.

Frech MJ, Backus KH (2004) Characterization of inhibitory postsynaptic currents in rod bipolar cells of the mouse retina. Visual neuroscience 21:645-652.

Fu Y, Yau KW (2007) Phototransduction in mouse rods and cones. Pflugers Archiv : European journal of physiology 454:805-819.

Gabriel R, Lesauter J, Banvolgyi T, Petrovics G, Silver R, Witkovsky P (2004) AII amacrine neurons of the rat retina show diurnal and circadian rhythms of parvalbumin immunoreactivity. Cell Tissue Res 315:181-186.

Gambrill AC, Barria A (2011) NMDA receptor subunit composition controls synaptogenesis and synapse stabilization. Proceedings of the National Academy of Sciences of the United States of America 108:5855-5860.

Ghosh KK, Haverkamp S, Wassle H (2001) Glutamate receptors in the rod pathway of the mammalian retina. The Journal of neuroscience : the official journal of the Society for Neuroscience 21:8636-8647.

Ghosh KK, Bujan S, Haverkamp S, Feigenspan A, Wassle H (2004) Types of bipolar cells in the mouse retina. The Journal of comparative neurology 469:70-82.

Gray JA, Shi Y, Usui H, During MJ, Sakimura K, Nicoll RA (2011) Distinct modes of AMPA receptor suppression at developing synapses by GluN2A and GluN2B: single-cell NMDA receptor subunit deletion in vivo. Neuron 71:1085-1101.

Graydon CW, Lieberman EE, Rho N, Briggman KL, Singer JH, Diamond JS (2018) Synaptic Transfer between Rod and Cone Pathways Mediated by AII Amacrine Cells in the Mouse Retina. Current biology : CB 28:2739-2751 e2733.

Greenlee MHW, Wilson MC, Sakaguchi DS (2002) Expression of SNAP-25 during mammalian retinal development: thinking outside the synapse. Seminars in cell & developmental biology 13:99-106.

Greger IH, Watson JF, Cull-Candy SG (2017) Structural and Functional Architecture of AMPA-Type Glutamate Receptors and Their Auxiliary Proteins. Neuron 94:713-730.

Grimes WN, Li W, Chavez AE, Diamond JS (2009) BK channels modulate pre- and postsynaptic signaling at reciprocal synapses in retina. Nature neuroscience 12:585-592.

Grimes WN, Zhang J, Graydon CW, Kachar B, Diamond JS (2010) Retinal parallel processors: more than 100 independent microcircuits operate within a single interneuron. Neuron 65:873-885.

Grimes WN, Zhang J, Tian H, Graydon CW, Hoon M, Rieke F, Diamond JS (2015) Complex inhibitory microcircuitry regulates retinal signaling near visual threshold. Journal of neurophysiology 114:341-353.

Grunder T, Kohler K, Guenther E (2000a) Distribution and developmental regulation of AMPA receptor subunit proteins in rat retina. Investigative ophthalmology & visual science 41:3600-3606.

Grunder T, Kohler K, Kaletta A, Guenther E (2000b) The distribution and developmental regulation of NMDA receptor subunit proteins in the outer and inner retina of the rat. J Neurobiol 44:333-342.

Guenther E, Schmid S, Wheeler-Schilling T, Albach G, Grunder T, Fauser S, Kohler K (2004) Developmental plasticity of NMDA receptor function in the retina and the influence of light. FASEB J 18:1433-1435.

Guo C, Hirano AA, Stella SL, Jr., Bitzer M, Brecha NC (2010) Guinea pig horizontal cells express GABA, the GABA-synthesizing enzyme GAD 65, and the GABA vesicular transporter. The Journal of comparative neurology 518:1647-1669.

Hack I, Koulen P, Peichl LEO, BrandstÄTter JH (2002) Development of glutamatergic synapses in the rat retina: The postnatal expression of ionotropic glutamate receptor subunits. Visual neuroscience 19:1-13.

Hall BJ, Ripley B, Ghosh A (2007) NR2B signaling regulates the development of synaptic AMPA receptor current. The Journal of neuroscience : the official journal of the Society for Neuroscience 27:13446-13456.

Han KS, Cooke SF, Xu W (2017) Experience-Dependent Equilibration of AMPAR-Mediated Synaptic Transmission during the Critical Period. Cell reports 18:892-904.

Hansen KB, Yi F, Perszyk RE, Menniti FS, Traynelis SF (2017) NMDA Receptors in the Central Nervous System. Methods Mol Biol 1677:1-80.

Hansen KB, Wollmuth LP, Bowie D, Furukawa H, Menniti FS, Sobolevsky AI, Swanson GT, Swanger SA, Greger IH, Nakagawa T, McBain CJ, Jayaraman V, Low CM, Dell'Acqua ML, Diamond JS, Camp CR, Perszyk RE, Yuan H, Traynelis SF (2021) Structure, Function, and Pharmacology of Glutamate Receptor Ion Channels. Pharmacol Rev 73:298-487.

Hartveit E (1999) Reciprocal synaptic interactions between rod bipolar cells and amacrine cells in the rat retina. Journal of neurophysiology 81:2923-2936.

Hartveit E, Veruki ML (1997) AII amacrine cells express functional NMDA receptors. Neuroreport 8:1219-1223.

Hartveit E, Zandt BJ, Madsen E, Castilho A, Morkve SH, Veruki ML (2018) AMPA receptors at ribbon synapses in the mammalian retina: kinetic models and molecular identity. Brain structure & function 223:769-804.

He Q, Xu HP, Wang P, Tian N (2013) Dopamine D1 receptors regulate the light dependent development of retinal synaptic responses. PloS one 8:e79625.

Helmstaedter M, Briggman KL, Turaga SC, Jain V, Seung HS, Denk W (2013) Connectomic reconstruction of the inner plexiform layer in the mouse retina. Nature 500:168-174.

Henley JM, Wilkinson KA (2016) Synaptic AMPA receptor composition in development, plasticity and disease. Nature reviews Neuroscience 17:337-350.

Henneberger C, Juttner R, Schmidt SA, Walter J, Meier JC, Rothe T, Grantyn R (2005) GluR- and TrkB-mediated maturation of GABA receptor function during the period of eye opening. The European journal of neuroscience 21:431-440.

Herring BE, Shi Y, Suh YH, Zheng CY, Blankenship SM, Roche KW, Nicoll RA (2013) Cornichon proteins determine the subunit composition of synaptic AMPA receptors. Neuron 77:1083-1096.

Ho MT, Pelkey KA, Topolnik L, Petralia RS, Takamiya K, Xia J, Huganir RL, Lacaille JC, McBain CJ (2007) Developmental expression of Ca2+-permeable AMPA receptors underlies depolarization-induced long-term depression at mossy fiber CA3 pyramid synapses. The Journal of neuroscience : the official journal of the Society for Neuroscience 27:11651-11662.

Hooks BM, Chen C (2020) Circuitry Underlying Experience-Dependent Plasticity in the Mouse Visual System. Neuron 106:21-36.

Hoon M, Okawa H, Della Santina L, Wong RO (2014) Functional architecture of the retina: development and disease. Progress in retinal and eye research 42:44-84.

Jarsky T, Tian M, Singer JH (2010) Nanodomain control of exocytosis is responsible for the signaling capability of a retinal ribbon synapse. The Journal of neuroscience : the official journal of the Society for Neuroscience 30:11885-11895.

Johnson J, Tian N, Caywood MS, Reimer RJ, Edwards RH, Copenhagen DR (2003) Vesicular neurotransmitter transporter expression in developing postnatal rodent retina: GABA and glycine precede glutamate. The Journal of neuroscience : the official journal of the Society for Neuroscience 23:518-529.

Jones RS, Carroll RC, Nawy S (2012) Light-induced plasticity of synaptic AMPA receptor composition in retinal ganglion cells. Neuron 75:467-478.

Kaeser PS, Regehr WG (2014) Molecular mechanisms for synchronous, asynchronous, and spontaneous neurotransmitter release. Annu Rev Physiol 76:333-363.

Kamalova A, Nakagawa T (2021) AMPA receptor structure and auxiliary subunits. The Journal of physiology 599:453-469.

Kamboj SK, Swanson GT, Cull-Candy SG (1995) Intracellular spermine confers rectification on rat calcium-permeable AMPA and kainate receptors. The Journal of physiology 486 (Pt 2):297-303.

Kato AS, Siuda ER, Nisenbaum ES, Bredt DS (2008) AMPA receptor subunit-specific regulation by a distinct family of type II TARPs. Neuron 59:986-996.

Kavalali ET (2015) The mechanisms and functions of spontaneous neurotransmitter release. Nature reviews Neuroscience 16:5-16.

Kim MH, Strazza P, Jr., Puthussery T, Gross OP, Taylor WR, von Gersdorff H (2023) Functional maturation of the rod bipolar to AII-amacrine cell ribbon synapse in the mouse retina. Cell reports 42:113440.

Koh DS, Burnashev N, Jonas P (1995) Block of native Ca(2+)-permeable AMPA receptors in rat brain by intracellular polyamines generates double rectification. The Journal of physiology 486 (Pt 2):305-312.

Koike C, Numata T, Ueda H, Mori Y, Furukawa T (2010a) TRPM1: a vertebrate TRP channel responsible for retinal ON bipolar function. Cell Calcium 48:95-101.

Koike C, Obara T, Uriu Y, Numata T, Sanuki R, Miyata K, Koyasu T, Ueno S, Funabiki K, Tani A, Ueda H, Kondo M, Mori Y, Tachibana M, Furukawa T (2010b) TRPM1 is a component of the retinal ON bipolar cell transduction channel in the mGluR6 cascade. Proceedings of the National Academy of Sciences of the United States of America 107:332-337.

Kolb H, Nelson R (1983) Rod pathways in the retina of the cat. Vision Research 23:301-312.

Kothmann WW, Trexler EB, Whitaker CM, Li W, Massey SC, O'Brien J (2012) Nonsynaptic NMDA receptors mediate activity-dependent plasticity of gap junctional coupling in the AII amacrine cell network. The Journal of neuroscience : the official journal of the Society for Neuroscience 32:6747-6759.

Koulen P, Garner CC, Wassle H (1998a) Immunocytochemical localization of the synapse-associated protein SAP102 in the rat retina. The Journal of comparative neurology 397:326-336.

Koulen P, Brandstätter JH, Enz R, Bormann J, Wässle H (1998b) Synaptic clustering of GABACreceptor ρ-subunits in the rat retina. European Journal of Neuroscience 10:115-127.

Koulen P, Fletcher EL, Craven SE, Bredt DS, Wassle H (1998c) Immunocytochemical localization of the postsynaptic density protein PSD-95 in the mammalian retina. The Journal of neuroscience : the official journal of the Society for Neuroscience 18:10136-10149.

Kumar SS, Bacci A, Kharazia V, Huguenard JR (2002) A developmental switch of AMPA receptor subunits in neocortical pyramidal neurons. The Journal of neuroscience : the official journal of the Society for Neuroscience 22:3005-3015.

Lagnado L, Schmitz F (2015) Ribbon Synapses and Visual Processing in the Retina. Annual review of vision science 1:235-262.

Li W, Trexler EB, Massey SC (2002) Glutamate receptors at rod bipolar ribbon synapses in the rabbit retina. The Journal of comparative neurology 448:230-248.

Liao F, Liu H, Milla-Navarro S, Villa P, Germain F (2023) Origin of Retinal Oscillatory Potentials in the Mouse, a Tool to Specifically Locate Retinal Damage. Int J Mol Sci 24.

Liu M, Shi R, Hwang H, Han KS, Wong MH, Ren X, Lewis LD, Brown EN, Xu W (2018) SAP102 regulates synaptic AMPAR function through a CNIH-2-dependent mechanism. Journal of neurophysiology 120:1578-1586.

Liu XB, Murray KD, Jones EG (2004) Switching of NMDA receptor 2A and 2B subunits at thalamic and cortical synapses during early postnatal development. The Journal of neuroscience : the official journal of the Society for Neuroscience 24:8885-8895.

Lu W, Constantine-Paton M (2004a) Eye Opening Rapidly Induces Synaptic Potentiation and Refinement. Neuron 43:237-249.

Lu W, Constantine-Paton M (2004b) Eye opening rapidly induces synaptic potentiation and refinement. Neuron 43:237-249.

Lujan B, Dagostin A, von Gersdorff H (2019) Presynaptic Diversity Revealed by Ca(2+)-Permeable AMPA Receptors at the Calyx of Held Synapse. The Journal of neuroscience : the official journal of the Society for Neuroscience 39:2981-2994.

MacNeil MA, Masland RH (1998) Extreme Diversity among Amacrine Cells: Implications for Function. Neuron 20:971-982.

Magazanik LG, Buldakova SL, Samoilova MV, Gmiro VE, Mellor IR, Usherwood PN (1997) Block of open channels of recombinant AMPA receptors and native AMPA/kainate receptors by adamantane derivatives. The Journal of physiology 505 (Pt 3):655-663.

Manookin MB, Beaudoin DL, Ernst ZR, Flagel LJ, Demb JB (2008) Disinhibition combines with excitation to extend the operating range of the OFF visual pathway in daylight. The Journal of neuroscience : the official journal of the Society for Neuroscience 28:4136-4150.

Masland RH (2001) The fundamental plan of the retina. Nature neuroscience 4:877-886.

Masland RH (2012) The tasks of amacrine cells. Visual neuroscience 29:3-9.

Matt L, Kirk LM, Chenaux G, Speca DJ, Puhger KR, Pride MC, Qneibi M, Haham T, Plambeck KE, Stern-Bach Y, Silverman JL, Crawley JN, Hell JW, Diaz E (2018) SynDIG4/Prrt1 Is Required for Excitatory Synapse Development and Plasticity Underlying Cognitive Function. Cell reports 22:2246-2253.

Matta JA, Ashby MC, Sanz-Clemente A, Roche KW, Isaac JT (2011) mGluR5 and NMDA receptors drive the experience- and activity-dependent NMDA receptor NR2B to NR2A subunit switch. Neuron 70:339-351.

Matta JA, Pelkey KA, Craig MT, Chittajallu R, Jeffries BW, McBain CJ (2013) Developmental origin dictates interneuron AMPA and NMDA receptor subunit composition and plasticity. Nature neuroscience 16:1032-1041.

Maxeiner S, Luo F, Tan A, Schmitz F, Sudhof TC (2016) How to make a synaptic ribbon: RIBEYE deletion abolishes ribbons in retinal synapses and disrupts neurotransmitter release. The EMBO journal 35:1098-1114.

McGee TP, Bats C, Farrant M, Cull-Candy SG (2015) Auxiliary Subunit GSG1L Acts to Suppress Calcium-Permeable AMPA Receptor Function. The Journal of neuroscience : the official journal of the Society for Neuroscience 35:16171-16179.

McLaughlin AJ, Percival KA, Gayet-Primo J, Puthussery T (2020) Glycinergic Inhibition Targets Specific Off Cone Bipolar Cells In Primate Retina. eNeuro.

Mehta B, Ke JB, Zhang L, Baden AD, Markowitz AL, Nayak S, Briggman KL, Zenisek D, Singer JH (2014) Global Ca2+ signaling drives ribbon-independent synaptic transmission at rod bipolar cell synapses. The Journal of neuroscience : the official journal of the Society for Neuroscience 34:6233-6244.

Menger N, Wassle H (2000) Morphological and physiological properties of the A17 amacrine cell of the rat retina. Visual neuroscience 17:769-780.

Monyer H, Seeburg PH, Wisden W (1991) Glutamate-operated channels: developmentally early and mature forms arise by alternative splicing. Neuron 6:799-810.

Moore-Dotson JM, Klein JS, Mazade RE, Eggers ED (2015) Different types of retinal inhibition have distinct neurotransmitter release properties. Journal of neurophysiology 113:2078-2090.

Morales B, Choi SY, Kirkwood A (2002) Dark rearing alters the development of GABAergic transmission in visual cortex. The Journal of neuroscience : the official journal of the Society for Neuroscience 22:8084-8090.

Morgans CW, Zhang J, Jeffrey BG, Nelson SM, Burke NS, Duvoisin RM, Brown RL (2009) TRPM1 is required for the depolarizing light response in retinal ON-bipolar cells. Proceedings of the National Academy of Sciences of the United States of America 106:19174-19178.

Mørkve SH, Veruki ML, Hartveit E (2002) Functional characteristics of non-NMDA-type ionotropic glutamate receptor channels in AII amacrine cells in rat retina. The Journal of physiology 542:147-165.

Moser T, Grabner CP, Schmitz F (2020) Sensory Processing at Ribbon Synapses in the Retina and the Cochlea. Physiol Rev 100:103-144.

Moss SJ, Smart TG (2001) Constructing inhibitory synapses. Nature reviews Neuroscience 2:240-250.

Munch TA, da Silveira RA, Siegert S, Viney TJ, Awatramani GB, Roska B (2009) Approach sensitivity in the retina processed by a multifunctional neural circuit. Nature neuroscience 12:1308-1316.

Nakatsuka K, Hamasaki DI (1985) Destruction of the indoleamine-accumulating amacrine cells alters the ERG of rabbits. Investigative ophthalmology & visual science 26:1109-1116.

Nelson R, Kolb H (1985) A17: a broad-field amacrine cell in the rod system of the cat retina. Journal of neurophysiology 54:592-614.

Nomura A, Shigemoto R, Nakamura Y, Okamoto N, Mizuno N, Nakanishi S (1994) Developmentally regulated postsynaptic localization of a metabotropic glutamate receptor in rat rod bipolar cells. Cell 77:361-369.

Oesch N, Diamond J (2009) A night vision neuron gets a day job. Nature neuroscience 12:1209-1211.

Oesch NW, Diamond JS (2011) Ribbon synapses compute temporal contrast and encode luminance in retinal rod bipolar cells. Nature neuroscience 14:1555-1561.

Okawa H, Yu WQ, Matti U, Schwarz K, Odermatt B, Zhong H, Tsukamoto Y, Lagnado L, Rieke F, Schmitz F, Wong ROL (2019) Dynamic assembly of ribbon synapses and circuit maintenance in a vertebrate sensory system. Nature communications 10:2167.

Osswald IK, Galan A, Bowie D (2007) Light triggers expression of philanthotoxin-insensitive Ca2+-permeable AMPA receptors in the developing rat retina. The Journal of physiology 582:95-111.

Pampaloni NP, Plested AJR (2022) Slow excitatory synaptic currents generated by AMPA receptors. The Journal of physiology 600:217-232.

Pampaloni NP, Riva I, Carbone AL, Plested AJR (2021) Slow AMPA receptors in hippocampal principal cells. Cell reports 36:109496.

Pan ZH (2000) Differential expression of high- and two types of low-voltage-activated calcium currents in rod and cone bipolar cells of the rat retina. Journal of neurophysiology 83:513-527.

Pan ZH (2001) Voltage-activated Ca2+ channels and ionotropic GABA receptors localized at axon terminals of mammalian retinal bipolar cells. Visual neuroscience 18:279-288.

Pan ZH, Hu HJ, Perring P, Andrade R (2001) T-type Ca(2+) channels mediate neurotransmitter release in retinal bipolar cells. Neuron 32:89-98.

Paoletti P, Bellone C, Zhou Q (2013) NMDA receptor subunit diversity: impact on receptor properties, synaptic plasticity and disease. Nature reviews Neuroscience 14:383-400.

Pei W, Huang Z, Wang C, Han Y, Park JS, Niu L (2009) Flip and flop: a molecular determinant for AMPA receptor channel opening. Biochemistry 48:3767-3777.

Peichl L, Gonzalez-Soriano J (1994) Morphological types of horizontal cell in rodent retinae: a comparison of rat, mouse, gerbil, and guinea pig. Visual neuroscience 11:501-517.

Percival KA, Gayet J, Khanjian R, Taylor WR, Puthussery T (2022) Calcium-permeable AMPA receptors on AII amacrine cells mediate sustained signaling in the On-pathway of the primate retina. Cell reports 41:111484.

Philpot BD, Sekhar AK, Shouval HZ, Bear MF (2001) Visual experience and deprivation bidirectionally modify the composition and function of NMDA receptors in visual cortex. Neuron 29:157-169.

Protti DA, Llano I (1998) Calcium currents and calcium signaling in rod bipolar cells of rat retinal slices. The Journal of neuroscience : the official journal of the Society for Neuroscience 18:3715-3724.

Puller C, Haverkamp S, Neitz M, Neitz J (2014) Synaptic elements for GABAergic feed-forward signaling between HII horizontal cells and blue cone bipolar cells are enriched beneath primate S-cones. PloS one 9:e88963.

Quinlan EM, Philpot BD, Huganir RL, Bear MF (1999) Rapid, experience-dependent expression of synaptic NMDA receptors in visual cortex in vivo. Nature neuroscience 2:352-357.

Raviola E, Dacheux RF (1987) Excitatory dyad synapse in rabbit retina. Proceedings of the National Academy of Sciences of the United States of America 84:7324-7328.

Rodenas-Ruano A, Chavez AE, Cossio MJ, Castillo PE, Zukin RS (2012) REST-dependent epigenetic remodeling promotes the developmental switch in synaptic NMDA receptors. Nature neuroscience 15:1382-1390.

Rodieck RW (1998) The First Steps in Seeing. Sunderland, MA: Sinauer Associates.

Rozov A, Burnashev N (1999) Polyamine-dependent facilitation of postsynaptic AMPA receptors counteracts paired-pulse depression. Nature 401:594-598.

Sanes JR, Masland RH (2015) The types of retinal ganglion cells: current status and implications for neuronal classification. Annu Rev Neurosci 38:221-246.

Sans N, Petralia RS, Wang Y-X, Blahos J, Hell JW, Wenthold RJ (2000) A Developmental Change in NMDA Receptor-Associated Proteins at Hippocampal Synapses. The Journal of Neuroscience 20:1260-1271.

Schnell E, Sizemore M, Karimzadegan S, Chen L, Bredt DS, Nicoll RA (2002) Direct interactions between PSD-95 and stargazin control synaptic AMPA receptor number. Proceedings of the National Academy of Sciences of the United States of America 99:13902-13907.

Schubert T, Hoon M, Euler T, Lukasiewicz PD, Wong RO (2013) Developmental regulation and activity-dependent maintenance of GABAergic presynaptic inhibition onto rod bipolar cell axonal terminals. Neuron 78:124-137.

Schubert T, Kerschensteiner D, Eggers ED, Misgeld T, Kerschensteiner M, Lichtman JW, Lukasiewicz PD, Wong RO (2008) Development of presynaptic inhibition onto retinal bipolar cell axon terminals is subclass-specific. Journal of neurophysiology 100:304-316.

Schwenk J, Baehrens D, Haupt A, Bildl W, Boudkkazi S, Roeper J, Fakler B, Schulte U (2014) Regional diversity and developmental dynamics of the AMPA-receptor proteome in the mammalian brain. Neuron 84:41-54.

Schwenk J, Harmel N, Zolles G, Bildl W, Kulik A, Heimrich B, Chisaka O, Jonas P, Schulte U, Fakler B, Klocker N (2009) Functional proteomics identify cornichon proteins as auxiliary subunits of AMPA receptors. Science 323:1313-1319.

Schwenk J, Harmel N, Brechet A, Zolles G, Berkefeld H, Muller CS, Bildl W, Baehrens D, Huber B, Kulik A, Klocker N, Schulte U, Fakler B (2012) High-resolution proteomics unravel architecture and molecular diversity of native AMPA receptor complexes. Neuron 74:621-633.

Shanks NF, Savas JN, Maruo T, Cais O, Hirao A, Oe S, Ghosh A, Noda Y, Greger IH, Yates JR, 3rd, Nakagawa T (2012) Differences in AMPA and kainate receptor interactomes facilitate identification of AMPA receptor auxiliary subunit GSG1L. Cell reports 1:590-598.

Shekhar K, Lapan SW, Whitney IE, Tran NM, Macosko EZ, Kowalczyk M, Adiconis X, Levin JZ, Nemesh J, Goldman M, McCarroll SA, Cepko CL, Regev A, Sanes JR (2016) Comprehensive Classification of Retinal Bipolar Neurons by Single-Cell Transcriptomics. Cell 166:1308-1323 e1330.

Shen Y, Heimel JA, Kamermans M, Peachey NS, Gregg RG, Nawy S (2009) A transient receptor potential-like channel mediates synaptic transmission in rod bipolar cells. The Journal of neuroscience : the official journal of the Society for Neuroscience 29:6088-6093.

Sheng M, Cummings J, Roldan LA, Jan YN, Jan LY (1994) Changing subunit composition of heteromeric NMDA receptors during development of rat cortex. Nature 368:144-147.

Sherry DM, Wang MM, Bates J, Frishman LJ (2003) Expression of vesicular glutamate transporter 1 in the mouse retina reveals temporal ordering in development of rod vs. cone and ON vs. OFF circuits. The Journal of comparative neurology 465:480-498.

Shin J, Shen F, Huguenard JR (2005) Polyamines modulate AMPA receptor-dependent synaptic responses in immature layer v pyramidal neurons. Journal of neurophysiology 93:2634-2643.

Siddiqui TJ, Pancaroglu R, Kang Y, Rooyakkers A, Craig AM (2010) LRRTMs and neuroligins bind neurexins with a differential code to cooperate in glutamate synapse development. The Journal of neuroscience : the official journal of the Society for Neuroscience 30:7495-7506.

Siddiqui TJ, Tari PK, Connor SA, Zhang P, Dobie FA, She K, Kawabe H, Wang YT, Brose N, Craig AM (2013) An LRRTM4-HSPG complex mediates excitatory synapse development on dentate gyrus granule cells. Neuron 79:680-695.

Singer JH, Diamond JS (2003) Sustained Ca2+ entry elicits transient postsynaptic currents at a retinal ribbon synapse. Journal of Neuroscience 23:10923-10933.

Singer JH, Lassova L, Vardi N, Diamond JS (2004) Coordinated multivesicular release at a mammalian ribbon synapse. Nature neuroscience 7:826-833.

Sinha R, Siddiqui TJ, Padmanabhan N, Wallin J, Zhang C, Karimi B, Rieke F, Craig AM, Wong RO, Hoon M (2020) LRRTM4: A Novel Regulator of Presynaptic Inhibition and Ribbon Synapse Arrangements of Retinal Bipolar Cells. Neuron 105:1007-1017 e1005.

Sinha R, Grimes WN, Wallin J, Ebbinghaus BN, Luu K, Cherry T, Rieke F, Rudolph U, Wong RO, Hoon M (2021) Transient expression of a GABA receptor subunit during early development is critical for inhibitory synapse maturation and function. Current biology : CB 31:4314-4326 e4315.

Sommer B, Kohler M, Sprengel R, Seeburg PH (1991) RNA editing in brain controls a determinant of ion flow in glutamate-gated channels. Cell 67:11-19.

Sommer B, Keinanen K, Verdoorn TA, Wisden W, Burnashev N, Herb A, Kohler M, Takagi T, Sakmann B, Seeburg PH (1990) Flip and flop: a cell-specific functional switch in glutamate-operated channels of the CNS. Science 249:1580-1585.

Strettoi E, Masland RH (1996) The number of unidentified amacrine cells in the mammalian retina. Proceedings of the National Academy of Sciences of the United States of America 93:14906-14911.

Strettoi E, Dacheux RF, Raviola E (1990) Synaptic connections of rod bipolar cells in the inner plexiform layer of the rabbit retina. The Journal of comparative neurology 295:449-466.

Strettoi E, Masri RA, Grunert U (2018) AII amacrine cells in the primate fovea contribute to photopic vision. Scientific reports 8:16429.

Stroh S, Puller C, Swirski S, Holzel MB, van der Linde LIS, Segelken J, Schultz K, Block C, Monyer H, Willecke K, Weiler R, Greschner M, Janssen-Bienhold U, Dedek K (2018) Eliminating Glutamatergic Input onto Horizontal Cells Changes the Dynamic Range and Receptive Field Organization of Mouse Retinal Ganglion Cells. The Journal of neuroscience : the official journal of the Society for Neuroscience 38:2015-2028.

Tan HL, Roth RH, Graves AR, Cudmore RH, Huganir RL (2020) Lamina-specific AMPA receptor dynamics following visual deprivation in vivo. eLife 9.

Thoreson WB, Mangel SC (2012) Lateral interactions in the outer retina. Progress in retinal and eye research 31:407-441.

Tian N (2004) Visual experience and maturation of retinal synaptic pathways. Vision Res 44:3307-3316.

Tian N, Copenhagen DR (2001) Visual deprivation alters development of synaptic function in inner retina after eye opening. Neuron 32:439-449.

Tian N, Copenhagen DR (2003) Visual Stimulation Is Required for Refinement of ON and OFF Pathways in Postnatal Retina. Neuron 39:85-96.

Tomita S, Chen L, Kawasaki Y, Petralia RS, Wenthold RJ, Nicoll RA, Bredt DS (2003) Functional studies and distribution define a family of transmembrane AMPA receptor regulatory proteins. J Cell Biol 161:805-816.

Traynelis SF, Wollmuth LP, McBain CJ, Menniti FS, Vance KM, Ogden KK, Hansen KB, Yuan H, Myers SJ, Dingledine R (2010) Glutamate receptor ion channels: structure, regulation, and function. Pharmacol Rev 62:405-496.

Truckenbrodt S, Rizzoli SO (2014) Spontaneous vesicle recycling in the synaptic bouton. Frontiers in cellular neuroscience 8:409.

Tsukamoto Y, Omi N (2013) Functional allocation of synaptic contacts in microcircuits from rods via rod bipolar to AII amacrine cells in the mouse retina. The Journal of comparative neurology 521:3541-3555.

Tsukamoto Y, Morigiwa K, Ueda M, Sterling P (2001) Microcircuits for night vision in mouse retina. The Journal of neuroscience : the official journal of the Society for Neuroscience 21:8616-8623.

Twomey EC, Yelshanskaya MV, Vassilevski AA, Sobolevsky AI (2018) Mechanisms of Channel Block in Calcium-Permeable AMPA Receptors. Neuron 99:956-968 e954.

van Wyk M, Wassle H, Taylor WR (2009) Receptive field properties of ON- and OFF-ganglion cells in the mouse retina. Visual neuroscience 26:297-308.

Verdoorn T, Burnashev N, Monyer H, Seeburg P, Sakmann B (1991) Structural determinants of ion flow through recombinant glutamate receptor channels. Science 252:1715-1718.

Veruki ML, Morkve SH, Hartveit E (2003) Functional properties of spontaneous EPSCs and non-NMDA receptors in rod amacrine (AII) cells in the rat retina. The Journal of physiology 549:759-774.

Veruki ML, Zhou Y, Castilho A, Morgans CW, Hartveit E (2018) Extrasynaptic NMDA receptors on rod pathway amacrine cells: molecular composition, activation, and signaling. The Journal of neuroscience : the official journal of the Society for Neuroscience.

Veruki ML, Zhou Y, Castilho A, Morgans CW, Hartveit E (2019) Extrasynaptic NMDA Receptors on Rod Pathway Amacrine Cells: Molecular Composition, Activation, and Signaling. The Journal of neuroscience : the official journal of the Society for Neuroscience 39:627-650.

Vistamehr S, Tian N (2004) Light deprivation suppresses the light response of inner retina in both young and adult mouse. Visual neuroscience 21:23-37.

Voinescu PE, Kay JN, Sanes JR (2009) Birthdays of retinal amacrine cell subtypes are systematically related to their molecular identity and soma position. The Journal of comparative neurology 517:737-750.

Volgyi B, Xin D, Bloomfield SA (2002) Feedback inhibition in the inner plexiform layer underlies the surround-mediated responses of AII amacrine cells in the mammalian retina. The Journal of physiology 539:603-614.

Volgyi B, Deans MR, Paul DL, Bloomfield SA (2004) Convergence and segregation of the multiple rod pathways in mammalian retina. The Journal of neuroscience : the official journal of the Society for Neuroscience 24:11182-11192.

von Engelhardt J, Mack V, Sprengel R, Kavenstock N, Li KW, Stern-Bach Y, Smit AB, Seeburg PH, Monyer H (2010) CKAMP44: a brain-specific protein attenuating short-term synaptic plasticity in the dentate gyrus. Science 327:1518-1522.

von Kriegstein K, Schmitz F (2003) The expression pattern and assembly profile of synaptic membrane proteins in ribbon synapses of the developing mouse retina. Cell Tissue Res 311:159-173.

Wassle H (2004) Parallel processing in the mammalian retina. Nature reviews Neuroscience 5:747-757.

Wassle H, Grunert U, Rohrenbeck J (1993) Immunocytochemical staining of AII-amacrine cells in the rat retina with antibodies against parvalbumin. The Journal of comparative neurology 332:407-420.

Wisner SR, Saha A, Grimes WN, Mizerska K, Kolarik HJ, Wallin J, Diamond JS, Sinha R, Hoon M (2023) Sensory deprivation arrests cellular and synaptic development of the night-vision circuitry in the retina. Current biology : CB.

Xue J, Cooper NGF (2001) The modification of NMDA receptors by visual experience in the rat retina is age dependent. Mol Brain Res 91:196-203.

Yan W, Laboulaye MA, Tran NM, Whitney IE, Benhar I, Sanes JR (2020) Mouse Retinal Cell Atlas: Molecular Identification of over Sixty Amacrine Cell Types. The Journal of neuroscience : the official journal of the Society for Neuroscience 40:5177-5195.

Yoshii A, Sheng MH, Constantine-Paton M (2003) Eye opening induces a rapid dendritic localization of PSD-95 in central visual neurons. Proceedings of the National Academy of Sciences of the United States of America 100:1334-1339.

Zhang C, McCall MA (2012) Receptor targets of amacrine cells. Visual neuroscience 29:11-29.

Zhang C, Hellevik A, Takeuchi S, Wong RO (2022a) Hierarchical partner selection shapes rod-cone pathway specificity in the inner retina. iScience 25:105032.

Zhang G, Liu JB, Yuan HL, Chen SY, Singer JH, Ke JB (2022b) Multiple Calcium Channel Types with Unique Expression Patterns Mediate Retinal Signaling at Bipolar Cell Ribbon Synapses. The Journal of neuroscience : the official journal of the Society for Neuroscience 42:6487-6505.

Zhang J, Yang Z, Wu SM (2005) Development of cholinergic amacrine cells is visual activity-dependent in the postnatal mouse retina. The Journal of comparative neurology 484:331-343.

Zhang J, Li W, Trexler EB, Massey SC (2002) Confocal Analysis of Reciprocal Feedback at Rod Bipolar Terminals in the Rabbit Retina. The Journal of Neuroscience 22:10871-10882.

Zhao JP, Phillips MA, Constantine-Paton M (2006) Long-term potentiation in the juvenile superior colliculus requires simultaneous activation of NMDA receptors and L-type Ca2+ channels and reflects addition of newly functional synapses. The Journal of neuroscience : the official journal of the Society for Neuroscience 26:12647-12655.

Zheng CY, Petralia RS, Wang YX, Kachar B, Wenthold RJ (2010) SAP102 is a highly mobile MAGUK in spines. The Journal of neuroscience : the official journal of the Society for Neuroscience 30:4757-4766.

Zhou C, Dacheux RF (2004) All amacrine cells in the rabbit retina possess AMPA-, NMDA-, GABA-, and glycine-activated currents. Visual neuroscience 21:181-188.

Zhou Y, Tencerova B, Hartveit E, Veruki ML (2016) Functional NMDA receptors are expressed by both AII and A17 amacrine cells in the rod pathway of the mammalian retina. Journal of neurophysiology 115:389-403.

7 SUPPLEMENTARY FIGURES

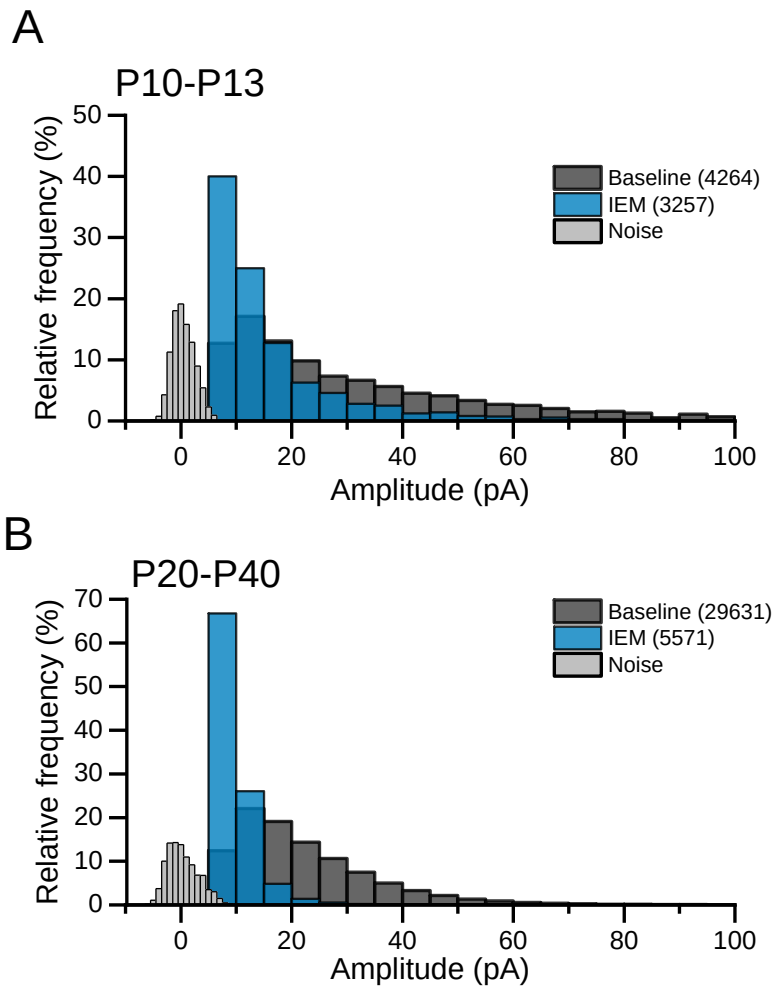

Supplementary Figure 1. Amplitude distributions of mEPSCs in AII amacrine cells before and after bath application of IEM1460.

(A) mEPSCs amplitude distributions (bin size 5 pA) in P10-P13 mice, before (gray) and after bath application of IEM1460 (25 µM, blue). **(B)** Same as **(A)**, but for P20-P40 mice. In both cases, bath application of IEM1460 produces a leftward shift of mEPSC amplitude distribution in such a way that the fit invaded the electrical noise distribution. It worth noting that this shift was more pronounced in the mature group. Total number of events per condition are shown in parentheses. The distribution of electrical noise for baseline condition is shown in gray (bin size 0.5 pA). N=cells/animals. P10-P13: n=8/6, P20-P40: n=7/4. Experiments were performed in the continuous presence of strychnine (3 µM), SR95531 (10 µM), TPMPA (50 µM), APV (25 µM) and TTX (0.5 µM) in order to isolate AMPAR-mEPSCs.

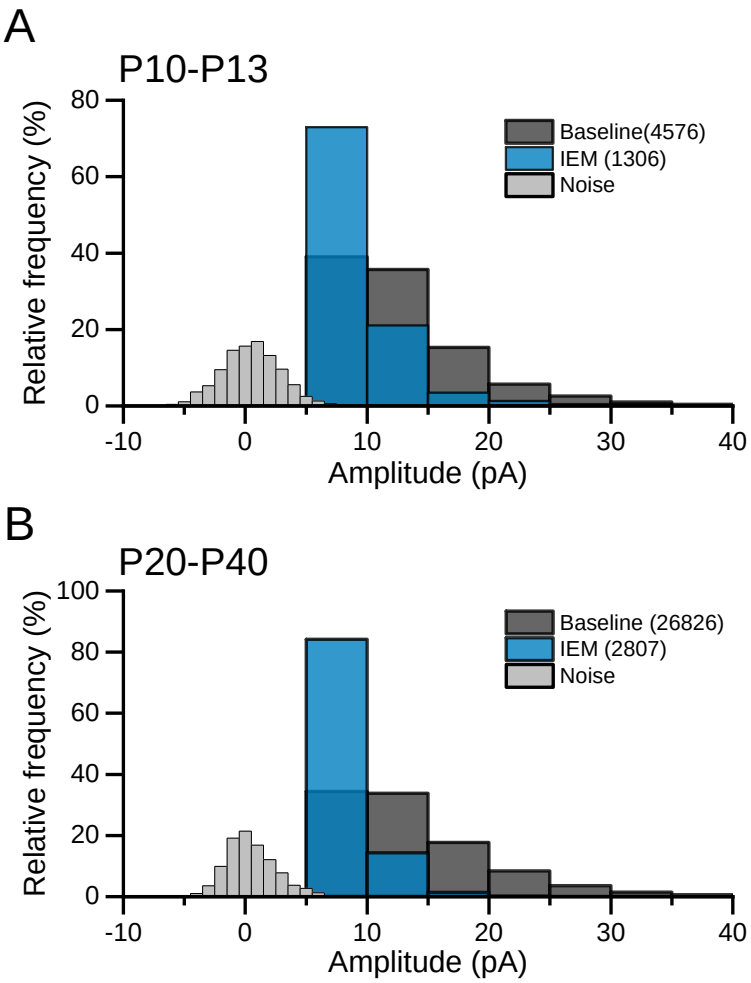

Supplementary Figure 2. Amplitude distributions of mEPSCs in A17 amacrine cells before and after bath application of IEM1460.

(A) mEPSCs amplitude distributions (bin size 5 pA) in P10-P13 mice, before (gray) and after bath application of IEM1460 (25 µM, blue). **(B)** Same as **(A)**, but for P20-P40 mice. In both cases, bath application of IEM1460 produces a similar leftward shift of mEPSC amplitude distribution in such a way that the fit invaded the electrical noise distribution. Total number of events per condition are shown in parentheses. The distribution of electrical noise for baseline condition is shown in gray (bin size 0.5 pA). N=cells/animals. P10-P13: n=6/4, P20-P40: n=5/3. Experiments were performed in the continuous presence of strychnine (3 µM), SR95531 (10 µM), TPMPA (50 µM), APV (25 µM) and TTX (0.5 µM) in order to isolate AMPAR-mEPSCs.

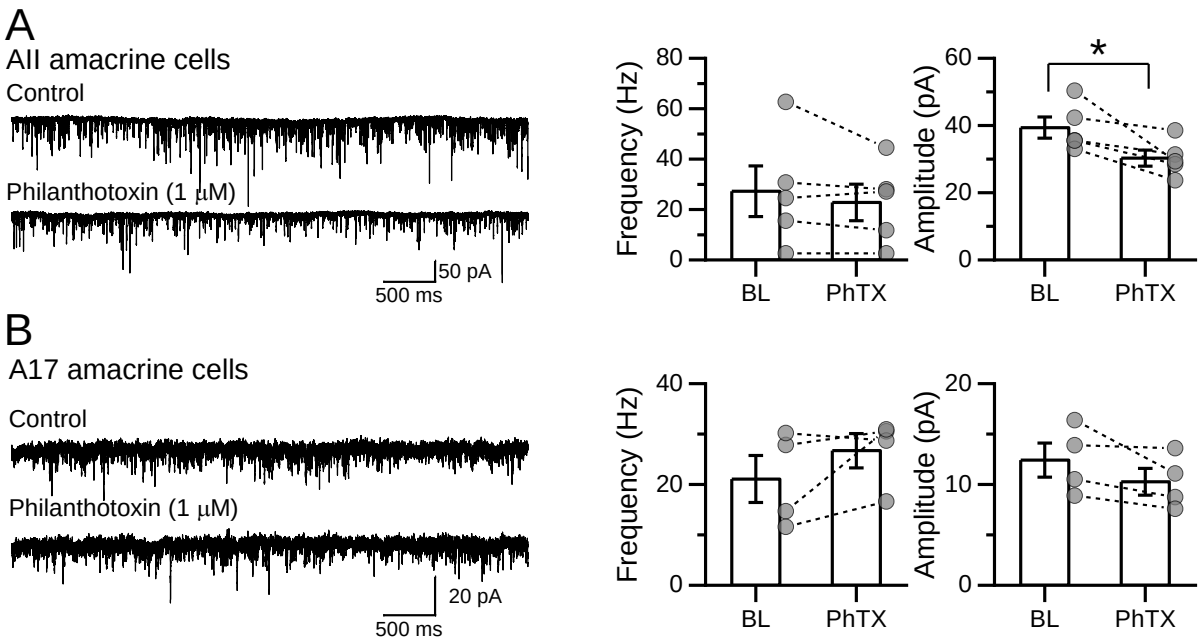

Supplementary Figure 3. Philanthotoxin suppresses mEPSCs amplitude in AII, but not in A17 amacrine cells before eye opening.

(A) Representative AMPAR-mEPSCs (left) recorded at -60 mV in AII amacrine cells from P10-P13 mice before (top) and after (bottom) bath application of the CP-AMPAR blocker, PhTX (1 μM). Bath application of PhTX decreased mEPSC mean amplitude without affecting mEPSC mean frequency (right). **(B)** Same as **(A)** but for A17 amacrine cells (left). Bath application of PhTX did not affect mEPSC amplitude or frequency (right). N=cells/animals. AII AC: 5/4, A17 AC: 4/3. Experiments were performed in the continuous presence of strychnine (3 μM), SR95531 (10 μM), TPMPA (50 μM), APV (25 μM) and TTX (0.5 μM) in order to isolate AMPAR-mEPSCs and avoid Nav channel-mediated currents. Data are presented as mean ± SEM. *p<0.05.

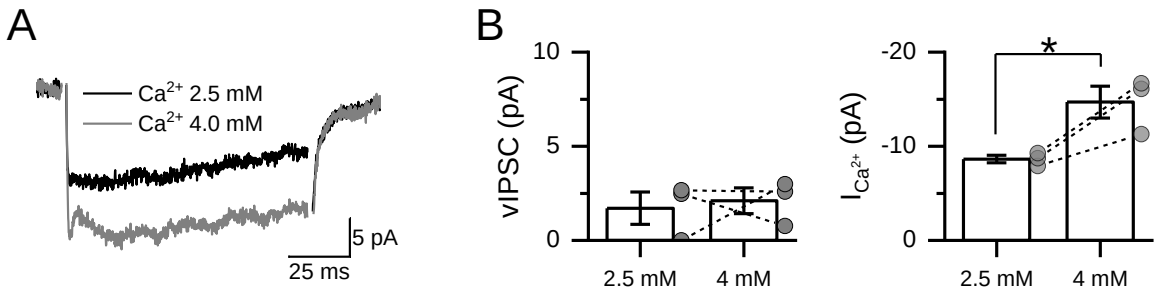

Supplementary Figure 4. Increasing extracellular Ca^{2+} does not trigger reciprocal feedback inhibition onto RBCs before eye opening.

(A) Averaged vIPSC currents recorded from P10-P13 mice before (black) and after (gray) incrementing extracellular Ca^{2+} concentration from 2.5 to 4.0 mM. **(B)** The vIPSC mean amplitude remain unaltered, whereas I_{Ca2+} amplitude significantly increased after bath application of ACSF-Ca^{2+}[4 mM]. N=3 cells/ 3 animals. Experiments were performed in the presence of strychnine (3 µM) and TTX (0.5 µM) in order to block glycinergic and non-reciprocal GABAergic feedback inputs to RBCs, respectively. Data are presented as mean ± SEM. *p<0.05.

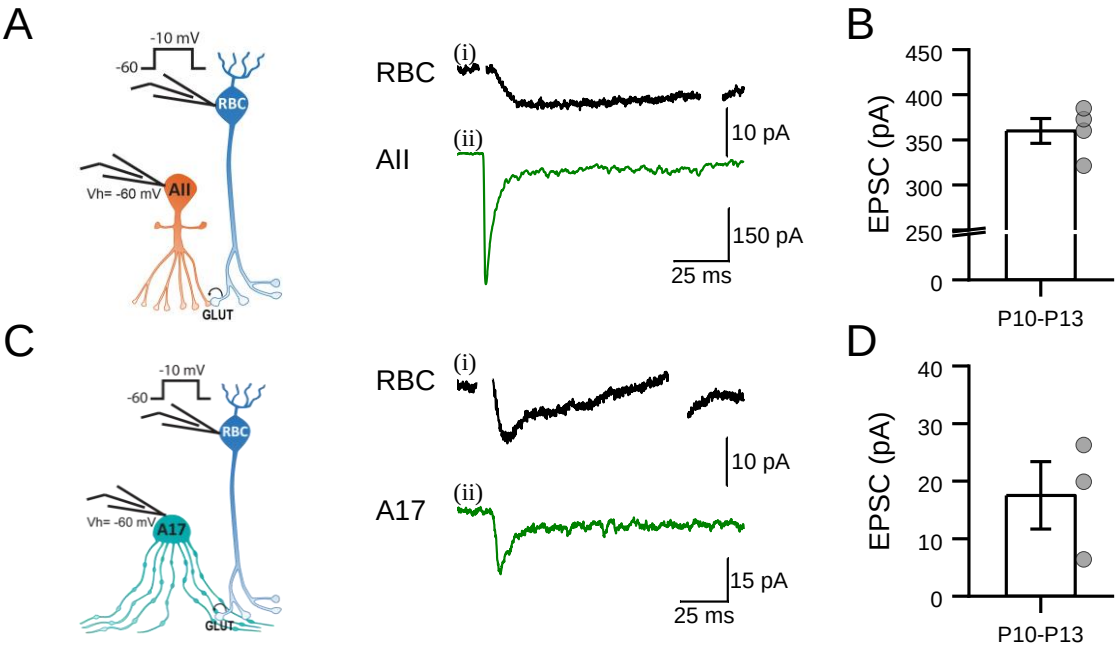

Supplementary Figure 5. Glutamate release at RBC dyad synapse is functional before eye opening.

(A) Schematic representation (left) of a dual recording between synaptically coupled RBC-AII pair from P10-P13 mice. A voltage-step from -60 to -10 mV was applied to the presynaptic RBC (i) in order to elicit a EPSC (ii) in the postsynaptic AII amacrine cell. **(B)** Summary plot showing EPSC mean amplitude recorded in the postsynaptic AII amacrine cell. N=4 pairs/3 animals. **(C)** Schematic representation (left) of a dual recording between synaptically coupled RBC-A17 pair from P10-P13 mice. A voltage-step from -60 to -10 mV was applied in RBC (i) in order to elicit a EPSC (ii) in the postsynaptic A17 amacrine cell. **(D)** Summary plot showing EPSC mean amplitude recorded in the postsynaptic A17 amacrine cell. N=3 pairs/2 animals. Experiments were performed in the continuous presence of strychnine (3 µM) and TTX (0.5 µM). Data are presented as mean ± SEM.

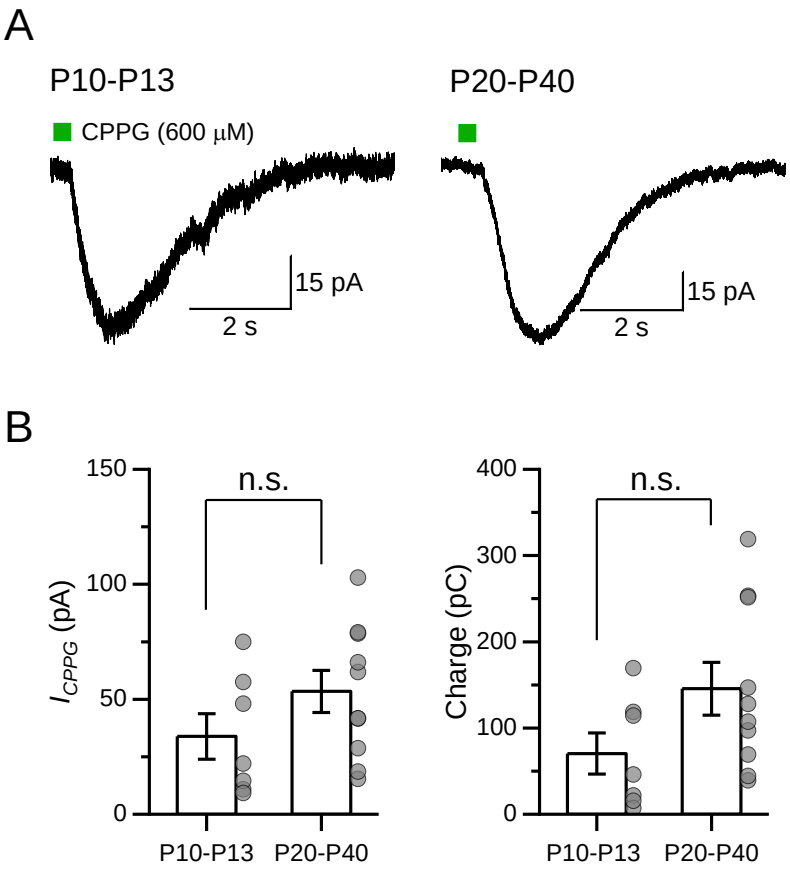

Supplementary Figure 6. CPPG Glutamate release at RBC-A17 synapse is functional before eye opening.

(A) Averaged CPPG-evoked EPSCs (V_{hold}=-60 mV) recorded in A17 ACs before (left) and after (right) eye opening. EPSCs were elicited by a puff of CPPG (600 μM, 300 ms) in the OPL directly onto RBC dendrites in the presence of L-AP4 (10 μM). **(B)** Quantification of the peak currents (left) and charge (right) showed no significant differences between CPPG-evoked responses at both ages. N=cells/animals. P10-P13:7/3, P20-P40:10/8. Data are presented as mean ± SEM.

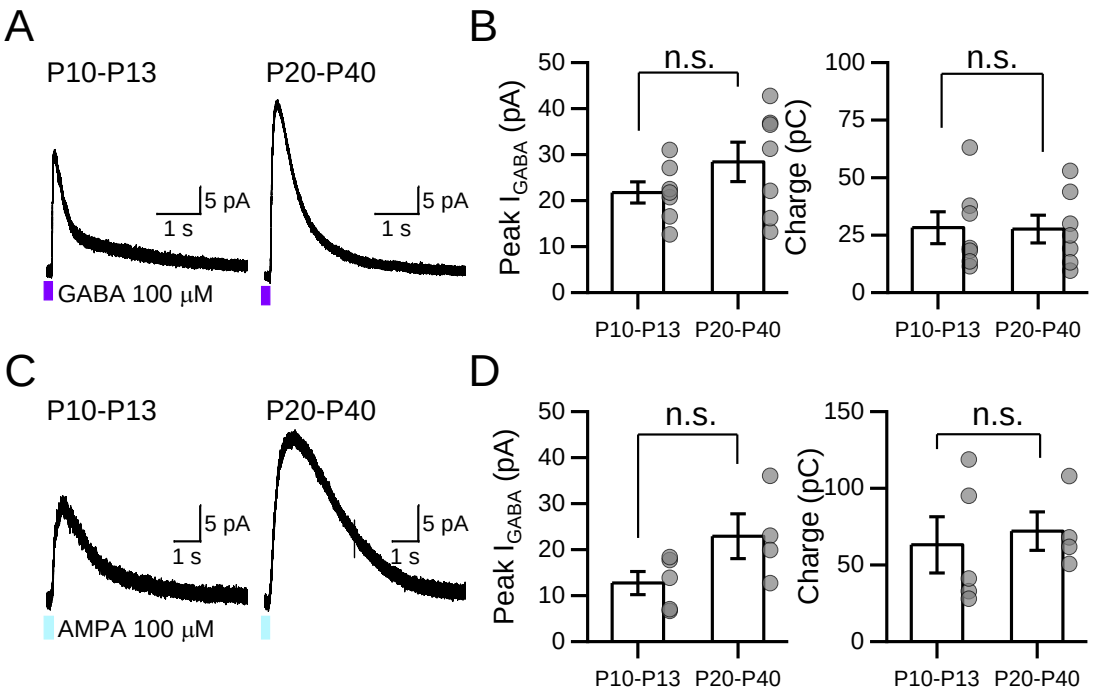

Supplementary Figure 7. GABARs and GABA release are functional before eye opening.

(A) Averaged GABAR-mediated currents (I_{GABA}) recorded in RBCs (V_{hold}=0 mV) from P10-P13 (left) and P20-P40 (right) mice. A brief application of GABA (100 µM, 25 ms) in the IPL directly onto RBC axon terminals was used to evoke I_{GABA}. **(B)** Summary data showing that I_{GABA} mean amplitude (left) and charge (right) remained unchanged throughout development, suggesting that GABAR are function before eye opening. N=cells/animals. P10-P13:7/3, P20-P40:7/3. **(C)** Averaged AMPA-evoked IPSCs recorded in RBCs from P10-P13 (left) and P20-P40 (right) mice. IPSCs were evoked by puff application of AMPA (100 µM, 25 ms) in the IPL, while RBCs were voltage-clamped (V_{hold}=0 mV). **(D)** Summary data showing that I_{GABA} mean amplitude (left) and charge (right) remain unchanged throughout development. N=cells/animals. P10-P13: 5/4, P20-P40: 4/4. Experiments were done in the continuous presence of strychnine (3 µM) and TTX (0.5 µM). Data are presented as mean ± SEM.

8 SUPPLEMENTARY TABLES

Supplementary Table 1. Descriptive statistics and test used in this thesis.

Figure		Measured variable	Descriptive stat. Mean ± SEM	Statistical test	Test statistics	N (cells/animals)
5	B	Cumulative prob. IEI	-	Two sample Kolmogorov-Smirnov test	**P10-P13 vs P20-P40** D(400)=0.805, p= 1.7084 x 10^{-113} **DR vs P10-P13** D(400)=0.9175, p= 3.1641 x 10^{-147} **DR vs P20-P40** D(400)=0.2125, p= 2.1161 x 10^{-8}	**P10-P13:** 8/6 **P20-P40:** 8/6 **DR:** 9/7
		Frequency (Hz)	**P10-P13:** 4.50±0.79 **P20-P40:** 42.02±4.57 **DR:** 107.83±12.66	One-way ANOVA Tukey test	F(2,22) = 40.419, p= 4.2942 x 10^{-8} **P10-P13 vs P20-P40**, p=0.0133 **DR vs P10-P13**, p=0 **DR vs P20-P40**, p= 3.3702 x 10^{-5}	
	C	Cumulative prob. amplitude	-	Two sample Kolmogorov-Smirnov test	**P10-P13 vs P20-P40** D(39)=0.4615, p= 0.0004 **DR vs P10-P13** D(39)=0.2821, p= 0.08974 **DR vs P20-P40** D(39)=0.2308 p= 0.25231	
		Amplitude (pA)	**P10-P13:** 30.07±2.01 **P20-P40:** 17.22±1.94 **DR:** 23.47±1.86	One-way ANOVA Tukey test	F(2,22) = 10.5962, p= 5.9865 x 10^{-4} **P10-P13 vs P20-P40**, p= 0.00039 **DR vs P10-P13**, p= 0.05869 **DR vs P20-P40**, p= 0.07651	
	E	Rise (ms)	**P10-P13:**0.285±0.019 **P20-P40:**0.410±0.018 **DR:**0.476±0.018	One-way ANOVA Tukey test	F(2,22) = 28.5511, p= 7.7014 x 10^{-7} **P10-P13 vs P20-P40**, p= 0.00028 **DR vs P10-P13**, p= 4.7696 x 10^{-7} **DR vs P20-P40**, p= 0.04176	
		Decay (ms)	**P10-P13:**0.693±0.052 **P20-P40:**0.982±0.053 **DR:**1.100±0.060	One-way ANOVA Tukey test	F(2,22) = 14.1098, p= 1.1404 x 10^{-4} **P10-P13 vs P20-P40**, p= 0.00442 **DR vs P10-P13**, p= 9.2287 x 10^{-5} **DR vs P20-P40**, p= 0.30788	
		Half-width (ms)	**P10-P13:**1.013±0.044 **P20-P40:**1.294±0.057 **DR:**1.433±0.037	Kruskal-Wallis ANOVA Dunn's Test	Chi Sqr= 16.5742, p= 2.5174 x 10^{-4} **P10-P13 vs P20-P40**, p= 0.04464 **DR vs P10-P13**, p= 0.00016 **DR vs P20-P40**, p= 0.36982	
6	C	Rectification Index	**P10-P13** (-):0.87±0.06 (+):0.31±0.05 **P20-P40** (-):0.64±0.05 (+):0.22±0.04 **DR** (+):0.23±0.07	Two sample t Test	**P10-P13** t(10)= 6.9027, p= 4.1807 x 10^{-5} **P20-P40** t(7)= 6.9776, p= 2.1582 x 10^{-4} **DR vs P20-P40** t(7)= -0.0539, p= 0.95853	**P10-P13** (-):6/4 (+):6/5 **P20-P40** (-):4/4 (+):5/4 **DR:** 4/4
7	B	I_{AMPA} amplitude (pA)	**P10-P13** BL: 752.5±164.6 IEM: 256.3±106.8	Paired sample t test	**P10-P13** t(3)= 5.4327, p= 0.01224 **P20-P40**	**P10-P13:** 4/3 **P20-P40:** 5/4

			P20-P40 BL: 553.3±107.2 IEM: 145.1±22.1		t(4)= 4.36484, p= 0.01202	
	C	I_{AMPA} charge (pC)	**P10-P13** BL:1230.4±432.1 IEM: 380.6±181.0 **P20-P40** BL:1054.2±178.2 IEM:192.6±28.4	Paired sample t test	**P10-P13** t(3)= 3.3512, p= 0.04402 **P20-P40** t(4)= 5.73253, p= 0.00459	
	D	Percentage of block	**P10-P13:** 68.94±7.03 **P20-P40:** 71.70±3.74	Two sample t Test	t(7)= -0.36783, p= 0.72387	
8	**B**	Cumulative prob. IEI	**P10-P13** **BL vs IEM**	Two sample Kolmogorov-Smirnov test	D(500)=0.06, p= 0.30234	**P10-P13:** 8/6 **P20-P40:** 7/4
		Frequency (Hz)	**P10-P13** BL: 4.50±0.79 IEM: 3.44±0.44	Paired sample t test	t(7)= 1.5989, p= 0.15387	
		Cumulative prob. amplitude	**P20-P40** **BL vs IEM**	Two sample Kolmogorov-Smirnov test	D(80)=0.25, p= 0.01319	
		Amplitude (pA)	**P10-P13** BL: 30.07±2.01 IEM: 16.97±1.68	Paired sample t test	t(7)= 4.69741, p= 0.00222	
	D	Cumulative prob. IEI	**P20-P40** **BL vs IEM**	Two sample Kolmogorov-Smirnov test	D(62)= 0.70968, p= 3.3307×10^{-15}	
		Frequency (Hz)	**P20-P40** BL: 89.66±16.51 IEM: 10.67±1.92	Wilcoxon Signed Ranks Test	Z=2.282, p=0.02249	
		Cumulative prob. amplitude	**P20-P40** **BL vs IEM**	Two sample Kolmogorov-Smirnov test	D(80)= 0.4375, p= 2.9278×10^{-7}	
		Amplitude (pA)	**P20-P40** BL: 21.60±1.94 IEM: 10.15±0.71	Paired sample t test	t(6)= 5.16013, p= 0.00209	
	E	Percentage of block	**P10-P13:** 41.16±7.17 **P20-P40:** 49.90±7.07	Two sample t Test	t(13)= -0.86335, p= 0.40359	
9	**A**	I_{NMDA} amplitude (pA)	**P10-P13:** 1.75±1.35 **P20-P40:** 0.27±0.98 **DR:** -12.75±1.90	Kruskal-Wallis ANOVA Dunn's Test	Chi Sqr= 11.51579, p= 0.00316 **P10-P13 vs P20-P40**, p= 1 **DR vs P10-P13**, p= 0.00414 **DR vs P20-P40**, p= 0.03073	**P10-P13:** 7/5 **P20-P40:** 5/5 **DR:** 6/3
	B		**P20-P40 (Rat)** 25.90±4.61	-	-	**P20-P40 (Rat):**4/1
10	**B**	Cumulative prob. IEI	-	Two sample Kolmogorov-Smirnov test	**P10-P13 vs P20-P40** D(100)=0.26, p= 0.00222 **DR vs P10-P13** D(100)=0.29, p= 4.11741×10^{-4} **DR vs P20-P40** D(100)=0.08, p= 0.90841	**P10-P13:** 8/5 **P20-P40:** 8/6 **DR:** 7/5
		Frequency (Hz)	**P10-P13:** 10.78±3.06 **P20-P40:**36.25±10.32 **DR:** 30.68±3.01	Kruskal-Wallis ANOVA Dunn's Test	Chi Sqr= 9.78261, p= 0.00751 **P10-P13 vs P20-P40**, p= 0.03658	

					DR vs P10-P13, p= 0.01316 **DR vs P20-P40**, p= 1	
	C	Cumulative prob. amplitude	-	Two sample Kolmogorov-Smirnov test	**P10-P13 vs P20-P40** D(39)=0.07692, p= 0.9999 **DR vs P10-P13** D(39)=0.2821, p= 0.08974 **DR vs P20-P40** D(39)=0.23077 p= 0.25231	
		Amplitude (pA)	**P10-P13:** 11.92±0.86 **P20-P40:** 10.41±1.11 **DR:** 9.82±0.71	Kruskal-Wallis ANOVA	Chi Sqr= 4.29154, p= 0.11698	
	E	Rise (ms)	**P10-P13:**0.355±0.011 **P20-P40:**0.353±0.021 **DR:**0.414±0.035	One-way ANOVA	F(2,20) = 2.08342, p= 0.1507	
		Decay (ms)	**P10-P13:**0.881±0.071 **P20-P40:**0.764±0.064 **DR:**1.001±0.097	One-way ANOVA	F(2,22) = 2.30499, p= 0.12566	
		Half-width (ms)	**P10-P13:**1.169±0.076 **P20-P40:**1.131±0.075 **DR:**1.329±0.102	One-way ANOVA	F(2,22) = 1.49865, p= 0.24747	
11	**C**	Rectification Index	**P10-P13** (-):0.92±0.20 (+):0.76±0.07	Mann-Whitney Test	U=22, p=0.84645	**P10-P13** (-):6/5 (+):8/5 **P20-P40** (-):7/5 (+):8/5 **DR:** 6/4
			P20-P40 (-):0.89±0.13 (+):0.35±0.09 **DR** (+):0.30±0.07	Two sample t Test	**P20-P40** t(13)= 3.4209, p= 0.00456 **DR vs P20-P40** t(12)= 0.41658, p= 0.68434	
12	**B**	I_{AMPA} amplitude (pA)	**P10-P13** BL: 173.29±31.25 IEM: 49.28±9.27 **P20-P40** BL: 176.41±37.80 IEM: 48.80±13.03	Paired sample t test	**P10-P13** t(4)= 5.2169, p= 0.00644 **P20-P40** t(4)= 5.0020, p= 0.00748	**P10-P13:** 5/3 **P20-P40:** 5/3
	C	I_{AMPA} charge (pC)	**P10-P13** BL:453.34±122.68 IEM: 118.38±36.37 **P20-P40** BL:379.74±124.31 IEM:95.35±31.52	Paired sample t test	**P10-P13** t(4)= 3.8746, p= 0.01792 **P20-P40** t(4)= 2.9466, p= 0.04211	
	D	Percentage of block	**P10-P13:** 71.79±3.33 **P20-P40:** 73.07±2.10	Two sample t Test	t(8)= -0.32601, p= 0.75278	
13	**B**	Cumulative prob. IEI	**P10-P13** **BL vs IEM**	Two sample Kolmogorov-Smirnov test	D(4562)= 0.56423, p= 0	**P10-P13:** 6/4 **P20-P40:** 5/3
		Frequency (Hz)	**P10-P13** BL: 10.42±3.45 IEM: 2.49±0.49	Paired sample t test	t(5)= 2.6214, p= 0.04702	
		Cumulative prob. amplitude	**P10-P13** **BL vs IEM**	Two sample Kolmogorov-Smirnov test	D(27)=0.4074, p= 0.02167	
		Amplitude (pA)	**P10-P13**	Wilcoxon	Z=2.0966, p=0.03125	

			BL: 11.52±0.74 IEM: 8.75±0.61	Signed Ranks Test		
	D	Cumulative prob. IEI	**P20-P40** **BL vs IEM**	Two sample Kolmogorov-Smirnov test	D(459)= 0.69935, p= 2.3778 x 10^{-98}	
		Frequency (Hz)	**P20-P40** BL: 45.31±15.32 IEM: 4.74±2.80	Paired sample t test	t(4)= 3.1217, p= 0.03547	
		Cumulative prob. amplitude	**P20-P40** **BL vs IEM**	Two sample Kolmogorov-Smirnov test	D(59)= 0.5593, p= 7.6682 x 10^{-9}	
		Amplitude (pA)	**P20-P40** BL: 11.39±1.62 IEM: 7.43±0.36	Paired sample t test	t(4)= 3.03128, p=0.03873	
	E	Percentage of block	**P10-P13:** 23.87±2.66 **P20-P40:** 31.36±6.25	Two sample t Test	t(9)= -1.1758, p= 0.26984	
14	**C**	Rectification Index	**P10-P13** (+):0.76±0.07 **P10-P13 GluA2$^{-/-}$** (+): 0.35±0.11 **P20-P40** (+):0.35±0.09	One-way ANOVA Tukey test	F(2,19) = 7.41118, p= 0.00418 **P10-P13 WT vs P20-P40 WT,** p=0.00782 **P10-P13 WT vs P10-P13 GluA2$^{-/-}$**, p= 0.01366 **P10-P13 GluA2$^{-/-}$ vs P20-P40 WT** , p= 1	**P10-P13 GluA2$^{-/-}$** (+):6/1 **P10-P13 WT** (+):8/5 **P20-P40 WT** (+):8/5
15	**B**	vIPSC amplitude (pA)	**P10-P13:** 1.28±0.27 **P20-P40:**13.67±1.37	Mann-Whitney Test	U=11, p=6.0859 x 10^{-9}	**P10-P13:**19/15 **P20-P40:**35/21
		I_{Ca}^{2+} amplitude (pA)	**P10-P13:** -8.58±1.12 **P20-P40:** -21.12±1.76	Mann-Whitney Test	U=607, p= 5.7545 x 10^{-7}	
16	**B**	vIPSC amplitude (pA)	**P10-P13 GluA2$^{-/-}$** 11.26±2.95 **P20-P40 GluA2$^{-/-}$** 8.51±1.25	Mann-Whitney Test	U=252, p=0.12874	**P10-P13:**32/5 **P20-P40:**21/3
		I_{Ca}^{2+} amplitude (pA)	**P10-P13 GluA2$^{-/-}$** -10.10±1.50 **P20-P40 GluA2$^{-/-}$** -18.74±1.53	Mann-Whitney Test	U=528.5, p= 4.7984 x 10^{-4}	
17	**B**	vIPSC amplitude (pA)	**NR:** 19.26±2.29 **DR:** 6.84±0.97	Mann-Whitney Test	U=1308.5, p=1.9397 x 10^{-6}	**NR:**27/5 **DR:**59/20
		I_{Ca}^{2+} amplitude (pA)	**NR:** -7.22±1.09 **DR:** -12.72±0.94	Mann-Whitney Test	U=1000, p= 9.2187 x 10^{-4}	
18	**B**	vIPSC amplitude (pA)	**DR:** 4.56±1.23 **LE1:** 11.07±2.05 **LE2:** 15.19±1.72	Kruskal-Wallis ANOVA Dunn's Test	Chi Sqr= 16.82262, p=2.2234 x 10^{-4} **DR vs LE1**, p= 0.04226 **DR vs LE2** p= 1.23971 x 10^{-4} **LE1 vs LE2**, p= 0.17775	**DR:** 22/8 **LE1:** 32/5 **LE2:** 28/4
		I_{Ca}^{2+} amplitude (pA)	**DR:** -10.84±1.15 **LE1:** -10.89±1.60 **LE2:** -11.38±1.42	Kruskal-Wallis ANOVA	Chi Sqr= 16.82262, p= 0.83903	
19	**B**	I_{NMDA} amplitude (pA)	**P10-P13:** 50.33±9.22 **P20-P40:**57.30±14.11 **DR:**19.30±3.17	One-way ANOVA	(2,9) = 2.96045, p= 0.10281	**P10-P13:** 5/5 **P20-P40:** 4/3 **DR:** 3/2

				Tukey test		
20	**A**	I_{NMDA} amplitude (pA)	**P10-P13** BL: 50.33±9.22 Zn: 32.15±5.67 Ro:19.34±4.70	One-way ANOVA RM Tukey test	$F(2,8) = 27.40423$, $p= 2.6320 \times 10^{-4}$ BL-Zn, p= 0.00635 BL-Ro, $p= 2.0405 \times 10^{-4}$ Zn-Ro, p= 0.03802	**P10-P13:** 5/5 **P20-P40:** 4/3 **DR:** 3/2
	B		**P20-P40** BL: 57.30±14.11 Zn: 37.65±11.20 Ro: 31.90±9.94	One-way ANOVA RM Tukey test	$F(2,6) = 12.44029$, p= 0.00733 BL-Zn, p= 0.0241 BL-Ro, p= 0.00749 Zn-Ro, p= 0.56045	
	C		**DR** BL: 19.30±3.17 Zn: 12.68±2.87 Ro: 11.55±3.46	One-way ANOVA RM Tukey test	$F(2,4) = 33.80186$, p= 0.00312 BL-Zn, p= 0.00637 BL-Ro, p= 0.00354 Zn-Ro, p= 0.55735	
S3	**A**	Frequency (Hz)	**P10-P13 All AC** BL:27.23±10.06 PhTx:22.84±7.25	Paired sample t test	$t(4)= 1.2152$, p= 0.29111	**P10-P13:**5/4
		Amplitude (pA)	**P10-P13 All AC** BL:39.36±3.15 PhTx:30.30±2.41	Paired sample t test	$t(4)= 2.88081$, p= 0.04498	
	B	Frequency (Hz)	**P10-P13 A17 AC** BL:21.07±4.65 PhTx:26.70±3.39	Wilcoxon Signed Ranks Test	Z= 1.64317, p= 0.10035	**P10-P13:**4/3
		Amplitude (pA)	**P10-P13 A17 AC** BL: 12.41±1.68 PhTx:10.26±1.33	Paired sample t test	$t(3)= 1.98517$, p= 0.14134	
S4	**B**	vIPSC amplitude (pA)	**P10-P13** 2.5 mM: 0.06±1.48 4.0 mM: 2.11±0.68	Paired sample t test	$t(2)= -1.92365$, p= 0.1943	**P10-P13:**3/3
		I_{Ca}^{2+} amplitude (pA)	**P10-P13** 2.5 mM: -8.64±0.40 4.0 mM: -14.69±1.70	Paired sample t test	$t(2)= 4.56397$, p= 0.04481	
S5	**B**	EPSC (pA)	**P10-P13** 359.84±13.82	-	-	**P10-P13:**4/3
	D	EPSC (pA)	**P10-P13** 17.51±5.86	-	-	**P10-P13:**3/2
S6	**B**	I_{CPPG} (pA)	**P10-P13** 33.85±9.89 **P20-P40** 53.42±9.14	Two sample t Test	$t(15)= -1.42632$, p= 0.17426	**P10-P13:**7/3 **P20-P40:**10/8
		Charge (pC)	**P10-P13** 70.35±23.91 **P20-P40** 145.56±30.61	Two sample t Test	$t(15)= -1.79563$, p= 0.09272	
S7	**B**	I_{GABA} (pA)	**P10-P13** 21.76±2.32 **P20-P40** 28.42±4.28	Two sample t Test	$t(12)= -1.36874$, p= 0.19616	**P10-P13:**7/3 **P20-P40:**7/3
		Charge (pC)	**P10-P13** 28.25±6.93 **P20-P40** 27.62±6.03	Two sample t Test	$t(12)= 0.06803$, p= 0.94688	

	D	I_{GABA} (pA)	**P10-P13** 12.73±2.52 **P20-P40** 22.91±4.88	Two sample t Test	t(7)= -1.97801, p= 0.08844	**P10-P13:**5/4 **P20-P40:**4/4
		Charge (pC)	**P10-P13** 63.12±18.38 **P20-P40** 72.06±12.46	Two sample t Test	t(7)= -0.379911, p= 0.71528	